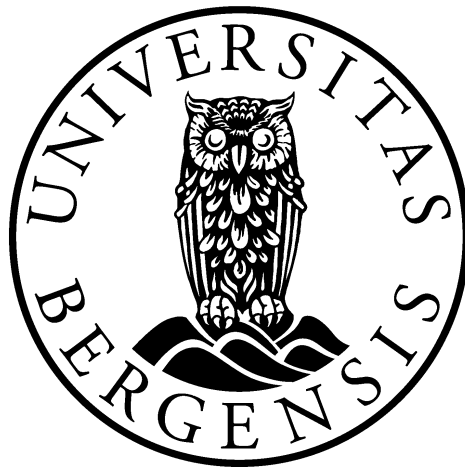


# Polarization-independent CP-violation in SUSY theories

Alexander Vereshagin



Dissertation for the degree of Philosophiae Doctor (PhD)

Department of Physics and Technology  
University of Bergen

September 22, 2012



# Scientific environment

The research has been conducted under the supervision of Prof. Per Osland, in the theoretical particle physics group, part of the Subatomic Section at the Department of Physics and Technology, University of Bergen, Norway.

Part of the work has been performed in collaboration with Jan Kalinowski and Krzysztof Rolbiecki from Institute of Theoretical Physics, University of Warsaw, Poland.

The research was supported by the Quota Program in the period of 2002 – 2005.

Part of this study was conducted in parallel with another research, performed in collaboration with Vladimir Vereshagin and Kirill Semenov-Tian-Shansky from St. Petersburg State University; the main results of the latter activity are summarized in a series of papers: A. Vereshagin *et al.*, Phys. Rev. D **59** (1999) 016002; J. Math. Sci. **125** (2005) 144–158 [*translated from*: Zap. nauchn. sem. POMI **291** (2002) 78–108]; Phys. Rev. D **69** (2004) 025002; Phys. Rev. D **73** (2006) 025020; Phys. Rev. D **77** (2008) 025028.



# Acknowledgements

It is a pleasure to thank my supervisor and collaborator Prof. Per Osland for guiding me through the SUSY phenomenology and Feynman graph computation routines. His help with calculations, continuous advice, patience and friendly support made this work possible. I am also very grateful to Prof. Vladimir Vereshagin for invaluable discussions and explanations.

Further, I would like to thank Prof. Alfred Bartl for pointing out an error in our intermediate calculations and communicating results of Ref. [27] prior to publication, as well as Prof. Jan Kalinowski and Krzysztof Rolbiecki for our fruitful collaboration at the later stage of this research.

I greatly appreciate kind hospitality of Nordic Institute for Theoretical Physics (NORDITA) during my stays as a visiting student in Copenhagen and Stockholm.

I wish also to thank my fellow students Frank Saether and Audun Nyre for interesting discussions and friendly atmosphere during my studies in University of Bergen.

Finally, I am indebted to my wife Natalie for constant encouragement, kind help and support during completion of this Thesis.

Alexander Vereshagin



# Abstract

Supersymmetry (SUSY) is a beautiful mathematical concept which binds internal symmetries of a quantum field theory with global symmetries of the space-time. Applications of this approach may stretch from unsolved puzzles in particle physics to global problems in cosmology. The elimination of the hierarchy problem in Supersymmetric versions of the Standard Model was the initial strongest motivation to explore SUSY. However, there are other philosophical and technical problems that may find a solution if SUSY is proven to be the part of physical reality. This includes improved ultraviolet convergence of the theory, a way out of the strong restrictions imposed for field-theoretical models by general Coleman-Mandula theorem, potential solution of the so-called “cold dark matter problem” in cosmology, and many others.

Building a (realistic) supersymmetric quantum field theory model normally requires introduction of new particles (“superparticles”), and it is not yet clear how one can confirm supersymmetry without detecting some of them. The regular search for supersymmetric events started back in 1980th, but, unfortunately, no direct evidence is still found. Yet, the SUSY studies contribute a big part of particle physics activities; the search for Supersymmetry is one of the main focuses of the on-going experimental program at CERN and at proposed electron–positron linear collider. In particular, it is currently believed that the known sources of CP-violation inside the Standard Model are not sufficient to explain the observed dominance of matter over anti-matter, while SUSY extensions of the Standard Model provide additional sources of CP-violation. It is known that the complex phases of the higgsino and gaugino mass parameters in the Minimal Supersymmetric Standard Model (MSSM) allow for CP violation at low orders of perturbation theory, without invoking the Cabibbo–Kobayashi–Maskawa matrix or the Higgs sector. If the phases are significant, one may expect experimental evidence of CP violation that does not fit the explanation within the (non-supersymmetric) Standard Model.

In the light of the International Linear Collider project, it is natural to consider the products of electron–positron annihilation. Typically, to detect a CP-odd observable in a two particle creation process one has to detect spin component (polarization) of some of the particles in addition to the particle momenta, since any scalar product of momenta is even under C and P. It is shown, however, that for chargino pair creation in electron-positron annihilation it is in principle possible to detect CP-violation without measuring polarizations, provided the two final charginos have different masses.

It is shown that one can construct a CP-odd observable out of unpolarized cross-sections. This observable, although vanishes at the tree level, acquires non-vanishing contributions starting from 1-loop order. Most of the results are obtained in the simplest version of unconstrained MSSM, however one can easily see that the results hold in a much larger class of less restricted Supersymmetric models.





# List of papers contributing to the Thesis

A part of the results presented in this Thesis was published in:

1. P. Osland and A. Vereshagin, *CP violation in unpolarized  $e^+ e^- \rightarrow$  charginos at one loop level*, Phys. Rev. D **76** (2007) 036001 [Erratum-*ibid.* 119902].
2. P. Osland, J. Kalinowski, K. Rolbiecki and A. Vereshagin, *Polarization-independent CP-odd Observable in  $e^+e^-$  Chargino Production at One Loop*, eConf C **0705302** (2007) SUS10.



# Contents

<b>1</b>	<b>Introduction</b>	<b>1</b>
<b>2</b>	<b>CP-odd observables</b>	<b>7</b>
<b>3</b>	<b>Polarized tree-level cross section</b>	<b>11</b>
3.1	Tree level approximation: notations . . . . .	12
3.2	The tree level cross section . . . . .	14
3.3	P, C, and CP transformations at tree-level . . . . .	15
<b>4</b>	<b>The one-loop corrections: contributing graphs</b>	<b>19</b>
4.1	Contributing graphs: overview . . . . .	19
4.2	1PI one-loop graphs (“boxes”): skeletons . . . . .	21
4.3	1PI one-loop diagrams in the heavy slepton limit . . . . .	25
4.4	One-loop corrections to the 3-point vertices: skeletons . . . . .	26
4.5	One-loop corrections to the 3-point vertices . . . . .	29
<b>5</b>	<b>Loop integral calculations</b>	<b>35</b>
5.1	Passarino–Veltman-like integrals . . . . .	35
5.2	Loop momenta parametrizations . . . . .	35
5.3	Some symmetries of the loop integrals . . . . .	39
5.4	Reduction of $J$ 's with negative index (uncrossed box) . . . . .	41
5.5	Reduction of $J$ 's with negative index (crossed box) . . . . .	42
5.6	“Three-point” tensor integrals (uncrossed box) . . . . .	42
5.7	“Three-point” tensor integrals (crossed box) . . . . .	45
5.8	“Three-point” $J$ with one negative index . . . . .	46
5.9	$J$ with two Lorentz indices . . . . .	50
<b>6</b>	<b>Box contributions to CP-odd observables</b>	<b>53</b>
6.1	Loop contribution overview . . . . .	53
6.2	Analysis of box contributions . . . . .	54
6.3	Full 1 loop CP-odd contribution . . . . .	60
6.4	Interference with chargino decay . . . . .	62
<b>7</b>	<b>Conclusions</b>	<b>63</b>
<b>APPENDICES:</b>		

<b>A</b>	<b>The Fiertz transformation</b>	<b>67</b>
A.1	General Fiertz transformation . . . . .	67
A.2	Cross-channel s-neutrino exchange via Fiertz . . . . .	69
<b>B</b>	<b><math>U(1)</math> Ward identities and the <math>\gamma f_i \bar{f}_j</math> coupling</b>	<b>73</b>
<b>C</b>	<b>The Lagrangian vertices and Feynman rules</b>	<b>77</b>
C.1	Handling C-conjugate and Majorana fermions . . . . .	77
C.2	MSSM Lagrangian vertices used in analytical calculations . . . . .	81
C.2.1	Standard Model vertices used at tree level and in box calculations . . . . .	81
C.2.2	MSSM (SUSY) vertices used at tree level and in box calculations . . . . .	82

# List of Figures

3.1	Tree level diagrams for $e^+ + e^- \rightarrow \tilde{\chi}_i^+ + \tilde{\chi}_j^-$ process: superpartners of ordinary particles pictured by double lines for later convenience. Throughout the Thesis we drop “tilde” (“ $\tilde{\phantom{x}}$ ”) sign from the chargino symbols $\tilde{\chi}_i$ when drawn in diagrams. . . . .	11
4.1	“Vertical” skeleton with ordinary particle exchanges between initial and final states. . . . .	21
4.2	“Vertical” skeleton with sparticle exchanges between initial and final states. . . . .	22
4.3	“Horizontal” fermion lines: “clashing” specifies intermediate particles. . . . .	22
4.4	“Horizontal” fermion lines: both the internal fermions are sparticles. . . . .	23
4.5	“Crossed” fermion lines: both the internal fermions are neutrino. . . . .	23
4.6	“Crossed” fermion lines: both the internal fermions are neutralino. . . . .	23
4.7	“Crossed” fermion lines: neutrino and neutralino. . . . .	24
4.8	Box diagrams without slepton lines: all chargino and neutralino mass eigenstates contribute. . . . .	25
4.9	Electron-electron vertex corrections: skeleton graphs. . . . .	27
4.10	Chargino-chargino vertex corrections: skeleton graphs. . . . .	28
4.11	Electron-chargino vertex corrections: skeleton graphs . . . . .	28
4.12	$eeZ$ vertex corrections: all mass eigenstates of intermediate sparticles shall be accounted for. . . . .	29
4.13	$Z\chi\chi$ vertex corrections (1st and 2nd skeletons from Fig. 4.10): all selectron and sneutrino mass eigenstates contribute. Note however that the first diagram vanishes for one of the internal selectron mass states ( $\tilde{e}_1$ ) and the last diagram vanishes if the two internal selectrons have different masses. . . . .	30
4.14	$Z\chi\chi$ vertex corrections (3rd skeleton from Fig. 4.10): all chargino and neutralino mass eigenstates shall be accounted for. . . . .	31
4.15	$Z\chi\chi$ vertex corrections (4th skeleton from Fig. 4.10): all mass eigenstates of intermediate sparticles shall be accounted for. . . . .	32
4.16	$e^+\chi_i^+\tilde{\nu}$ vertex corrections (1st and 2nd skeletons from Fig. 4.11): all chargino and neutralino mass eigenstates shall be accounted for. . . . .	33
4.17	$e^+\chi_i^+\tilde{\nu}$ vertex corrections (3rd and 4th skeletons from Fig. 4.11): all eigenstates of the intermediate sparticles shall be accounted for. . . . .	34
5.1	Momenta assignment in the “crossed” and “uncrossed” box diagrams: arrows on particle lines denote the momentum direction. . . . .	36
6.1	The couplings of Eq. (6.3) vs. $\phi_\mu$ for various values of $\tan\beta$ . . . . .	56

6.2	The ratio (2.17) at various values of $\phi_\mu$ and $\tan\beta$ . The polar scattering angle is $\theta = \pi/3$ while $\sqrt{s} = 600$ GeV. . . . .	57
6.3	Same parameters as in Fig. 6.2, except $\sqrt{s} = 800$ GeV. . . . .	58
6.4	The ratio (2.17) for various values of the polar angle $\theta$ . The other parameters are fixed as $\tan\beta = 5$ , $\sqrt{s} = 800$ GeV. . . . .	59
6.5	The couplings of Eq. (6.3) vs. $\Delta m$ , for two values of $\tan\beta$ . Some points are obtained with fixed $ \mu  = 300$ GeV and varying $M_2$ , others are obtained with fixed $M_2 = 200$ GeV and varying $ \mu $ . In all cases $\phi_\mu = \pi/2$ . . . . .	59
6.6	Box-only contribution (dashed lines) vs. full one-loop result (full lines) in the heavy sfermions limit for $\tan\beta = 2$ and 10. . . . .	60
6.7	Selectron exchange box diagram. . . . .	61
6.8	The contribution of the selectron exchange box diagram to the observable (2.17) (here denoted as $A_{\text{CP}}$ ). The selectron mass is 403 GeV. . . . .	61
A.1	Tree level sneutrino exchange. . . . .	69
A.2	Tree level photon exchange. . . . .	70
C.1	Example of diagram with “clashed” fermion arrows. The outside arrows show the chosen direction of fermion flow. . . . .	79

# Notation

Throughout the thesis, ‘natural’ units are chosen, which means that the speed of light,  $c$ , and  $\hbar$  are taken to be unity.

Vectors in three-dimensional Euclidian space are indicated by boldface letters.

Indices from the middle of the Greek alphabet ( $\mu, \nu, \dots$ ) usually run over the space-time labels 0, 1, 2, 3 (Lorentz indices). It is assumed that raising and lowering of Lorentz indices is achieved by convolution with the conventional diagonal metric tensor  $g_{\mu\nu}$  ( $g_{00} = 1$ ,  $g_{11} = g_{22} = g_{33} = -1$ ). Summation over repeated indices is implied, unless otherwise indicated.

$\varepsilon_{\mu\nu\rho\sigma}$  denotes completely anti-symmetric rank 4 tensor ( $\varepsilon^{0123} = -\varepsilon_{0123} = 1$ ).

Unless otherwise indicated, the Dirac matrices  $\gamma^\mu$ ,  $\mu = 0, 1, 2, 3$ , are defined such that  $[\gamma^\mu, \gamma^\nu]_+ = 2g^{\mu\nu}$  and  $\gamma_5 = i\gamma^0\gamma^1\gamma^2\gamma^3$ .

We use the ‘Feynman slash-notations’:  $\not{p} = p_\mu\gamma^\mu$ .

For simplicity the chargino particle  $\tilde{\chi}_i$  is often (in particular, in the diagrams) denoted as simple  $\chi_i$  omitting ‘ $\sim$ ’.

The sparticles are indicated by double lines in the diagrams. To distinguish the spin we use dashed double lines for sfermions:  $\text{---} \text{---}$ , and solid double lines for chargino and neutralino:  $\text{=====}$ .

Other notations are defined in the text where appropriate.





# Chapter 1

## Introduction

Although it is more than 40 years old<sup>1</sup>, Supersymmetry (SUSY) is still a purely theoretical construct with, although intrinsically beautiful, complicated mathematical technique involved. The regular search for supersymmetric particles was largely inspired by the introduction of the SUSY extension of the Standard Model in the beginning of 1980th (see, e.g., [2, 3, 4]). However, no direct evidence was found since then and a certain part of the scientific community started to become pessimistic about SUSY realization in Nature<sup>2</sup>. Yet, the SUSY studies contribute a big part of particle physics activities in the world, both theoretical and experimental<sup>3</sup>. One can ask: why a concept that was not supported by experiment for more than 40 years is still of major interest for many physicists? Why supersymmetric extension of the Standard Model (MSSM and beyond) is intensively studied? There are, of course, decent reasons for such an attention.

Historically, one of the main attractions of supersymmetry-driven extensions of the Standard Model was the way how supersymmetry eliminates the *hierarchy problem*<sup>4</sup>. The quadratic divergencies normally present in the theory got canceled by loops with super-particles, and the Higgs mass is then controlled by the SUSY breaking scale. As Steven Weinberg writes in his book [4]: “The hope of a solution of the hierarchy problem along these lines has been the single strongest motivation for trying to incorporate supersymmetry in a realistic theory”.

Nevertheless, supersymmetry is much more than a “trick to solve a technical problem”. There are other (big and small) benefits SUSY promises. The first and main one: generally good ultraviolet convergence and *nonrenormalization* of some of the coupling constants [10], which ensures that certain relations between tree level couplings are still valid for “true” — renormalized — theory. This has very far-reaching consequences. For example, the gauge coupling unification is much more precise in supersymmetric theories. The string theories incorporating gravity behave much better when SUSY is incorporated. There are many other

---

<sup>1</sup>The first publications by Golfand and Likhthman appeared in 1971; in 1974 Wess and Zumino independently proposed similar algebra [1].

<sup>2</sup>The new wave of skepticism towards supersymmetric theories arose recently when preliminary experimental results from CERN were reported and apparently ruled out one of the simplest classes of SUSY theories (cMSSM; see, e.g., [5]; for a review of recent experimental results see, e.g., [6]). These results however cannot invalidate the SUSY concept itself, neither can they rule out other (perhaps more complicated) possible SUSY model modifications. We shall also mention here that the models considered in this Thesis do not belong to the cMSSM (also known as MSUGRA) type and thus not questioned by the just mentioned experimental results.

<sup>3</sup>Recently announced Higgs boson detection at CERN [7] puts the Higgs mass (around 125 GeV) in the range acceptable for SUSY extensions of the Standard Model (see, e.g., [8]).

<sup>4</sup>Interconnected to the so-called *naturalness problem* [9]

benefits as well. And on top of all of them, there is a theoretical result, which shows, that SUSY (or perhaps, something even more sophisticated mathematically) is, in some sense, unavoidable. It is the celebrated Coleman-Mandula theorem [11] and its constructive extension by Haag, Lopuszanski, and Sohnius [12].

The Coleman-Mandula theorem was proven under quite general assumptions<sup>5</sup> about the finiteness of the number of particle types below any given mass, the existence of scattering at almost all energies, and the analyticity of the S-matrix. The theorem states that the most general *Lie algebra* of symmetry operators that commute with the S-matrix, that take single-particle states into single-particle states consists of the generators  $P_\mu$  and  $J_{\mu\nu}$  of the Poincaré group, plus ordinary internal symmetry generators that act on one-particle states with matrices that are diagonal in and independent of both momentum and spin. For those trying to build a theory, this, in fact, leaves very little freedom: the internal symmetries will (by Noether's theorem) enforce conserved charges, and the latter have to be confirmed by experiment. The Haag, Lopuszanski, and Sohnius theorem is a way out: relaxing the requirement of a Lie algebra, and allowing instead for larger class of *Graded Lie algebras* (which can transform fermions to bosons and vice versa), one is allowed to include a much richer class of symmetries: namely, supersymmetry. The history of physics repeatedly demonstrates that Nature seems to respect a general principle: “whatever is not explicitly forbidden, is implemented”<sup>6</sup>. That is why even after so many years without experimental justification SUSY is expected to be a part of physical reality.

Apart from attractive features of SUSY for the field theory models, it may also offer explanations for observed phenomena outside the frames of particle physics. In particular, the solution of the so-called “cold dark matter problem” in cosmology may be provided by supersymmetry: in many SUSY breaking scenarios the lightest supersymmetric particles can serve as candidates for the cold dark matter constituent (a status of Dark Matter searches was recently summarized in [13]). These considerations, however, fall outside the scope of this Thesis.

As long as it applies to quantum field theory, so far there was not proposed any way of incorporating SUSY without introducing new particles (“superparticles”). It is not yet clear how one can confirm supersymmetry without detection of a supersymmetric particle, which the rich SUSY phenomenology predicts. Hence, all SUSY advantages cannot eliminate the need of SUSY particle detection. Supersymmetry is one of the primary targets of high energy experiments currently conducted and planned. After a long history of unsuccessful experimental attempts (which effectively reduced the amount of parameter space that Supersymmetry parameters are still allowed to occupy), the launched Large Hadron Collider at CERN and the widely appreciated  $e^+e^-$  linear collider proposal give further hopes for detection of SUSY particles.

As mentioned above, a hope to solve the hierarchy problem in the Standard Model of Electroweak Interactions was one of the main drivers to incorporate SUSY in this model. Starting from the so-called MSSM (Minimal Supersymmetric Standard Model, see, e.g., [2, 14]), there were proposed many modifications of SUSY models, differing by gauge group content and, therefore, by particle spectrum. Only experiment can decide whether any of those models is actually realized in nature. Once a “new physics” event that can be potentially

---

<sup>5</sup>We follow the treatment given in [4], where the (somewhat simplified) proof of Coleman-Mandula theorem is provided.

<sup>6</sup>This wording is usually attributed to S. L. Glashow.

explained by SUSY will be observed, the first problem which will arise is to distinguish the SUSY scenarios that the detected event supports. CP-violation phenomena are considered as one of such “filters”.

The CP-transformation is a product of two discrete transformations of quantum states: the C conjugation, which transforms particles to anti-particles, and P (parity) conjugation, which mirrors particle 3-momenta in momentum space. If the theory (i.e., the S-matrix) is invariant under CP-transformation (CP-symmetric), then the matter and anti-matter have the same properties and thus have to be produced at the same rate. As argued by A. Sakharov [15], the CP-symmetry violation is necessary to produce baryons (“matter”) at the rates exceeding the production of anti-baryons and thus to explain the apparent matter-domination in the observed universe.

In contrast to supersymmetry, the existence of CP-violation phenomena for Weak interactions was confirmed long ago [16] and was studied well both theoretically and experimentally. The classical example is again provided by the Standard Model, where the CP-asymmetry is introduced by including a complex phase in the CKM matrix describing quark mixing of the three generations of quarks [17].

The detection of CP-violation phenomena usually requires quite advanced experimental setup and the effects one needs to measure are typically small (on the order of a percent). One may wonder why we study such small effects in a class of models, which is not even confirmed to have relation to nature. One of the answers is given by the fact that we lack a fundamental understanding of the origin of CP-violation in the universe and cannot yet explain the apparent dominance of matter over anti-matter. In particular, it is currently believed that the known sources of CP-violation inside the Standard Model are not sufficient to explain the observed baryon asymmetry [17]. SUSY extensions of the Standard Model are known to provide additional sources of CP-violation and this is another reason for Supersymmetry to attract attention: any CP-violating reaction not predicted by the Standard Model, if observed, would give a “new life” to SUSY models.

It is known that the complex phases of the higgsino and gaugino mass parameters in the Minimal Supersymmetric Standard Model (MSSM [18, 3]) allow for CP violation at low orders of perturbation theory, without invoking the Cabibbo–Kobayashi–Maskawa matrix or the Higgs sector. If the phases are significant, one may expect experimental evidence of CP violation that does not fit the explanation within the (non-supersymmetric) Standard Model, leave alone the consequences for CP-conserving processes. It has long been known that these phases, if  $\mathcal{O}(1)$ , could lead to values for the electron and neutron electric dipole moments that would violate the experimental bounds unless the superparticles had masses of  $\mathcal{O}(\text{TeV})$  or higher [19]. However, it has recently been realized that there could well be cancellations among various contributions to such CP-violating effects [20, 21], such that the experimental constraints are respected, even with some phases of  $\mathcal{O}(1)$  and some superparticles light.

The couplings with potentially CP-violating phases affect many cross sections and rates. However, the most informative way to study such couplings would be in some CP-odd observable that would be accessible in future experiments. In the light of the International Linear Collider project [22], it is natural to consider the products of  $e^+e^-$  annihilation. The chargino pair creation

$$e^+ + e^- \rightarrow \tilde{\chi}_i^+ + \tilde{\chi}_j^- \quad (1.1)$$

then immediately comes to mind. At tree level the neutralino couplings do not enter in the amplitude and the only CP-violating phase that enters is  $\phi_\mu$  due to the higgsino mass

parameter

$$\mu \equiv |\mu| e^{i\phi_\mu} . \quad (1.2)$$

This phase is indeed accessible at tree level if one in mixed events ( $i \neq j$ ) measures the transverse polarization of one of the charginos [23, 24, 25]. There is also an additional CP violating effect in chargino decays, at the one-loop level [26].

It, however, turns out that if one does not consider the decay of a final-state chargino, the tree-level cross section of the above process conserves CP (in the  $m_e = 0$  limit) [23], even if one considers polarized electron-positron beams [27]. At the same time, there is no physical *symmetry* which would prohibit the cross section from acquiring a CP-odd part: the result of [27] is mainly dictated by the V-A structure of the tree-level couplings (see the general discussion of the effective form factors given in [28, 29]). Hence, the CP-violation may manifest itself starting from one loop, or at higher loop orders. Since by the very construction MSSM is renormalizable and the tree-level cross section is CP-even, any non-vanishing CP-odd contribution should be *finite* at one (and higher) loop orders — that is the logic of renormalization and that is why many regularization problems [30] should drop out for this effect; of course, as long as it is present at higher loop orders.

Typically, to build a (scalar) CP-odd observable in a  $2 \rightarrow 2$  process one has to employ spin (polarization) of one of the particles in addition to the particle momenta, since any scalar product of momenta is even under C and P [31, 17]. However, the careful analysis in Section 2 shows, that when the mass indices of the two final charginos of the process (1.1) are different<sup>7</sup>, then the mass index interchange should also be accounted for in CP-transformation. In such case it turns out that a CP-odd observable is easily constructed out of unpolarized cross-sections. So, the CP-violation may in principle be observed in the reaction (1.1) without any spin detection and with unspecified polarization for the initial beams. Below we will show that such spin-independent observables do exist and they do not vanish at one-loop order. This is one of the main results of this Thesis.

While the identified effect is induced by loop corrections, and thus of  $\mathcal{O}(\alpha)$ , there could be enhancements due to factors  $\tan\beta$  or  $\cot\beta$ . In any case, we think an independent CP-violating effect is worth attention, if some kind of supersymmetry should be realized in nature. In particular, it may provide information on whether the chargino sector contains more than two mass states, and information on the neutralino sector, including the phase of the U(1) gaugino mass parameter,  $M_1$ , via the  $W^\pm \tilde{\chi}_i^\mp \tilde{\chi}_k^0$  couplings.

Following many authors we work within the simplest version of unconstrained MSSM making no assumptions about the symmetry breaking mechanisms [32], neither do we impose any constraints on the CP-violating phases. The R-parity and the lepton flavor violation is not permitted, though, as noted in [27], the modification for less constrained models can be done. Besides, just to simplify sample calculations we assume that all slepton masses are large,<sup>8</sup> and, of course, neglect everything proportional to the electron mass. We do not calculate the one-loop cross section here, neither do we give a systemized review of the magnitude of the CP-odd observables in various parameter points. Instead, we pick a specific parameter set that allows us to neglect certain diagrams and show that the effect is indeed non-zero at the one-loop order.

<sup>7</sup>We use a “mass index”, taking values 1 and 2, to distinguish the two chargino mass states.

<sup>8</sup>One could refer to the parameter space area around the so-called SPS 2 benchmark point [33], but remember that the latter classification assumes an mSUGRA breaking mechanism (which seem not to be favored by recent CERN results [6]) with no CP-violating phases.

As mentioned above, there are other possible CP-violating contributions like chargino decay that may interfere with the effect we discuss in this Thesis. While this interference potentially increases or reduces the observed effect, it will become clear from the structure of one-loop diagrams considered below that the effect can never be totally (analytically) canceled.

The Thesis is organized as follows:

- In Chapter 2 we apply CP-transformation to the in- and out- states of the reaction (1.1), which gives us certain transformation rules for kinematical variables and the particle masses. These transformations shall be applied to the cross-section to get its CP-conjugated version. This approach identifies a candidate for the (polarization-independent!) CP-odd observable to be explored in the following chapters. We also briefly discuss possible kinematical structures that can contribute to polarization-dependent CP-violation observables.
- In Chapter 3 we calculate the tree-level approximation to the amplitude of the process (2.1) assuming *polarized*  $e^+e^-$  beams. We demonstrate that: a) the observable we identified is zero at tree-level, and b) the amplitude of the reaction (1.1) is CP-even even if the initial electron and positron beams are polarized<sup>9</sup>. We argue that as long as there is no physical symmetry that prohibits the amplitude of the reaction to acquire a CP-odd part, we have to look at higher loop orders to see whether the CP-violating parts indeed cancel.
- In order to compute the 1-loop corrections, in Chapter 4 we assemble and classify all one-loop diagrams contributing to the amplitude of our process and in Chapter 5 we describe the technique which was used for automatic analytic calculations of our observable at the one-loop level.
- In Chapter 6 we discuss the obtained results. We show that to prove the existence of a CP-violation effect at one-loop level it is sufficient to compute the so-called box diagrams. This computation (under the assumption of heavy sleptons) is done as a part of this Thesis. Since the obtained analytical formulae for the box diagram contribution of the CP-violating observable are still too lengthy to reduce them to compact form, we instead provide the analytical expression for the part that involves the  $Z$ -boson exchange box diagrams and discuss its structure (which is representative for the entire box diagram contribution). Further, fixing some of the masses we study the entire box contribution to the observable as function of the higgsino complex phase  $\phi_\mu$  and  $\tan\beta$ . Finally, we compare the obtained box contribution to the complete one-loop result for the observable; the latter was obtained with help of the numerical code by K. Rolbiecki and J. Kalinowski (see, e.g., [34] and references therein). As was predicted, the boxes turn out to provide the major contribution: we briefly discuss the reasons why it happens. The main results quoted in this chapter were published in [35, 36].
- Conclusions are given Chapter 7.
- In Appendix A we demonstrate how a Fiertz transformation can simplify the  $t$ -channel sneutrino exchange amplitude at the tree level, effectively getting rid of the C-conjugation matrices in the vertices. In Appendix B we employ relevant Ward-Takahashi

---

<sup>9</sup>This (tree-level) result was first obtained in [27] using different analytical methods.

identities to illustrate a known fact (see, e.g., [37]) that the photon cannot couple to two fermions of different masses: we use this fact when accounting for various loop diagrams. Since Fierz transformation turned out to be not efficient for 1-loop calculations, in Appendix C we provide a modification to conventional Feynman rules that allow simple automatic handling of the vertices with C-matrices (here we follow the approach from [38]). For the sake of completeness in this Appendix we also list Lagrangian vertices needed to obtain the analytical results quoted in Chapter 3 and Chapter 6 (the complete collection can be found in, e.g., [39]).

## Chapter 2

# CP-odd observables

We shall consider chargino production in electron-positron annihilation with transversely polarized beams:

$$e^+(p_1, P_+) + e^-(p_2, P_-) \rightarrow \tilde{\chi}_i^+(k_1) + \tilde{\chi}_j^-(k_2), \quad (2.1)$$

where  $\tilde{\chi}_i^+$  and  $\tilde{\chi}_j^-$  denote charginos, and  $P_\pm^\mu$  are the positron and electron polarization vectors; the latter are convenient to define as four-vectors, which in the center-of-mass system look like [40]:

$$\begin{aligned} P_+ &\stackrel{c.m.}{=} (0, \mathbf{P}_+^\perp), & \mathbf{P}_+^\perp \cdot \mathbf{p}_1 &\stackrel{c.m.}{=} -\mathbf{P}_+^\perp \cdot \mathbf{p}_2 \stackrel{c.m.}{=} 0, \\ P_- &\stackrel{c.m.}{=} (0, \mathbf{P}_-^\perp), & \mathbf{P}_-^\perp \cdot \mathbf{p}_2 &\stackrel{c.m.}{=} -\mathbf{P}_-^\perp \cdot \mathbf{p}_1 \stackrel{c.m.}{=} 0, \end{aligned} \quad (2.2)$$

and, therefore, in any system of frame  $p_{1,2}^\mu P_{\pm\mu} = 0$ .

The crucial point here is that for  $i \neq j$ , the charginos do not form a particle-antiparticle pair. Hence, while the initial state (for suitably chosen polarizations,  $P_+ \leftrightarrow P_-$ ) is in the c.m. frame odd under charge conjugation, the final state has no such symmetry.

Let us take a closer look at this. The chargino mass matrix  $M_\chi$  is diagonalized by matrices  $X$  and  $Y$  producing two chargino (fermion) mass states in the MSSM Lagrangian (see also Appendix C):

$$M_\chi = \begin{pmatrix} M_2 & \sqrt{2}m_W \sin \beta \\ \sqrt{2}m_W \cos \beta & \mu \end{pmatrix}, \quad Y^* M_\chi X^\dagger = \begin{pmatrix} m_{\chi_1} & 0 \\ 0 & m_{\chi_2} \end{pmatrix}, \quad 0 < m_{\chi_1} < m_{\chi_2}.$$

For a given mass (mass index)  $i$ , the chargino field operator  $\tilde{\chi}_i(x)$  permits conventional plane wave expansion:

$$\begin{aligned} \tilde{\chi}_i(x) &= \int \frac{d^3\mathbf{p}}{(2\pi)^3 2p_0} \sum_{\sigma=\pm\frac{1}{2}} \{ e^{-ipx} c(\mathbf{p}, \sigma, i) u(p, \sigma) + e^{ipx} d^\dagger(\mathbf{p}, \sigma, i) v(p, \sigma) \} \\ \overline{\tilde{\chi}_i}(x) &= \int \frac{d^3\mathbf{p}}{(2\pi)^3 2p_0} \sum_{\sigma=\pm\frac{1}{2}} \{ e^{-ipx} d(\mathbf{p}, \sigma, i) \bar{v}(p, \sigma) + e^{ipx} c^\dagger(\mathbf{p}, \sigma, i) \bar{u}(p, \sigma) \} \end{aligned}$$

where  $c^\dagger(\mathbf{p}, \sigma, i)$  creates the *particle* which is (conventionally) a *positive* chargino (with the spin projection  $\sigma$  and the mass  $m_{\chi_i}$ ), while  $d^\dagger(\mathbf{p}, \sigma, i)$  creates the *antiparticle* — the *negative* chargino with the same mass. Their conjugates  $c(\mathbf{p}, \sigma, i)$  and  $d(\mathbf{p}, \sigma, i)$ , of course, annihilate particle and antiparticle, respectively.

The P conjugation acts on the creation operator of any particle with momentum  $\mathbf{p}$ , spin projection  $\sigma$  and other quantum numbers abbreviated as  $n$  in the following way:

$$\mathcal{P}a^\dagger(\mathbf{p}, \sigma, n)\mathcal{P}^{-1} = \eta_n a^\dagger(-\mathbf{p}, \sigma, n),$$

thus resulting only in a reversal of 3-momenta and a multiplicative factor  $\eta_n$ , usually called intrinsic P-parity (see, e.g. [41], however the intrinsic P- and C- parities are not essential for the current discussion). The C conjugation acts on the creation operator of the positive chargino with mass  $m_i$  as

$$\mathcal{C}c^\dagger(\mathbf{p}, \sigma, i)\mathcal{C}^{-1} = \xi_i d^\dagger(\mathbf{p}, \sigma, i),$$

where  $d^\dagger(\mathbf{p}, \sigma, i)$  is the creation operator for a negative chargino with otherwise the same quantum numbers (3-momentum, polarization, mass), and  $\xi_i$  is the corresponding intrinsic C-parity. Hence, under P and C, and CP conjugation the  $S$ -matrix element

$$\langle \tilde{\chi}_i^+(\mathbf{k}_1), \tilde{\chi}_j^-(\mathbf{k}_2) | S | e^+(\mathbf{p}_1, P_+), e^-(\mathbf{p}_2, P_-) \rangle \quad (2.3)$$

of the process (2.1) gets transformed into:

$$\text{P : } \eta_j^* \eta_i \eta_e \eta_e^* \langle \tilde{\chi}_i^+(-\mathbf{k}_1), \tilde{\chi}_j^-(\mathbf{k}_2) | S | e^+(-\mathbf{p}_1, P_+), e^-(-\mathbf{p}_2, P_-) \rangle, \quad (2.4)$$

$$\begin{aligned} \text{C : } & \xi_j^* \xi_i \xi_e \xi_e^* \langle \tilde{\chi}_i^-(\mathbf{k}_1), \tilde{\chi}_j^+(\mathbf{k}_2) | S | e^-(\mathbf{p}_1, P_+), e^+(\mathbf{p}_2, P_-) \rangle \\ & \equiv (\text{phase}) \times \langle \tilde{\chi}_j^+(\mathbf{k}_2), \tilde{\chi}_i^-(\mathbf{k}_1) | S | e^+(\mathbf{p}_2, P_-), e^-(\mathbf{p}_1, P_+) \rangle, \end{aligned} \quad (2.5)$$

and

$$\begin{aligned} \text{CP : } & \eta_j^* \eta_i \eta_e \eta_e^* \xi_j^* \xi_i \xi_e \xi_e^* \langle \tilde{\chi}_i^-(\mathbf{k}_1), \tilde{\chi}_j^+(\mathbf{k}_2) | S | e^-(\mathbf{p}_1, P_+), e^+(\mathbf{p}_2, P_-) \rangle \\ & \equiv (\text{phase}) \times \langle \tilde{\chi}_j^+(\mathbf{k}_2), \tilde{\chi}_i^-(\mathbf{k}_1) | S | e^+(\mathbf{p}_2, P_-), e^-(\mathbf{p}_1, P_+) \rangle, \end{aligned} \quad (2.6)$$

where the phase factors involving intrinsic parities  $\eta$  and  $\xi$  will not be discussed since they do not affect the rates.

From Eqs. (2.4)–(2.6) one sees, that the P-conjugation just results in the change of sign of the particle three-momenta, which can be written as

$$\mathbf{p}_{1,2} \leftrightarrow -\mathbf{p}_{1,2}, \quad \mathbf{k}_{1,2} \leftrightarrow -\mathbf{k}_{1,2}; \quad (2.7)$$

the C-conjugation amounts to the following substitution in the cross section:

$$\mathbf{p}_1 \leftrightarrow \mathbf{p}_2, \quad \mathbf{k}_1 \leftrightarrow \mathbf{k}_2, \quad m_i \leftrightarrow m_j, \quad P_+ \leftrightarrow P_-; \quad (2.8)$$

and, finally, the CP-transformation is equivalent to the change

$$\mathbf{p}_1 \leftrightarrow -\mathbf{p}_2, \quad \mathbf{k}_1 \leftrightarrow -\mathbf{k}_2, \quad m_i \leftrightarrow m_j, \quad P_+ \leftrightarrow P_- . \quad (2.9)$$

Alternatively, the transformations (2.7) – (2.9) can be written in 4-vector notations where, as usual, it is assumed that raising and lowering of indices is achieved by the conventional metrics  $g_{\mu\nu} = \text{diag}(1, -1, -1, -1)$ :

$$\text{P : } p_a^\mu \leftrightarrow p_{a\mu}, \quad k_a^\mu \leftrightarrow k_{a\mu}, \quad a = 1, 2; \quad (2.10)$$

$$\text{C : } p_1^\mu \leftrightarrow p_2^\mu, \quad k_1^\mu \leftrightarrow k_2^\mu, \quad m_i \leftrightarrow m_j, \quad P_+^\mu \leftrightarrow P_-^\mu; \quad (2.11)$$

$$\text{CP : } p_1^\mu \leftrightarrow p_{2\mu}, \quad k_1^\mu \leftrightarrow k_{2\mu}, \quad m_i \leftrightarrow m_j, \quad P_+^\mu \leftrightarrow P_-^\mu; \quad (2.12)$$



(one can check that the Lorentz-invariance is maintained automatically).

Our goal is to find CP-sensitive observables. Let us write the cross section as

$$d\sigma = d\sigma_0 + (\text{terms linear in } |\mathbf{P}_-| \text{ or } |\mathbf{P}_+|) + (\dots)|\mathbf{P}_-||\mathbf{P}_+|, \quad (2.13)$$

where  $d\sigma_0$  does not depend on polarization vectors and will be referred to as the *unpolarized* part. The second and higher power of  $|P_-|$  or  $|P_+|$  cannot arise, to see this we just note that the only way a polarization vector can enter the cross section is due to the “spin sums” (helicity projection operators) for the Dirac spinors:

$$u(p)\bar{u}(p) = \frac{1}{2}(1 + \gamma_5 \mathcal{P})(\not{p} + m), \quad v(p)\bar{v}(p) = \frac{1}{2}(1 + \gamma_5 \mathcal{P})(\not{p} - m); \quad (2.14)$$

these terms appear in the cross section as a result of squaring the amplitude, and the latter contain only one Dirac spinor for each external particle.

Consider first the unpolarized part. Poincaré invariance forces it to depend only on masses  $m_i, m_j$  and on two independent scalar variables, say, on Mandelstam’s  $s \equiv (p_1 + p_2)^2$  and  $t \equiv (p_1 - k_1)^2$ . The latter do not change under the transformations (2.7)–(2.9), so the CP-transformation for the unpolarized cross-section is reduced to the interchange of the chargino masses in the resulting formula<sup>1</sup>. Hence, for the equal mass fermions in the final state ( $m_i = m_j$ ) the unpolarized cross section is always P-, C- and CP-even<sup>2</sup>. *In contrast, if the chargino masses are different, CP-violating terms can arise even in the unpolarized cross-section.* That is the effect we will consider in this Thesis, so unless otherwise stated the final chargino masses are taken non-equal.

As shown later in this Thesis, the tree-level cross section (polarized and unpolarized) of our process is CP even (this was also confirmed by results of [27]), but CP-odd terms do arise in the one loop contributions. Therefore, the natural building block for experimental observable is the ratio

$$\frac{d\sigma_0^{\text{odd}}}{d\sigma_0}, \quad (2.15)$$

where  $d\sigma^{\text{odd}}$  is the CP-odd part of corresponding cross-section:

$$d\sigma_0^{\text{odd}} = \frac{1}{2} [d\sigma_0 - d\sigma_0^{\text{CP}}], \quad d\sigma_0^{\text{CP}} \equiv d\sigma_0(m_j \leftrightarrow m_i). \quad (2.16)$$

Since the CP-violation first enters at one loop, one should calculate  $d\sigma_0^{\text{odd}}$  at the one-loop level to estimate the effect. In contrast, at least in the kinematical regions far from the resonance area, one can expect (see, e.g. [42]) that the tree level gives a reasonable approximation to  $d\sigma_0$  in the denominator of Eq. (2.15). Since the one loop order of the cross section itself requires much more involved calculations than one loop  $d\sigma_0^{\text{odd}}$  alone, we will deal only with the ratio

$$\frac{d\sigma_0^{\text{odd}}|_{1 \text{ loop}}}{d\sigma_0|_{\text{tree}}}. \quad (2.17)$$

---

<sup>1</sup>Of course, the coupling constants at vertices with charginos should be considered as functions of the chargino masses.

<sup>2</sup>The famous forward-backward asymmetry term in the *unpolarized* cross-section of, say,  $e^+e^- \rightarrow \mu^+\mu^-$  scattering, which is often referred to as parity violating, in fact only indicates the presence of parity violating term in the interaction, the unpolarized cross-section itself being, of course, P-even.

In this research we are not going to focus on the polarization-dependent part of the cross-section (2.13). Let us, however, look which Lorentz structures may contribute to the latter part. Considering all possible ways to construct the Lorentz-scalar out of kinematical parameters, one may easily see that in addition to the masses and Mandelstam variables the cross-section can also depend on invariants linear and bilinear in the polarization four-vectors:

$$P_{+\mu}P_-^\mu, \quad \varepsilon_{\mu\nu\rho\sigma}a^\mu b^\nu P_+^\rho P_-^\sigma, \quad \text{and} \quad k_{1\mu}P_\pm^\mu = -k_{2\mu}P_\pm^\mu, \quad \varepsilon_{\mu\nu\rho\sigma}a^\mu b^\nu c^\rho P_\pm^\sigma, \quad (2.18)$$

where  $a, b, c = p_1, p_2, k_1, k_2$ . According to Eq. (2.9), the first of the above terms is clearly CP-even. The others can lead to CP-violation.

To track the CP-behavior of the above invariants it is convenient to switch to the c.m. frame, where the polarization vectors satisfy the conditions (2.2). In this frame the initial and final-state momenta become, respectively,  $\mathbf{p}_1 = \mathbf{p}$ ,  $\mathbf{p}_2 = -\mathbf{p}$  and  $\mathbf{k}_1 = \mathbf{k}$ ,  $\mathbf{k}_2 = -\mathbf{k}$ , while the CP-transformation (2.9) amounts to the interchange

$$\mathbf{p} \leftrightarrow \mathbf{p}, \quad \mathbf{k} \leftrightarrow \mathbf{k}, \quad m_i \leftrightarrow m_j, \quad \mathbf{P}_+^\perp \leftrightarrow \mathbf{P}_-^\perp.$$

In that specific case when the final-state chargino masses are equal ( $i = j$ ), this is equivalent (c.m. frame only!) to  $P_+^\mu \leftrightarrow P_-^\mu$ , so, for any momenta  $a$  and  $b$ , the second term listed in Eq. (2.18) is CP-odd. The latter, of course, then holds in any frame, because the considered term is a Lorentz scalar. Therefore there is a possibility to have CP-violation even for the reaction producing two charginos with same mass index. Indeed, as an example one can take  $\varepsilon_{\mu\nu\rho\sigma}p_1^\mu p_2^\nu P_+^\rho P_-^\sigma$  term, which is P- and CP-odd in both  $i = j$  and  $i \neq j$  cases. In terms of three-vectors, the CP-odd behavior of the latter term is of course due to the vector product  $\mathbf{P}_+^\perp \times \mathbf{P}_-^\perp$ . Besides, CP-odd quantities can be formed out of the last two terms in (2.18).

One can, therefore, conclude that the reaction (2.1) in principle permits CP-violating observables both linear and bilinear in polarization vectors. In the following Chapter we show that at the tree level the terms linear in polarization vanish in the limit  $m_e = 0$  (one can attribute this fact to specific properties of V and A couplings: see [43], [27]), and, due to the structure of the model there is no CP violation in bilinear term. However, the loop contribution may in principle bring CP-violating terms both linear and bilinear in polarization vectors. We do not consider such observables, focusing instead on CP-violation in unpolarized cross-section.

## Chapter 3

# Polarized tree-level cross section

In this chapter we calculate the tree-level approximation to the process (2.1) assuming polarized  $e^+e^-$  beams. It is only this chapter that deals with beam polarization. For the sake of simplicity and to match with results by other authors, the notations in this chapter differ slightly from those used in the rest of the Thesis. Those additional notations are introduced in the text below. The un-polarized part of the tree-level cross section is also used later to normalize physical observables at 1-loop level.

The graphs contributing to the tree amplitude  $\mathcal{M}_{\text{tree}}$  are pictured<sup>1</sup> in Fig. 3.1. They are:  $s$ -channel Higgs (and the unphysical Goldstone), photon and  $Z$  exchanges, and  $t$ -channel sneutrino exchange.

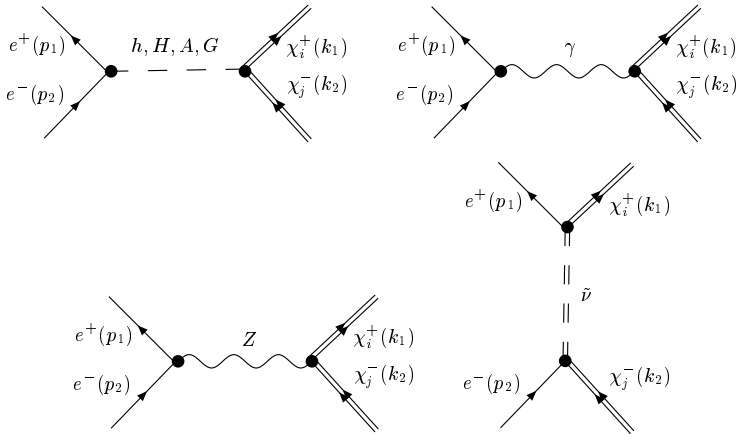


Figure 3.1: Tree level diagrams for  $e^+ + e^- \rightarrow \tilde{\chi}_i^+ + \tilde{\chi}_j^-$  process: superpartners of ordinary particles pictured by double lines for later convenience. Throughout the Thesis we drop “tilde” (“ $\sim$ ”) sign from the chargino symbols  $\tilde{\chi}_i$  when drawn in diagrams.

We neglect the scalar exchange diagrams, because all the Higgs/Goldstone–electron–electron (as well as the charged Higgs/Goldstone–neutrino–electron) Lagrangian couplings

<sup>1</sup>All pictures are drawn by the *JaxoDraw* tool [44].

are proportional to the electron mass, and the latter is small compared to the energies we are interested in: in the following we drop all the contributions proportional to  $m_e$ . In fact, this observation will allow us to exclude many diagrams at the one-loop level. Besides, the photon exchange contributes only if the final charginos have equal masses  $m_i = m_j$  and therefore, as discussed in Chapter 2, will not contribute to unpolarized CP-violating observable (2.15).

### 3.1 Tree level approximation: notations

There are many ways to fix the coordinates. For example, one can associate the axes with particle three-momenta and thus let them transform under P conjugation. In this case the components of all momenta are unchanged, but the polarization vectors change sign. However, to make the P and C non-invariant terms show up explicitly in the cross-section (and to be able to apply simple substitution rules (2.7)–(2.9)), we prefer to fix a rigid coordinate system (unaffected by P or C transformations) in the c.m. frame with  $\theta$  and  $\phi$  the polar and azimuthal angles.

Keeping in mind, that the two final-state charginos can have different masses,  $m_i$  and  $m_j$ , in the limit of zero electron mass, we parameterize the momenta in our process as

$$\begin{aligned} e^+ : \quad p_1 &= E(1, 0, 0, \boldsymbol{\omega}) , \\ e^- : \quad p_2 &= E(1, 0, 0, -\boldsymbol{\omega}) , \\ \tilde{\chi}_i^+ : \quad k_1 &= E_+(1, \boldsymbol{\omega}\beta_+ \sin\theta \cos\phi, \boldsymbol{\omega}\beta_+ \sin\theta \sin\phi, \boldsymbol{\omega}\beta_+ \cos\theta) , \\ \tilde{\chi}_j^- : \quad k_2 &= E_-(1, -\boldsymbol{\omega}\beta_- \sin\theta \cos\phi, -\boldsymbol{\omega}\beta_- \sin\theta \sin\phi, -\boldsymbol{\omega}\beta_- \cos\theta) , \end{aligned} \quad (3.1)$$

and it is implied that

$$E_+ + E_- = 2E, \quad E_+\beta_+ = E_-\beta_-, \quad E_{\pm}^2(1 - \beta_{\pm}^2) = m_{\pm}^2, \quad (3.2)$$

with  $m_+ \equiv m_i$  and  $m_- \equiv m_j$ . The factor  $\boldsymbol{\omega} = \pm 1$  in (3.1) is reserved for P and C transformation: it is equal to +1 as long as we work with the original process (2.1); to construct the cross section for the P-conjugated process one just has to take  $\boldsymbol{\omega} = -1$  (we shall discuss it below).

It is also convenient to introduce

$$\beta = \frac{E_+\beta_+ + E_-\beta_-}{2E} = \frac{E_{\pm}\beta_{\pm}}{E}; \quad (3.3)$$

this stresses that, in general, the final-state particles (charginos) will have different velocities, and that  $\beta$  is the “energy-weighted” velocity. As usual, the Mandelstam variables are denoted as  $s = (p_1 + p_2)^2 = 4E^2$ ,  $t = (p_1 - k_1)^2$ .

Furthermore,  $\phi_+$  and  $\phi_-$  denote the azimuthal orientations of the *transversely* polarized initial beams:

$$\begin{aligned} P_+ &= \left| \mathbf{P}_+^{\perp} \right| (0, \cos\phi_+, \sin\phi_+, 0), \\ P_- &= - \left| \mathbf{P}_-^{\perp} \right| (0, \cos\phi_-, \sin\phi_-, 0). \end{aligned} \quad (3.4)$$

The over-all minus sign leads to conventional formulas. The polarization-dependent projection operators look as follows:

$$u(p)\bar{u}(p) = \frac{1}{2}(1 + \gamma_5 \boldsymbol{P})(\not{p} + m), \quad v(p)\bar{v}(p) = \frac{1}{2}(1 + \gamma_5 \boldsymbol{P})(\not{p} - m). \quad (3.5)$$

As stated elsewhere, CP violation may enter in the two diagrams involving the  $Z$  and the sneutrino. The relevant Lagrangian terms are listed in Appendix C; here we prefer to extract additional factors from the couplings<sup>2</sup>. We rewrite the  $Z\tilde{\chi}_i^+\tilde{\chi}_j^-$  coupling (cf. (C.15)) as:

$$i\frac{g}{4\cos\theta_W}\gamma^\mu\left\{G_{Vij} + \gamma^5 G_{Aij}\right\} \equiv i\frac{e}{\sin 2\theta_W}\gamma^\mu\left\{G_{vij} - \gamma^5 G_{a ij}\right\}. \quad (3.6)$$

The  $e^\pm\tilde{\chi}_k^\mp\tilde{\nu}$  coupling (cf. (C.19), assuming  $m_e = 0$ ) for “electron in” is being rewritten as:

$$-i\frac{g}{2}X_{1k}^\dagger C(1 - \gamma^5) \equiv ieC_{\tilde{\nu},k}C(1 - \gamma^5), \quad (3.7)$$

and for “positron in”:

$$i\frac{g}{2}X_{k1}(1 + \gamma^5)C^{-1} \equiv ieC_{\tilde{\nu},k}^*(1 + \gamma^5)C^{-1}. \quad (3.8)$$

Here  $C$  is the appropriate charge conjugation matrix<sup>3</sup> and the subscripts  $i, j, k = 1, 2$  indicate the chargino types;  $X$  is the chargino mixing matrix (see Appendix C). Henceforth, whenever it cannot lead to confusion, we use  $G_v$  and  $G_a$  instead of  $G_{vij}$  and  $G_{a ij}$ , as well as  $C_i$  instead of  $C_{\tilde{\nu},i}$ .

Finally, we need the QED couplings for fermion – photon (cf. (C.8) and (C.14); we assume  $q_{in} = +1$  for electron and  $q_{out} = +1$  for positive chargino):

$$-ieq_{in}\gamma_\mu; \quad -ieq_{out}\gamma_\mu,$$

and the Standard Model coupling for electron –  $Z$ -boson (cf.<sup>4</sup> (C.9)):

$$-i\frac{g}{4\cos\theta_W}\gamma_\mu(-4\sin^2\theta_W + 1 - \gamma^5) \equiv -i\frac{e}{\sin 2\theta_W}\gamma_\mu(g_v - g_a\gamma^5). \quad (3.9)$$

Following the most common convention, we treat the *positive* chargino as a “particle” (together with the electron); its antiparticle is, of course, the negative chargino with the *same* mass (mass index). Hence, the equality  $q_{in}q_{out} = -1$  always holds, but we shall keep these coefficients in the formulas, in order to more easily keep track of the various contributions.

The Standard Model constants,  $g_v, g_a$  are real, while  $C_i, G_v, G_a$  are in general *complex* constants, which we parameterize further as:

$$\begin{aligned} C_i &= |C_i| \exp(i\phi_i), \\ G_v &= |G_v| \exp(i\psi_v), \\ G_a &= |G_a| \exp(i\psi_a). \end{aligned} \quad (3.10)$$

Their imaginary parts, proportional to  $\sin\phi_i, \sin\psi_v$  and  $\sin\psi_a$ , may induce CP violation. Besides, it is convenient to define

$$G_L \equiv \frac{1}{2}(G_a + G_v) \equiv |G_L| \exp(i\psi_L). \quad (3.11)$$

<sup>2</sup>It is mainly to automatize the symbolic and, later, numerical calculations, as well as to match the notations by other authors.

<sup>3</sup>We effectively remove it by Fiertz transformation (see Appendix A) at the tree level; at 1-loop level we use modified Feynman rules which do not include charge conjugation matrix in vertices (Appendix C.1).

<sup>4</sup>The  $g_V$  and  $g_A$  couplings used in [36] are related to  $g_v$  and  $g_a$  (used above) as follows:  $g_V = 2g_v = (1 - 4\sin^2\theta_W), g_A = -2g_a = -1$ .

### 3.2 The tree level cross section

The tree amplitude  $\mathcal{M}$  of the process (2.1) is made up from photon and  $Z$  exchanges in the  $s$ -channel, and sneutrino exchange in the  $t$ -channel. Thus, the cross section is proportional to

$$|\mathcal{M}_{\text{tree}}|^2 \equiv \sum_{\tilde{\chi} \text{ spins}} [\mathcal{M}^*(\gamma) + \mathcal{M}^*(Z) + \mathcal{M}^*(\tilde{\nu})][\mathcal{M}(\gamma) + \mathcal{M}(Z) + \mathcal{M}(\tilde{\nu})];$$

as long as the final charginos have different masses  $m_i \neq m_j$ , the photon exchange drops out. Note that we sum over the spins of resulting chargino, but do not average over the spins of incoming  $e^\pm$ , so the extra  $\frac{1}{4}$  factor does not arise. This is because the initial beams are polarized. To get un-polarized cross section one would need to sum over the incoming polarizations and add the factor  $\frac{1}{4}$ . One usually distinguishes between the squared graphs:

$$X(\ell\ell) \equiv \sum_{\tilde{\chi} \text{ spins}} \mathcal{M}^*(\ell)\mathcal{M}(\ell), \quad \ell = \gamma, Z, \tilde{\nu}, \quad (3.12)$$

and the remaining interference terms. The latter are in general complex, however the imaginary parts cancel when the relevant contributions are taken in pairs:

$$X(\ell\ell') \equiv \sum_{\tilde{\chi} \text{ spins}} [\mathcal{M}^*(\ell)\mathcal{M}(\ell') + \mathcal{M}(\ell)\mathcal{M}^*(\ell')], \quad \ell\ell' = \gamma Z, \gamma\tilde{\nu}, Z\tilde{\nu}. \quad (3.13)$$

With the common normalization conditions the differential cross section (in the c.m. system) is:

$$\frac{d\sigma}{d\Omega} = \frac{\beta}{64\pi^2 s} |\mathcal{M}|^2, \quad \beta \equiv \frac{|\mathbf{p}_{\text{out}}|}{|\mathbf{p}_{\text{in}}|}.$$

Taking the  $e^4 = (4\pi\alpha)^2$  factor out of  $|\mathcal{M}|^2$  and separating the polarization independent (“un-polarized”,  $X_0$ ) and polarization-dependent (“transverse”,  $X_t$ ) parts:

$$|\mathcal{M}|^2 = (4\pi\alpha)^2 [X_0(\ell\ell') + \left| \mathbf{P}_+^\perp \right| \left| \mathbf{P}_-^\perp \right| \beta^2 \sin^2 \theta X_t(\ell\ell')]$$

we re-write the cross section in the form:

$$\begin{aligned} \frac{d\sigma}{d\Omega} &= \frac{\alpha^2 \beta}{4s} \sum_{\substack{\ell\ell' = \gamma\gamma, ZZ, \tilde{\nu}\tilde{\nu} \\ \gamma Z, \gamma\tilde{\nu}, Z\tilde{\nu}}} [X_0(\ell\ell') + \left| \mathbf{P}_+^\perp \right| \left| \mathbf{P}_-^\perp \right| \beta^2 \sin^2 \theta X_t(\ell\ell')] \\ &\equiv \frac{\alpha^2 \beta}{4s} [X_0 + \left| \mathbf{P}_+^\perp \right| \left| \mathbf{P}_-^\perp \right| \beta^2 \sin^2 \theta X_t]. \end{aligned} \quad (3.14)$$

To make the resulting expressions more compact, we introduce the following dimensionless products of coupling constants and propagators:<sup>5</sup>

$$\begin{aligned} \chi &= \frac{1}{\sin^2(2\theta_W)} \frac{s}{s - M_Z^2}, \\ \chi_{\tilde{\nu}} &= \frac{1}{2} |C_i| |C_j| \frac{s}{(t - M_{\tilde{\nu}}^2)}. \end{aligned} \quad (3.15)$$

<sup>5</sup> $\chi$  factor used in [36], p. 3 is less than this one by factor of 4.

Besides, it is convenient to abbreviate the QED angular distribution:

$$\mathcal{A} = 2 - \beta^2 \sin^2 \theta \quad (3.16)$$

(in the relativistic limit  $\beta \rightarrow 1$ , consequently  $\mathcal{A} \rightarrow 1 + \cos^2 \theta$ ).

The calculation of the cross-section is quite cumbersome even at the tree level: one of the simplifying tricks, the Fiertz transformation, is demonstrated in Appendix A. Even with such simplifications, we had to use REDUCE [45] package to assemble the intermediate algebraic blocks, and the expressions were then simplified manually. The results are presented below.

The polarization-independent contributions are:

$$\begin{aligned} X_0(\gamma\gamma) &= \delta_{ij} q_{\text{in}}^2 q_{\text{out}}^2 \mathcal{A}, \\ X_0(\gamma Z) &= \delta_{ij} 2q_{\text{in}} q_{\text{out}} \chi (g_v G_v \mathcal{A} - 2g_a G_a \beta \cos \theta), \\ X_0(ZZ) &= \chi^2 \left( (g_v^2 + g_a^2) \{ |G_v|^2 [\mathcal{A} - 2(m_i - m_j)^2/s] + |G_a|^2 [\mathcal{A} - 2(m_i + m_j)^2/s] \} \right. \\ &\quad \left. - 4g_v g_a (G_v^* G_a + G_v G_a^*) \beta \cos \theta \right), \\ X_0(\gamma\tilde{\nu}) &= -\delta_{ij} 2q_{\text{in}} q_{\text{out}} \chi_{\tilde{\nu}} [\mathcal{A} - 2\beta \cos \theta], \\ X_0(Z\tilde{\nu}) &= -2\chi \chi_{\tilde{\nu}} (g_v + g_a) \text{Re} \{ \exp[i(\phi_i - \phi_j)] \\ &\quad \times [G_v (\mathcal{A} - 2\beta \cos \theta - 2(m_i - m_j)^2/s) \\ &\quad + G_a (\mathcal{A} - 2\beta \cos \theta - 2(m_i + m_j)^2/s)] \}, \\ X_0(\tilde{\nu}\tilde{\nu}) &= 4\chi_{\tilde{\nu}}^2 [\mathcal{A} - 2\beta \cos \theta - 2(m_i^2 + m_j^2)/s]. \end{aligned} \quad (3.17)$$

The polarization-*dependent* cross section is made up from:

$$\begin{aligned} X_t(\gamma\gamma) &= -\delta_{ij} q_{\text{in}}^2 q_{\text{out}}^2 \cos[2\phi - (\phi_+ + \phi_-)], \\ X_t(\gamma Z) &= -\delta_{ij} 2q_{\text{in}} q_{\text{out}} \chi |G_v| g_v \cos[2\phi - (\phi_+ + \phi_-)], \\ X_t(ZZ) &= -\chi^2 (g_v^2 - g_a^2) (|G_v|^2 + |G_a|^2) \cos[2\phi - (\phi_+ + \phi_-)], \\ X_t(\gamma\tilde{\nu}) &= \delta_{ij} 2q_{\text{in}} q_{\text{out}} \chi_{\tilde{\nu}} \cos[2\phi - (\phi_+ + \phi_-)], \\ X_t(Z\tilde{\nu}) &= 4\chi \chi_{\tilde{\nu}} (g_v - g_a) \{ |G_L| \cos[2\phi - (\phi_+ + \phi_-) + \omega(\psi_L + \phi_i - \phi_j)] \\ &\quad + \omega \sin(\phi_+ - \phi_-) (|G_v| \sin(\phi_i - \phi_j + \psi_v) + |G_a| \sin(\phi_i - \phi_j + \psi_a)) \}, \\ X_t(\tilde{\nu}\tilde{\nu}) &= 0. \end{aligned} \quad (3.18)$$

Note that for  $i = j$  the coupling constants  $G_v$  and  $G_a$  become real, and the angles  $\psi_v$  and  $\psi_a$  vanish. In the formulae above,  $\omega$  should be taken equal to +1 as long as the rate of the reaction (2.1) is computed. Terms odd in  $\omega$  violate parity (discussed below).

### 3.3 P, C, and CP transformations at tree-level

Let us first discuss parity transformation. As stated in Section 3.1, we prefer to fix the coordinate frame unaffected by the C and P transformations. Hence, from (3.1) and (2.7) it is easy to see that to construct the cross section for the P-conjugated process one just has to take  $\omega = -1$  in Eq. (3.18), keeping the spin four-vectors  $P_{\pm}$  unchanged. It should be stressed that although it is the electron, and not the positron, that after the P conjugation moves in the direction of the third axis, the angles  $\theta$  and  $\phi$  should not be altered in the formulae for the cross-section: all the changes are taken care of by  $\omega$  and no further modification is needed.

There is no  $\omega$  dependence in the un-polarized cross-section (3.17), so it is P-even. As discussed in Chapter 2, this is, in fact, a consequence of the Lorentz-invariance.

The parity violation manifests itself in the interference term  $X_t(Z\bar{\nu})$  of the polarization-dependent cross-section part (3.18). In four-vector notations, the latter is built of terms like  $(a, b, c = p_1, p_2, k_1, k_2)$

$$\varepsilon_{\mu\nu\rho\sigma} a^\mu b^\nu P_+^\rho P_-^\sigma, \quad P_\pm^\mu a_\mu,$$

which are P-odd, as well as of those like

$$P_+^\mu P_{-\mu}, \quad a^\mu b_\mu, \quad \varepsilon_{\mu\nu\rho\sigma} a^\mu b^\nu c^\rho P_\pm^\sigma,$$

which are P-even. We note that there is a parity violating term in  $X_t(Z\bar{\nu})$  that has no dependence on the angle  $\phi$  specifying the chargino momenta. This apparent lack of correlation between angular dependence and parity violation is possible, since, for example, a factor  $\cos\theta$  can arise from P-even scalar products like  $p_1^\mu k_{1\mu}$ , or from P-odd terms like  $\varepsilon_{\mu\nu\rho\sigma} p_1^\mu k_1^\nu P_+^\rho P_-^\sigma$ . In the same way, the term  $\varepsilon_{\mu\nu\rho\sigma} p_1^\mu p_2^\nu P_+^\rho P_-^\sigma$  gives no dependence on the angles  $\theta$  and  $\phi$  at all, being, however, odd under parity.

To consider charge conjugation, we note that in the notations of Section 3.1 the C-transformation (2.8) (or (2.11)) is equivalent to

$$\begin{aligned} \omega &= -1, & \phi_+ &\leftrightarrow \phi_- + \pi, & \beta_+ &\leftrightarrow \beta_-, & E_+ &\leftrightarrow E_-, \\ m_i &\leftrightarrow m_j, & C_i &\leftrightarrow C_j, & G_{v,a\,ij} &\leftrightarrow G_{v,a\,ji} = G_{v,a\,ij}^*. \end{aligned} \quad (3.19)$$

This implies that the cross section for the C-conjugated process is obtained from Eqs. (3.17) – (3.18) by the following substitution:

$$\begin{aligned} \omega &= -1, & \phi_+ &\leftrightarrow \phi_- + \pi, \\ m_i &\leftrightarrow m_j, & |C_i| &\leftrightarrow |C_j|, & \phi_i &\leftrightarrow \phi_j, & \psi_{v,a,L} &\rightarrow -\psi_{v,a,L}. \end{aligned} \quad (3.20)$$

In particular, one can see that the above substitution of the polarization azimuthal angles amounts to

$$(\phi_+ + \phi_-) \leftrightarrow (\phi_+ + \phi_-), \quad (\phi_+ - \phi_-) \leftrightarrow -(\phi_+ - \phi_-). \quad (3.21)$$

Recalling that due to the Lagrangian structure (see Appendix C) for  $i = j$  the coupling constants  $G_v$  and  $G_a$  become real, and the angles  $\psi_v$  and  $\psi_a$  vanish, one immediately sees that in both cases  $i = j$  and  $i \neq j$  the C-conjugation (3.20) leaves the unpolarized contribution (3.17) unchanged. Since, as just discussed, the latter is also P-even, we conclude that the unpolarized cross-section is CP-even. Again, this conclusion we already made when looking at the symmetry properties of the cross section in Chapter 2.

Next step is to see that, while containing C-odd (and P-odd) terms, the polarized part (3.18) of the tree-level cross-section is still CP even. For all of the contributions, apart from  $X_t(Z\bar{\nu})$ , it is straightforward just because there is no  $\omega$  dependence (P-even) and, according to Eq. (3.21) the sum  $(\phi_+ + \phi_-)$  is C-even. However, the remaining term,  $X_t(Z\bar{\nu})$ , obviously contains P-odd terms. To demonstrate that the  $X_t(Z\bar{\nu})$  is CP-even it is enough to recall that due to the structure of the Lagrangian couplings the equality

$$\psi_L + \phi_i - \phi_j = 0 \quad (3.22)$$



always holds. Indeed, assembling the formulae (3.6)–(3.11), the expression of the couplings via the mixing matrices (C.15), and dropping overall real factors (irrelevant to complex phases), we see that

$$G_L \sim X_{i1} X_{1j}^\dagger, \quad C_i \sim X_{1i}^\dagger, \quad C_j \sim X_{1j}^\dagger,$$

up to real coefficients. The mixing  $X$ -matrices are unitary, so  $X_{i1}^\dagger = (X_{1i})^*$ , and thus

$$G_L \sim (C_i)^* C_j$$

up to a real coefficient. Thus, by definitions (3.10)–(3.11) of phases  $\psi_L$  and  $\phi_i, \phi_j$  the relation (3.22) holds. Therefore (and since  $(\phi_+ + \phi_-)$  is C-even), the first term of  $X_t(Z\tilde{\nu})$  is C- and CP-even. It is also easy to see, that the changes due to the C-transform (3.20) in the second term of  $X_t(Z\tilde{\nu})$  are compensated by changing the  $\omega$  sign, which represents the P-transform. Hence, the polarized part of the tree-level cross-section is CP-even.

The last result is somewhat surprising<sup>6</sup>: as we will show later, a CP-odd part does arise in the unpolarized cross-section at 1-loop level, so there is no physical/parameter *symmetry* that prohibits the CP-violation. Thus, the absence of CP-violation at tree-level can only be attributed to the specific coupling structure of the model (see also relevant discussion in [27]). On the other hand, the “good news” here is that the CP-even tree-level amplitude guarantees that the CP-odd term will get only finite corrections during renormalization: this is because the model (MSSM) is renormalizable by construction. We shall say more about it later on.

---

<sup>6</sup>It is important to mention that the same (tree-level) result was obtained independently by [27] using different analytical methods, which reduces the possibility of error in the calculations.



# Chapter 4

## The one-loop corrections: contributing graphs

### 4.1 Contributing graphs: overview

As we show in this Thesis, the one loop corrections do induce a CP-violating contribution to the process

$$e^+ + e^- \rightarrow \tilde{\chi}_i^+ + \tilde{\chi}_j^- \quad (4.1)$$

even in the case when the initial beams are not polarized. It should, perhaps, be stressed that we do not calculate the full one-loop cross section here, neither do we give a review of the magnitude of the CP-odd observables in various parameter points. Our intention is to demonstrate that *there are* domains in the parameter space where the CP-violation is present at the one-loop level. Therefore the strategy is to pick a specific parameter set that allows us to neglect certain diagrams and show that the effect is indeed non-zero at the one-loop order. For this purpose we are free to choose any point in parameter space. The simplest choice turned out to be a (possible) point, where all slepton masses are large (“heavy slepton limit”)<sup>1</sup>.

It is essential that the results are obtained *analytically*, rather than by numerical accounting of all the contributing diagrams<sup>2</sup>. In fact, it is the analytical properties of the results that ensure non-cancellation of the CP-violating terms arising from a certain set of contributing diagrams. However, the complete overview of the contributing graphs is, of course, required. With this purpose we introduce here some diagrammatic notations and classify contributing 1-loop diagrams in the following Sections.

The phenomenological structure of the model is complicated, and there are many graphs that contribute to our process at the one-loop level, thereby one requires suitable diagram drawing conventions and a convenient classification scheme to account for them all.

---

<sup>1</sup>One could refer to the parameter space area around the so-called “SPS 2” benchmark point [33], but remember that the latter classification assumes a specific (mSUGRA) breaking mechanism with no CP-violating phases. In this research we do not assume any particular SUSY-breaking mechanism, and of course, the phases do present. However, the existence of SPS 2 parameter point in (very constrained) mSUGRA model confirms that less constrained SUSY models indeed include heavy slepton limit as a part of the parameter space.

<sup>2</sup>Some results of numerical calculations of 1-loop cross-section to the process (4.1) can be found, e.g., in [34]. However, due to the very large number of contributing diagrams the authors obviously cannot analyze the analytical structure of the CP-odd contribution.

First, in the MSSM there are superparticles (sparticles) of spin 0 (sfermions) and  $\frac{1}{2}$  (chargino and neutralino). We found it convenient to indicate sparticles by double lines which, since  $R$ -parity conservation is imposed<sup>3</sup>, should not break or branch through a diagram. More precisely, the total number of double lines — that of bosonic (dashed double lines:  $\text{---} \text{---}$ ) plus that of fermionic (solid double lines:  $\text{=====}$ ) — attached to each vertex must be even.

Next, the model involves Majorana fermions (neutralino), which leads to certain subtleties with particle-antiparticle identification [48, 49, 38]. Following [38] we do not indicate the (double) fermion line direction for neutralino; in Appendix C we shortly explain how the vertices with neutralino are constructed out of Lagrangian couplings.

Besides, there is a specific feature of this kind of models — the fermion line arrows “clashing”. According to the standard convention, we define the positive chargino to be a *particle*, rather than antiparticle, and draw the arrows on the fermion lines in the direction of particle flow. Due to angular momentum conservation, the chain of fermion lines must be continuous, and in that specific vertex where electron meets chargino and sneutrino, the fermion arrows clash, say, due to charge conservation — see, e.g. the last diagram in Fig. 3.1. At the same time, this convention ensures that the clashing does not take place in, e.g., the triple vertex where neutrino meets chargino and selectron. Hence, the clashing of the fermion lines will always be present, whether the positive chargino is particle or antiparticle. It is, of course, caused by the  $C$ -matrix in the Lagrangian vertices. Appendix C.1 and references therein provide a recipe for selecting a consistent fermion line flow through the chains of fermion lines. However for correct application of the latter technique one shall first draw all diagrams with correct particle/antiparticle assignment, i.e., with arrow clashing.

To collect all the diagrams it is useful to classify them according to the fermion and the sparticle line topology, without explicit specification of the particles that correspond to each internal line. Due to the above-mentioned subtleties (e.g., “clashing” and Majorana fermions), the direction of a fermion’s arrow in these skeleton graphs is not always defined until the explicit particle assignment is made. In these cases we simply do not draw the arrow. In contrast, it also happens that the fermion lines themselves uniquely specify some particles in internal lines, in the latter situation we indicate them in the figures below.

Let us also note that the colored particles and the Faddeev–Popov ghosts can contribute to our process at the one-loop level only through loop corrections for the gauge boson propagator. As explained later in Chapter 6, the absence of CP-violation at the tree level ensures that the propagator corrections cannot induce CP-violation in our case<sup>4</sup>, neither can the (multiplicative) wave function renormalization. Hence, neither ghost nor color enters the diagrams we have to account for.

Further, there are neither 1PI triangle diagrams nor “fish-like” ones, because there are no four-point vertices with two fermions in the Lagrangian (renormalizability!). Thus, we are left with only two types of one-loop corrections that may contribute to  $d\sigma_0^{\text{odd}}$  from Eq. (2.17): they are the (1PI) box diagrams, and the tree diagrams from Fig. 3.1 (Chapter 3) with a triangle loop instead of one of the vertices. Accordingly, we classify all possible fermion skeletons for these one-loop graphs in Sections 4.2 (boxes) and 4.4 (triangles), and in Sections 4.3 and 4.5

<sup>3</sup>That is what the soft breaking terms are responsible for [46]. Recently the  $R$ -parity non-conserving extensions of the MSSM started to attract attention (see e.g. [47]), however here we do not consider these cases.

<sup>4</sup>Higgs boson propagators could in principle bring CP-violating terms into the amplitude, but as we discuss below all such terms are suppressed by  $m_e$  (electron mass) factor.

we make the specific particle assignments for boxes and triangles, respectively.

## 4.2 1PI one-loop graphs (“boxes”): skeletons

Let us first discuss the four-leg 1PI graphs contributing to the amplitude. Note, that since there is no four-point  $e^+e^-\chi^+\chi^-$  Lagrangian vertex, renormalizability of the MSSM tells us that the sum of all these graphs should be finite.

As just discussed, there is only one type of 1PI graphs that can contribute to the amplitude of the process 4.1 at the one-loop level: the box diagrams (4-propagator loops). Since the fermion lines should be continuous, one can divide these diagrams into three categories: with fermion (lepton) lines being “vertical”, “horizontal” or “crossed”.

For those with “vertical” fermion lines, the  $R$ -parity conservation allows two different possibilities (classes) for skeletons: those with ordinary particle exchanges between the fermion lines, and those with sparticle exchanges. The first class can be represented by two skeletons in Fig. 4.1; here and in what follows the wavy line denotes a suitable gauge boson ( $\gamma$ ,  $Z$  or  $W$ ). There are, of course, analogous diagrams with various scalars instead of gauge bosons, but it is trivially seen that those graphs involve the triple scalar-electron-electron or scalar-electron-neutrino couplings, thus proportional to the electron mass which we drop.

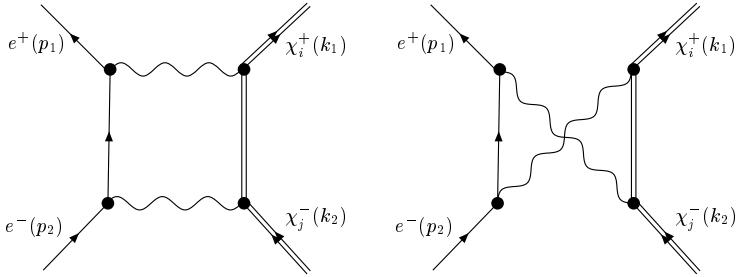


Figure 4.1: “Vertical” skeleton with ordinary particle exchanges between initial and final states.

The second class involves chargino/neutralino-electron vertices, so the non-spinor internal lines can only be sleptons ( $R$ -parity!): the two relevant skeletons are shown in Fig. 4.2.

One should of course keep in mind that there are many possibilities for different vector bosons, sleptons, as well as for intermediate lepton and chargino/neutralino lines within each class (skeleton).

For “horizontal” fermion lines there are more possibilities, however in the first three skeletons the particles on the internal lines are automatically fixed by the graph’s topology and available vertices. Indeed, as one can see from Fig. 4.3, in these three cases the above-mentioned fermion arrows “clashing” is unavoidable, but it is only chargino and electron lines that the Feynman rules allow to clash. This, in turn, defines charges of the sleptons and gauge bosons. In principle, the gauge boson lines in these skeletons can also be replaced by scalar exchanges, but the resulting diagrams will vanish in  $m_e = 0$  limit.

In the second “horizontal” class the internal fermions can only be charginos or neutralinos. According to our convention, we do not draw the fermion arrow until the explicit particle

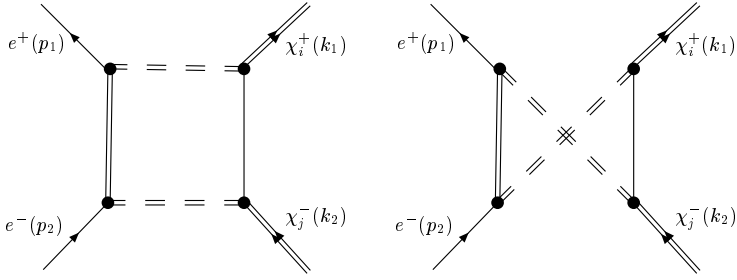


Figure 4.2: “Vertical” skeleton with sparticle exchanges between initial and final states.

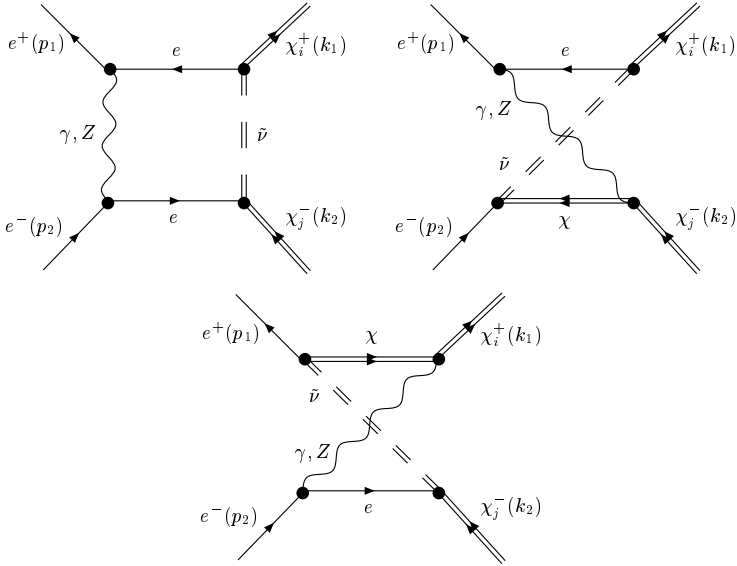


Figure 4.3: “Horizontal” fermion lines: “clashing” specifies intermediate particles.

assignment is made. For diagrams in this class the “clashing” alone cannot guide us in identifying the intermediate particles, and scalar exchanges are also possible, so there are two skeletons with various possibilities for all intermediate particles (Fig. 4.4).

At last, there are “crossed” boxes with crossing fermion lines. For the charge conservation these internal fermions must be neutral, only neutrino or neutralino are allowed. There is only one box with two internal neutrinos: Fig. 4.5 (the same diagram with  $W$  replaced by Higgs vanishes in  $m_e = 0$  limit). Besides, there are two possibilities for boxes with internal neutralino lines (here the Higgs coupling is, of course, not negligible): Fig. 4.6; and two possibilities for mixed neutrino-neutralino case: Fig. 4.7.

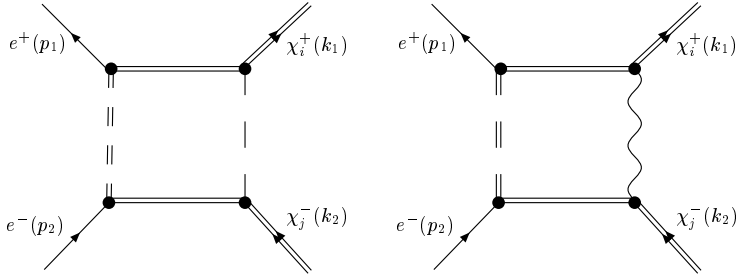


Figure 4.4: “Horizontal” fermion lines: both the internal fermions are sparticles.

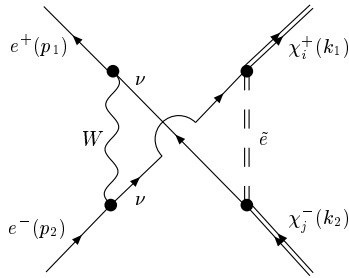


Figure 4.5: “Crossed” fermion lines: both the internal fermions are neutrino.

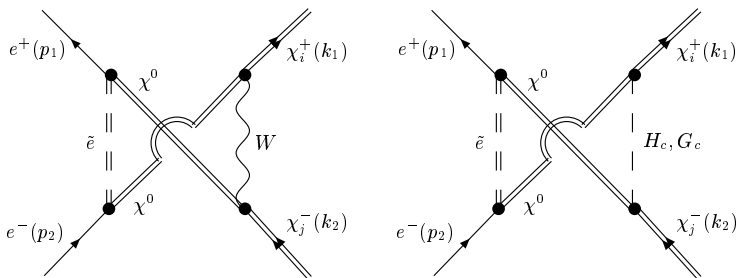


Figure 4.6: “Crossed” fermion lines: both the internal fermions are neutralino.

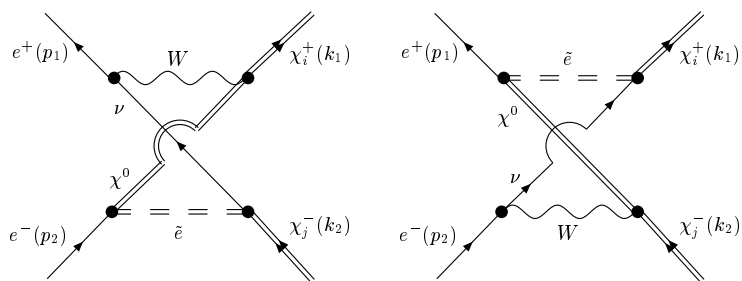


Figure 4.7: “Crossed” fermion lines: neutrino and neutralino.



### 4.3 1PI one-loop diagrams in the heavy slepton limit

The fermion skeletons classified in Section 4.2 contain internal lines with so far unspecified particle content. For actual calculations one, of course, needs to make the explicit particle assignment.

It is easy to see that all the box diagrams are *finite* by simple power counting. Hence, in the heavy slepton limit any box diagram that involves a slepton propagator shall be discarded: one can check that there are no scalar mass factors coming from the couplings. Consequently, among the diagrams considered in the previous Section, only those of the type shown in Figure 4.1 will contribute. These diagrams (now with specific particles assigned to the lines) are presented in Fig. 4.8.

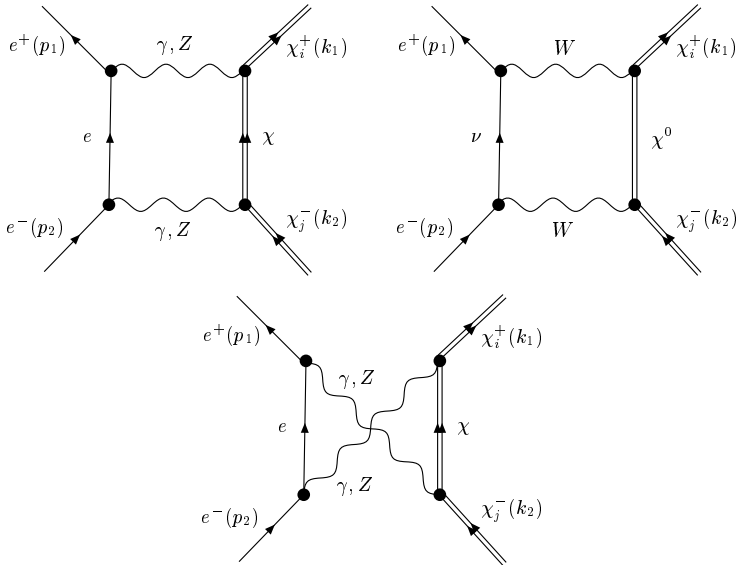


Figure 4.8: Box diagrams without slepton lines: all chargino and neutralino mass eigenstates contribute.

As we will show in Chapter 6, to verify the presence of CP-violation in the cross-section it is sufficient to calculate the above diagrams only.

#### 4.4 One-loop corrections to the 3-point vertices: skeletons

The rest of the one-loop diagrams are formed when vertices of tree graphs in Fig. 3.1 acquire one-loop corrections. As we show in Chapter 6, the calculation of the latter loops is not required to demonstrate the CP-violation at one loop order. Still, the numerical computations accounting for *all* the 1 loop graphs (including triangle diagrams) has also been performed<sup>5</sup>: some details are discussed in Chapter 6. Therefore, here we classify the 1-loop 3-points vertices for completeness purposes.


In principle, each triple vertex of the tree graphs in Fig. 3.1 acquires a correction at one loop. However, some of the corrections obviously vanish.

First of all, as mentioned in Chapter 3, the Lagrangian triple couplings of all scalars with electron and positron, as well as those with electron and neutrino are proportional to the electron mass, thereby all one-loop graphs that involve these couplings can be neglected. Moreover, at any loop order the Higgs/Goldstone- $e^+e^-$  three-point function is unavoidably proportional to the Yukawa coupling, since it is the Yukawa coupling that couples the Higgs sector to leptons<sup>6</sup>. This coupling is small, so the Higgs/Goldstone exchange (the first diagram in Fig. 3.1) should also be negligible at one loop and higher orders. Hence, one does not need to compute the one-loop corrections to Higgs/Goldstone- $e^+e^-$  vertices, and neither those to the Higgs/Goldstone- $\chi^+\chi^-$  vertices, since the latter ones are accompanied by tree level Higgs/Goldstone- $e^+e^-$  vertices in the relevant exchange diagrams.

Next, it is known (see, e.g., [50], see also Appendix B of this Thesis) that at any loop order the photon is prohibited from coupling to two different-mass fermions (charginos) by the  $U(1)$  Ward identities. Thus, one would need to calculate the one-loop corrections to the  $\gamma\chi_i\chi_j$  vertex, and, therefore, those to the  $\gamma ee$  coupling only for  $i = j$ , in which case the unpolarized cross-section is  $CP$ -even and therefore not considered here.

The remaining one-loop corrections — those to the vertices in the tree-level  $Z$  and  $\tilde{\nu}$  exchange diagrams (Fig. 3.1) — will, in general, contribute. As we have already noted, MSSM has no four-point couplings with two fermions, hence there are no “fish-like” (2-vertex) loops in this case and all one-loop corrections to triple vertices we need are those due to triangle diagrams. Again, we first classify the latter according to the geometry of their fermion lines.

The tree level triple vertices in the  $s$ -channel are those with two electrons or two charginos. There are four classes for the electron-electron vertex, shown in Fig. 4.9, where the unspecified wavy line denotes a suitable gauge boson. Note, that there are also diagrams with the same fermion skeleton, but with some of the internal wavy lines replaced by scalar (charged or neutral) ones. However, due to the presence of the above-mentioned scalar-electron vertices the latter diagrams vanish in the  $m_e = 0$  limit and therefore are not shown.

The chargino-chargino vertex corrections have similar fermion skeleton (Fig. 4.10), but the internal line content is richer, because there are also non-vanishing diagrams with scalar internal lines. Thus, in these skeleton graphs we use the zigzag line  to denote suitable scalars (Higgs  $h, H, A, H_c$  or Goldstone  $G, G_c$ ) particles or vector bosons ( $\gamma, Z$  or  $W$ ).

The skeletons for one-loop corrections to the upper  $t$ -channel vertex ( $e^+\chi_i^+\tilde{\nu}$ ) are collected in Fig. 4.11. Again, the internal wavy lines denote suitable vector bosons, while the zigzag

<sup>5</sup>The complete 1-loop results for the magnitude of CP-violating observable have been obtained in collaboration with J. Kalinowski and K. Rolbiecki using their numerical code. The obtained values have further confirmed the “box-only” results. See, please, [36], attached to this Thesis.

<sup>6</sup>At one loop one can also verify it by considering odd-even properties of relevant loop integrand as a function of the loop momentum.

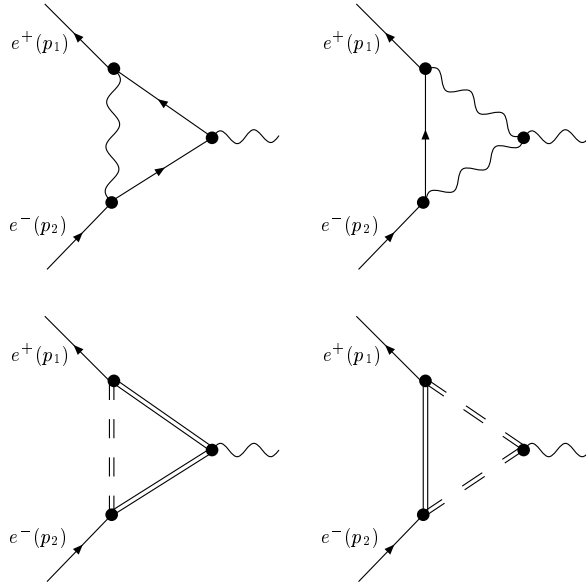


Figure 4.9: Electron-electron vertex corrections: skeleton graphs.

line can be either scalar or vector. Possible diagrams with some of the wavy lines replaced by scalars are proportional to electron mass and therefore dropped.

Finally, to obtain the lower  $t$ -channel vertex ( $e^-\chi_j^-\tilde{\nu}$ ) corrections one just has to reverse the directions of all fermion lines in Figure 4.11 and replace the external particles:  $e^+(p_1) \rightarrow e^-(p_2)$ ,  $\chi_i^+(k_1) \rightarrow \chi_j^-(k_2)$ .

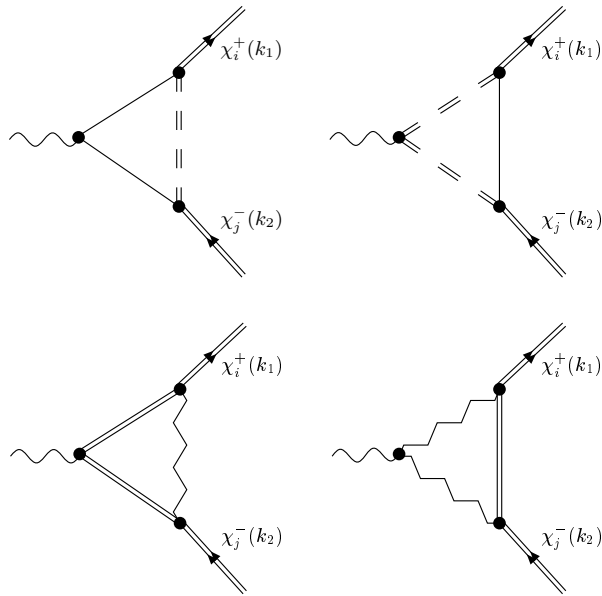


Figure 4.10: Chargino-chargino vertex corrections: skeleton graphs.

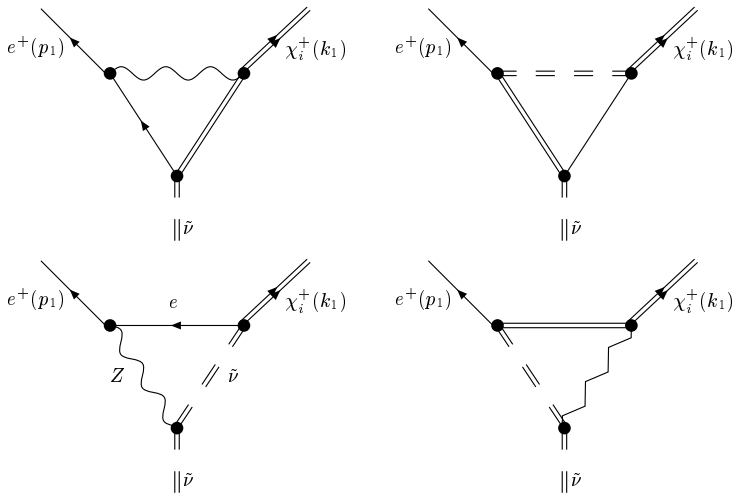


Figure 4.11: Electron-chargino vertex corrections: skeleton graphs

## 4.5 One-loop corrections to the 3-point vertices

In this Section we make the specific particle assignment for the triangle skeleton graphs collected in Section 4.4. As discussed below, contrary to the box diagrams (Sections 4.2 and 4.3), the heavy slepton limit does not allow to drop that many triangle graphs in calculations. That is why we first draw all the graphs (including those with slepton lines), and then discuss simplifications caused by the large slepton masses.

The 4 skeletons in Fig. 4.9 for 1-loop corrections to the  $eeZ$  vertex are represented by diagrams in Fig. 4.12. Note that the first 3 diagrams are just conventional Standard Model

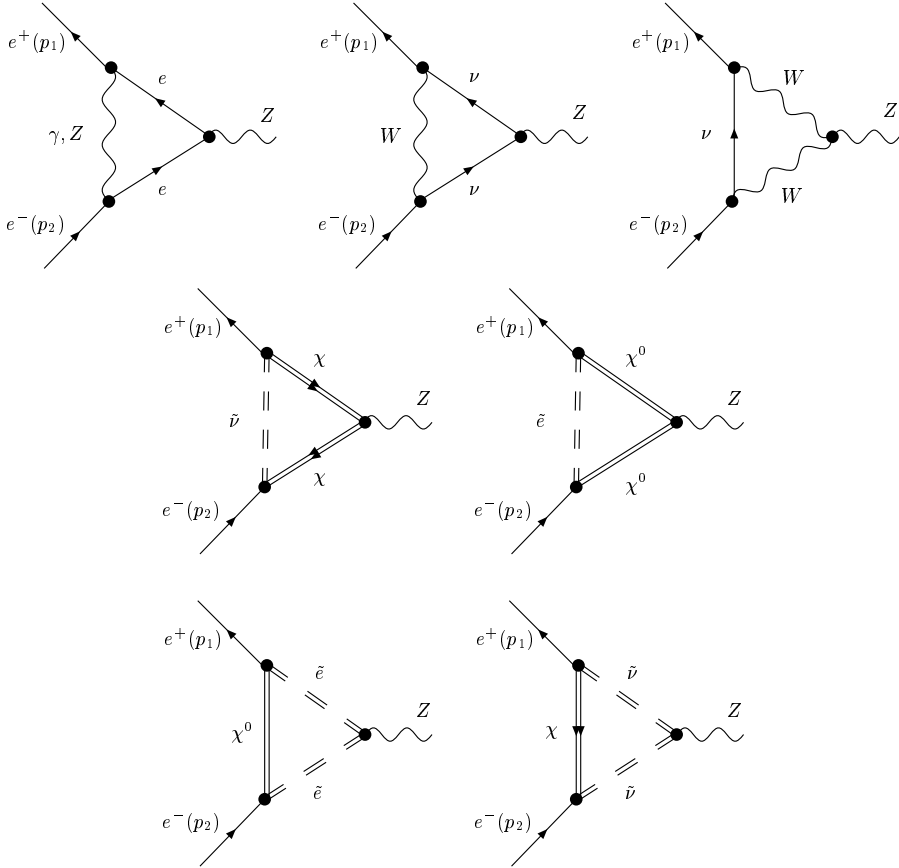


Figure 4.12:  $eeZ$  vertex corrections: all mass eigenstates of intermediate sparticles shall be accounted for.

corrections, while the rest unavoidably involve sleptons. Of course, all eigenstates of intermediate sparticles shall be taken into account, and for certain combinations of those eigenstates some of the graphs will vanish due to the structure of the couplings.

The number of 1-loop diagrams that contribute to the  $Z\chi\chi$  vertex correction is larger. Grouping them by the skeleton structure (Fig. 4.10) we draw these graphs in Figures 4.13, 4.14, and 4.15.

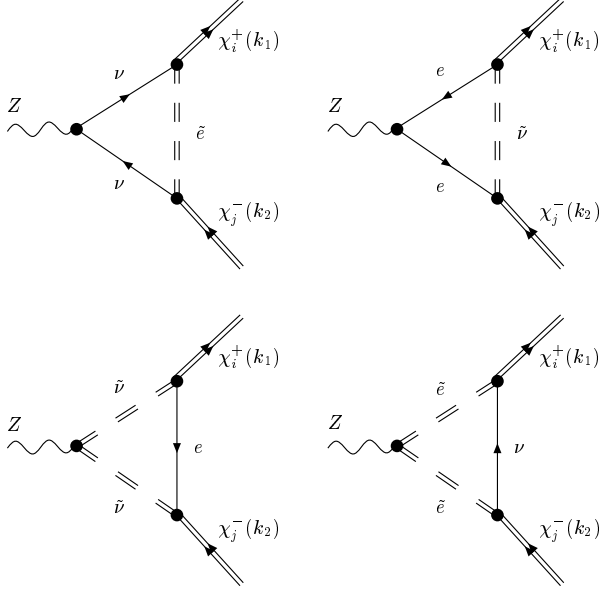


Figure 4.13:  $Z\chi\chi$  vertex corrections (1st and 2nd skeletons from Fig. 4.10): all selectron and sneutrino mass eigenstates contribute. Note however that the first diagram vanishes for one of the internal selectron mass states ( $\tilde{e}_1$ ) and the last diagram vanishes if the two internal selectrons have different masses.

The corrections to  $e^+\chi_i^+\tilde{\nu}$  are collected in Figs. 4.16 and 4.17 (again, they are grouped according to their 4 fermion skeletons from Figure 4.11). At last, the corrections to  $e^-\chi_i^-\tilde{\nu}$  vertex can easily be obtained from graphs in Figures 4.16 and 4.17 by reversing directions of the fermion lines and, of course, by substituting the external particles:  $e^+(p_1) \rightarrow e^-(p_2)$ ,  $\chi_i^+(k_1) \rightarrow \chi_j^-(k_2)$ .

Contrary to the box diagrams, there are not that many triangles that can be discarded in the limit of the heavy sleptons. The main reason here is that the triangle diagrams by themselves are not finite by power counting. Hence, even if a particular diagram contains the slepton propagator, its divergent part may still be needed to ensure finiteness of the full 1-loop observable. Besides, some of the mass factors may come from couplings.

Still, some simplifications can be made. For example, the first three graphs in Fig. 4.12 constitute the pure Standard Model correction. When combined with the tree approximation (which in the heavy slepton limit consists of the  $Z$ -exchange graph alone) to form the cross-section, these three loop graphs will result in multiplying Eqs. (3.17)–(3.17) by a factor, which does not involve the chargino masses. Then, essentially repeating the arguments of Section 3.3 one will conclude that this contribution is CP-even.

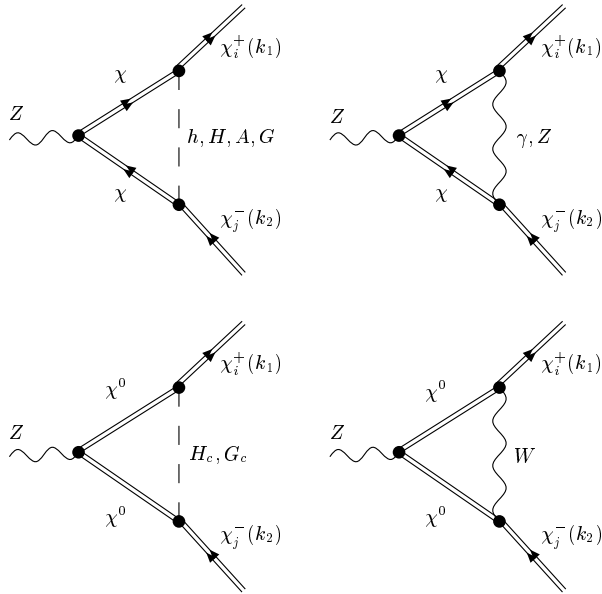


Figure 4.14:  $Z\chi\chi$  vertex corrections (3rd skeleton from Fig. 4.10): all chargino and neutralino mass eigenstates shall be accounted for.

There are a few other graphs that can be eliminated in a similar way once all the sleptons are made heavy. Besides, one can assume<sup>7</sup> all the Higgs bosons except  $h$  to be heavy (not to be mixed up with the Goldstones  $G$  and  $G_c$  which acquire, respectively,  $M_Z$  and  $M_W$  mass in our gauge), which leads to further simplifications. We do not focus further on these details, as they are not essential for confirming the presence of CP-violation.

<sup>7</sup>Again, by analogy with the SPS 2 benchmark point [33].

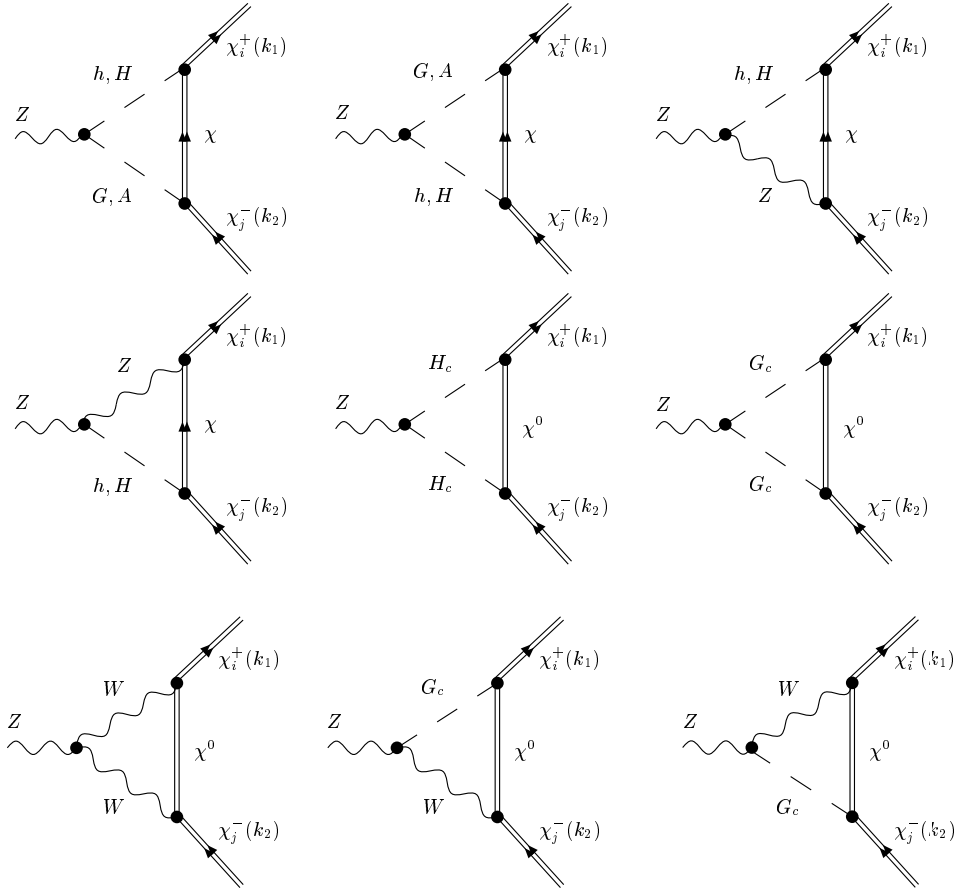


Figure 4.15:  $Z\chi\chi$  vertex corrections (4th skeleton from Fig. 4.10): all mass eigenstates of intermediate particles shall be accounted for.



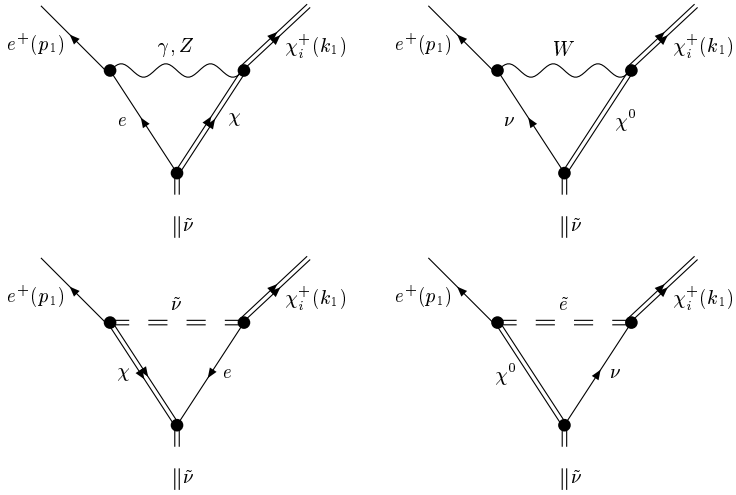


Figure 4.16:  $e^+\chi_i^+\tilde{\nu}$  vertex corrections (1st and 2nd skeletons from Fig. 4.11): all chargino and neutralino mass eigenstates shall be accounted for.

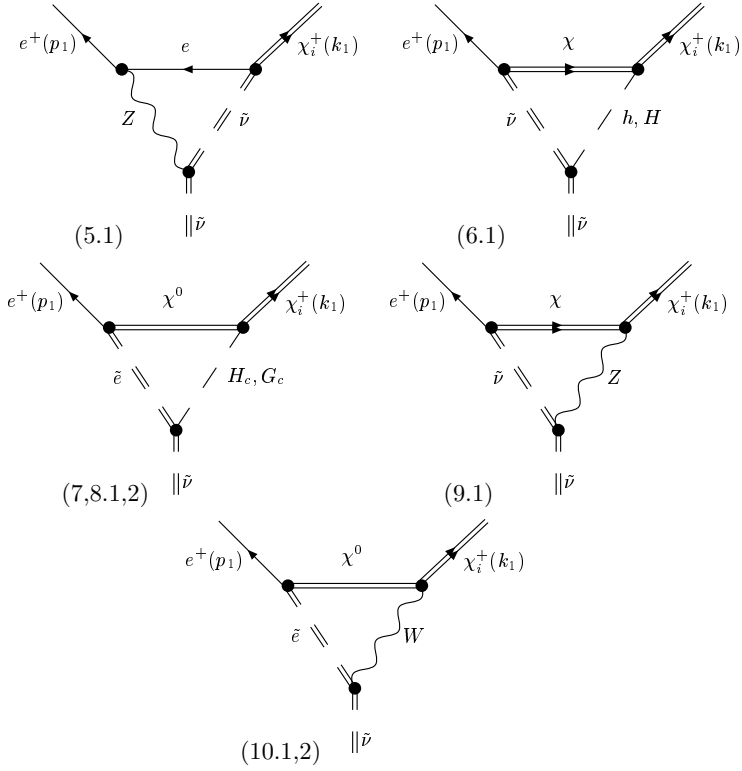


Figure 4.17:  $e^+ \chi_i^+ \tilde{\nu}$  vertex corrections (3rd and 4th skeletons from Fig. 4.11): all eigenstates of the intermediate particles shall be accounted for.

## Chapter 5

# Loop integral calculations

### 5.1 Passarino–Veltman-like integrals

As demonstrated in the previous Chapter, the 1-loop cross-section involves box and triangle diagrams with various topologies (described in Sections 4.2 and 4.4, respectively). It is well known, that the evaluation of those loop graphs can be reduced to handling the so-called Passarino-Veltman functions [51]. These are the scalar integrals, which we denote as:

$$J_{\nu_1, \nu_2, \nu_3, \nu_4} \equiv \int d^n q \frac{1}{d_1^{\nu_1} d_2^{\nu_2} d_3^{\nu_3} d_4^{\nu_4}}, \quad (5.1)$$

where  $d_i \equiv p_i^2 - m_i^2$ ;  $i = 1, 2, 3, 4$ ; are the corresponding propagator denominators and  $q$  is the loop momentum integration variable. Since the maximum number of propagators in the loops that we are going to deal with is 4 (box), we will not need  $J$ 's with more than 4 indices. Of course, for divergent integrals like, say,  $J_{1,1,0,0}$  we imply a regularization.

With some labor, we can reduce all the  $J$ 's to those with *positive* indices: the recipes of such a reduction will be given in Secs. 5.4–5.9, where we follow the algebraic approach developed in [52]. Once this reduction is done, the integrals with positive indices can be evaluated numerically<sup>1</sup> and, in principle, no more analytical work is required. However, for tracking the contributions to the CP-odd observable (2.17) it is useful to establish some symmetries for this basic set of integrals, which is done in Section 5.3.

The calculations are cumbersome, and choice of appropriate parametrization often allows one to reduce the analytical work. That is why in Section 5.2 below we fix 4 “symmetric” parametrizations for the loop momenta and use these parametrizations in subsequent calculations.

### 5.2 Loop momenta parametrizations

For various cases met in calculations it is convenient to parametrize the momentum inside graphs in different ways. The parametrizations we use for square loop graphs<sup>2</sup> are shown in Fig. 5.1. Note, that arrows on the lines here denote the momentum direction and have

---

<sup>1</sup>For the numerical work we used the FORTRAN code provided by the LoopTools package [53, 54].

<sup>2</sup>One would also need two more parametrizations for line topology like, e.g., in Fig 4.7. However, as long as we take the sleptons being heavy, diagrams of that type do not contribute.

nothing to do with the spin or charge flow. To adjust these conventions for triangle loops, we simply contract one of the inner box lines.

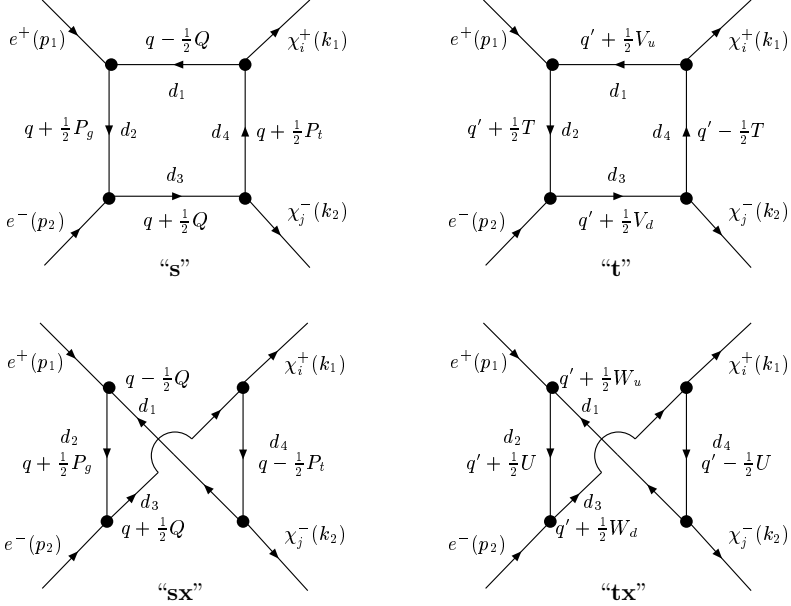


Figure 5.1: Momenta assignment in the “crossed” and “uncrossed” box diagrams: arrows on particle lines denote the momentum direction.

There is, of course, a connection between the external particle momenta and those on the inner lines. For the parametrizations we use it looks as follows:

$$\begin{aligned}
 \text{“s”}, \text{“sx”}: \quad Q &= p_1 + p_2 = k_1 + k_2, & P_g &= p_1 - p_2, & P_t &= k_1 - k_2; \\
 \text{“t”}: \quad T &= p_1 - k_1 = k_2 - p_2, & V_u &= -p_1 - k_1, & V_d &= p_2 + k_2; \\
 \text{“tx”}: \quad U &= k_1 - p_2 = p_1 - k_2, & W_u &= -p_1 - k_2, & W_d &= k_1 + p_2;
 \end{aligned} \tag{5.2}$$

The corresponding loop integration variables  $q$  and  $q'$  differ by the shift:

$$\begin{aligned}
 \text{“s”} \leftrightarrow \text{“t”}: \quad q - q' &= \frac{1}{2}(p_2 - k_1) = \frac{1}{2}(k_2 - p_1) = -\frac{1}{2}U, \\
 \text{“sx”} \leftrightarrow \text{“tx”}: \quad q - q' &= \frac{1}{2}(k_1 - p_1) = \frac{1}{2}(p_2 - k_2) = -\frac{1}{2}T,
 \end{aligned}$$

and it is, of course, impossible to establish such a connection between, say, “s” and “sx”.

Considering a particular diagram it is convenient to denote the masses of the particles propagating along the internal lines as  $m_1, m_2, m_3, m_4$ , and to call the denominators of the corresponding propagators  $d_1, d_2, d_3, d_4$ , so that  $d_i(p_i) = p_i^2 - m_i^2$ , where  $p_i$  stands for the momentum of  $i$ -th internal line. Below we list some trivial, though useful relations between these  $d$ 's and loop momenta in various parametrizations.

- “s”:

$$\begin{aligned}
d_1 &\equiv (q - \frac{1}{2}Q)^2 - m_1^2 = q^2 - qQ + \frac{1}{4}Q^2 - m_1^2, \\
d_2 &\equiv (q + \frac{1}{2}P_g)^2 - m_2^2 = q^2 + qP_g + \frac{1}{4}P_g^2 - m_2^2, \\
d_3 &\equiv (q + \frac{1}{2}Q)^2 - m_3^2 = q^2 + qQ + \frac{1}{4}Q^2 - m_3^2, \\
d_4 &\equiv (q + \frac{1}{2}P_t)^2 - m_4^2 = q^2 + qP_t + \frac{1}{4}P_t^2 - m_4^2,
\end{aligned} \tag{5.3}$$

and, hence,

$$\begin{aligned}
q^2 &= \frac{1}{2}(d_1 + d_3) - \frac{1}{4}Q^2 + \frac{1}{2}(m_1^2 + m_3^2), \\
qQ &= \frac{1}{2}(d_3 - d_1) + \frac{1}{2}(m_3^2 - m_1^2), \\
qP_g &= d_2 - q^2 - \frac{1}{4}P_g^2 + m_2^2 = d_2 - \frac{1}{2}(d_1 + d_3) + \frac{1}{4}(Q^2 - P_g^2) + \frac{1}{2}(2m_2^2 - m_1^2 - m_3^2), \\
qP_t &= d_4 - q^2 - \frac{1}{4}P_t^2 + m_4^2 \\
&= d_4 - \frac{1}{2}(d_1 + d_3) + \frac{1}{4}(Q^2 - P_t^2) + \frac{1}{2}(2m_4^2 - m_1^2 - m_3^2),
\end{aligned} \tag{5.4}$$

- “sx” (take “s” propagators and substitute  $P_t \rightarrow -P_t$ ):

$$\begin{aligned}
d_1 &\equiv (q - \frac{1}{2}Q)^2 - m_1^2 = q^2 - qQ + \frac{1}{4}Q^2 - m_1^2, \\
d_2 &\equiv (q + \frac{1}{2}P_g)^2 - m_2^2 = q^2 + qP_g + \frac{1}{4}P_g^2 - m_2^2, \\
d_3 &\equiv (q + \frac{1}{2}Q)^2 - m_3^2 = q^2 + qQ + \frac{1}{4}Q^2 - m_3^2, \\
d_4 &\equiv (q - \frac{1}{2}P_t)^2 - m_4^2 = q^2 - qP_t + \frac{1}{4}P_t^2 - m_4^2,
\end{aligned} \tag{5.5}$$

and, hence,

$$\begin{aligned}
q^2 &= \frac{1}{2}(d_1 + d_3) - \frac{1}{4}Q^2 + \frac{1}{2}(m_1^2 + m_3^2), \\
qQ &= \frac{1}{2}(d_3 - d_1) + \frac{1}{2}(m_3^2 - m_1^2), \\
qP_g &= d_2 - q^2 - \frac{1}{4}P_g^2 + m_2^2 = d_2 - \frac{1}{2}(d_1 + d_3) + \frac{1}{4}(Q^2 - P_g^2) + \frac{1}{2}(2m_2^2 - m_1^2 - m_3^2), \\
qP_t &= -\left(d_4 - q^2 - \frac{1}{4}P_t^2 + m_4^2\right) \\
&= -\left(d_4 - \frac{1}{2}(d_1 + d_3) + \frac{1}{4}(Q^2 - P_t^2) + \frac{1}{2}(2m_4^2 - m_1^2 - m_3^2)\right),
\end{aligned} \tag{5.6}$$

- “**t**”:

$$\begin{aligned}
d_1 &\equiv (q' + \frac{1}{2}V_u)^2 - m_1^2 = q'^2 + q'V_u + \frac{1}{4}V_u^2 - m_1^2, \\
d_2 &\equiv (q' + \frac{1}{2}T)^2 - m_2^2 = q'^2 + q'T + \frac{1}{4}T^2 - m_2^2, \\
d_3 &\equiv (q' + \frac{1}{2}V_d)^2 - m_3^2 = q'^2 + q'V_d + \frac{1}{4}V_d^2 - m_3^2, \\
d_4 &\equiv (q' - \frac{1}{2}T)^2 - m_4^2 = q'^2 - q'T + \frac{1}{4}T^2 - m_4^2,
\end{aligned} \tag{5.7}$$

and, hence,

$$\begin{aligned}
q'^2 &= \frac{1}{2}(d_2 + d_4) - \frac{1}{4}T^2 + \frac{1}{2}(m_2^2 + m_4^2), \\
q'T &= \frac{1}{2}(d_2 - d_4) + \frac{1}{2}(m_2^2 - m_4^2), \\
q'V_u &= d_1 - q'^2 - \frac{1}{4}V_u^2 + m_1^2 = d_1 - \frac{1}{2}(d_2 + d_4) + \frac{1}{4}(T^2 - V_u^2) + \frac{1}{2}(2m_1^2 - m_2^2 - m_4^2), \\
q'V_d &= d_3 - q'^2 - \frac{1}{4}V_d^2 + m_3^2 \\
&= d_3 - \frac{1}{2}(d_2 + d_4) + \frac{1}{4}(T^2 - V_d^2) + \frac{1}{2}(2m_3^2 - m_2^2 - m_4^2),
\end{aligned} \tag{5.8}$$

- “**tx**” (take “**t**” propagators and substitute  $V_{u,v} \rightarrow W_{u,v}$  and  $T \rightarrow U$ ):

$$\begin{aligned}
d_1 &\equiv (q' + \frac{1}{2}W_u)^2 - m_1^2 = q'^2 + q'W_u + \frac{1}{4}W_u^2 - m_1^2, \\
d_2 &\equiv (q' + \frac{1}{2}U)^2 - m_2^2 = q'^2 + q'U + \frac{1}{4}U^2 - m_2^2, \\
d_3 &\equiv (q' + \frac{1}{2}W_d)^2 - m_3^2 = q'^2 + q'W_d + \frac{1}{4}W_d^2 - m_3^2, \\
d_4 &\equiv (q' - \frac{1}{2}U)^2 - m_4^2 = q'^2 - q'U + \frac{1}{4}U^2 - m_4^2,
\end{aligned} \tag{5.9}$$

and, hence,

$$\begin{aligned}
q'^2 &= \frac{1}{2}(d_2 + d_4) - \frac{1}{4}U^2 + \frac{1}{2}(m_2^2 + m_4^2), \\
q'U &= \frac{1}{2}(d_2 - d_4) + \frac{1}{2}(m_2^2 - m_4^2), \\
q'W_u &= d_1 - q'^2 - \frac{1}{4}W_u^2 + m_1^2 = d_1 - \frac{1}{2}(d_2 + d_4) + \frac{1}{4}(U^2 - W_u^2) + \frac{1}{2}(2m_1^2 - m_2^2 - m_4^2), \\
q'W_d &= d_3 - q'^2 - \frac{1}{4}W_d^2 + m_3^2 \\
&= d_3 - \frac{1}{2}(d_2 + d_4) + \frac{1}{4}(U^2 - W_d^2) + \frac{1}{2}(2m_3^2 - m_2^2 - m_4^2).
\end{aligned} \tag{5.10}$$

Besides, the following equalities hold on the mass shell (we take  $m_e = 0$ , hence on the mass shell  $p_1^2 = p_2^2 = 0$ ,  $k_1^2 = m_i^2$ ,  $k_2^2 = m_j^2$ ):

for “s” and “sx” parametrizations:

$$\begin{aligned} Q^2 = s, \quad QP_g = 0, \quad QP_t = m_i^2 - m_j^2, \\ P_g^2 = -s, \quad P_t^2 = 2(m_i^2 + m_j^2) - s, \quad P_gP_t = u - t; \end{aligned}$$

for “t” parametrization:

$$\begin{aligned} T^2 = t, \quad TV_u = m_i^2, \quad TV_d = m_j^2, \\ V_u^2 = 2m_i^2 - t, \quad V_d^2 = 2m_j^2 - t, \quad V_uV_d = u - s; \end{aligned}$$

for “tx” parametrization:

$$\begin{aligned} U^2 = u, \quad UW_u = m_j^2, \quad UW_d = m_i^2, \\ W_u^2 = 2m_j^2 - u, \quad W_d^2 = 2m_i^2 - u, \quad W_uW_d = t - s; \end{aligned} \quad (5.11)$$

here, as usual,  $s \equiv (p_1 + p_2)^2$ ,  $t \equiv (p_1 - k_1)^2$ ,  $u \equiv (p_1 - k_2)^2$  are the conventional Mandelstam variables.

The above relations have been embedded into the REDUCE code which led to the simplifications of the results up to a level that allowed analytical analysis.

### 5.3 Some symmetries of the loop integrals

To simplify the automatic calculations, as well as for checking purposes, it is useful to establish some symmetries for the basic set of Passarino–Veltman-like integrals defined by Eq. (5.1). These symmetries are mainly dictated by the fact that the scalar<sup>3</sup>  $J$ 's may depend only on the Lorentz scalars listed in Eq. (5.11) and, of course, on the inner masses  $m_1, m_2, m_3, m_4$ .

As noted in Chapter 2, the CP-transformation for the unpolarized cross-section is reduced to the interchange of the chargino masses in the resulting cross-section formula. As we show below, such interchange often transforms one  $J$ -integral into another, which often leads to substantial cancellations. This is, in fact, the main reason to identify such symmetries.

We shall first look how the loop topology affects the value of the integral. Suppose that the integral  $J_{\nu_1, \nu_2, \nu_3, \nu_4}(m_i, m_j)$  for “uncrossed” (with the line geometry like, e.g., “s” in Fig. 5.1) and the integral  $J_{\nu_1, \nu_2, \nu_3, \nu_4}^{\text{cr}}(m_i, m_j)$  for “crossed” (like, e.g., “sx”) box diagrams are defined by Eq. (5.1). The arguments in brackets indicate that the positive and negative (upper and lower) outgoing charginos carry the masses  $m_i$  and  $m_j$ , respectively. Let us fix the inner masses  $m_1, m_2, m_3, m_4$  and the powers  $\nu_1, \nu_2, \nu_3, \nu_4$ , and compare  $J$  and  $J^{\text{cr}}$ .

We are free to choose any uncrossed parametrization for the uncrossed box and any crossed one for the crossed box, so let us choose “s” and “sx”, respectively. The immediate consequence is that  $J$  and  $J^{\text{cr}}$  differ only by the sign of  $P_t$  (note that when classifying graphs in Fig. 5.1, we always keep the external legs fixed!) or, in other words, under the transformation  $P_t \rightarrow -P_t$  these integrals transform into each other.

Next, as we already mentioned,  $J$  and  $J^{\text{cr}}$  may depend only on the scalar products (5.11) of the external 4-momenta (or, equivalently, those momenta that enter in  $d_i$ ) and on the inner masses  $m_1, m_2, m_3, m_4$ . Among the relevant scalar products only  $QP_t = m_i^2 - m_j^2$

<sup>3</sup>For divergent  $J$ 's we assume some regularization consistent with the Lorentz symmetry.

and  $P_g P_t = u - t$  change value (sign) together with  $P_t$ . Finally, again, due to the Lorentz invariance, in addition to the inner and external masses, the integrals may depend only on two independent scalar variables, so take  $m_i^2 \pm m_j^2$ ,  $m_1, m_2, m_3, m_4$  and Mandelstam's  $t$  and  $u$  as independent quantities ( $m_e = 0$ ). Hence,  $J_{\nu_1, \nu_2, \nu_3, \nu_4}$  and  $J_{\nu_1, \nu_2, \nu_3, \nu_4}^{\text{cr}}$  are related by the  $t \leftrightarrow u$ ,  $m_i \leftrightarrow m_j$  transformation. Note however that  $m_1, m_2, m_3, m_4$  should be kept fixed, thus the transformation has to be done carefully when one of the inner particles is a chargino.

Let us now make a few observations:

(i) As is clearly seen from Fig. (5.1) and Eq. (5.11), for  $\nu_4 = 0$  the integrals are equal:  $J_{\nu_1, \nu_2, \nu_3, 0}(m_i, m_j) = J_{\nu_1, \nu_2, \nu_3, 0}^{\text{cr}}(m_i, m_j)$ , and neither of them is affected by  $m_i \leftrightarrow m_j$  or  $t \leftrightarrow u$  interchange.

(ii) Next, if  $\nu_2 = 0$ , the product  $P_g P_t = u - t$  can not contribute and, therefore both  $J$  and  $J^{\text{cr}}$  can be considered as functions of Mandelstam's  $s$  and masses and transform into each other by  $m_i \leftrightarrow m_j$ , while  $m_1, m_2, m_3, m_4$  are kept fixed. Neither of the integrals is affected by the  $t \leftrightarrow u$  substitution.

(iii) Finally, if  $m_1 = m_3$  and *in addition*  $\nu_1 = \nu_3$ , the integrals are even in  $Q$ , and, therefore, also even in  $QP_t = m_i^2 - m_j^2$ . Hence, in this case  $J$  and  $J^{\text{cr}}$  are connected by the  $t \leftrightarrow u$  interchange alone and neither of them is affected by  $m_i \leftrightarrow m_j$  interchange.

For processing the diagrams in Fig. 4.8 we will mostly need the integrals with  $m_1 = m_3$ , so let us consider this case in detail<sup>4</sup>. In Table 5.1 we summarize the properties of the basic  $J$ 's appearing in our calculations (the values  $m_1, m_2, m_3, m_4$  should not be affected by the chargino mass interchanges below).

Uncrossed	Transformation between $J$ and $J^{\text{cr}}$	Crossed	Notes
$J_{1,1,1,1}$	$t \leftrightarrow u$	$J_{1,1,1,1}^{\text{cr}}$	Both $J$ 's are $m_i \leftrightarrow m_j$ -even
$J_{0,1,1,1}$	$t \leftrightarrow u, m_i \leftrightarrow m_j$	$J_{0,1,1,1}^{\text{cr}}$	
$J_{1,0,1,1}$	=	$J_{1,0,1,1}^{\text{cr}}$	Both $J$ 's are $t \leftrightarrow u$ and $m_i \leftrightarrow m_j$ -even
$J_{1,1,0,1}$	$t \leftrightarrow u, m_i \leftrightarrow m_j$	$J_{1,1,0,1}^{\text{cr}}$	
$J_{0,0,1,1}$	$m_i \leftrightarrow m_j$	$J_{0,0,1,1}^{\text{cr}}$	Both $J$ 's are $t \leftrightarrow u$ -even
$J_{0,1,0,1}$	$t \leftrightarrow u$	$J_{0,1,0,1}^{\text{cr}}$	Both $J$ 's are $m_i \leftrightarrow m_j$ -even
$J_{1,0,0,1}$	$m_i \leftrightarrow m_j$	$J_{1,0,0,1}^{\text{cr}}$	Both $J$ 's are $t \leftrightarrow u$ -even
$J_{1,1,1,0}$	=	$J_{1,1,1,0}^{\text{cr}}$	Both $J$ 's are $t \leftrightarrow u$ and $m_i \leftrightarrow m_j$ -even
$J_{0,1,1,0}$	=	$J_{0,1,1,0}^{\text{cr}}$	Both $J$ 's are $t \leftrightarrow u$ and $m_i \leftrightarrow m_j$ -even
$J_{1,0,1,0}$	=	$J_{1,0,1,0}^{\text{cr}}$	Both $J$ 's are $t \leftrightarrow u$ and $m_i \leftrightarrow m_j$ -even
$J_{1,1,0,0}$	=	$J_{1,1,0,0}^{\text{cr}}$	Both $J$ 's are $t \leftrightarrow u$ and $m_i \leftrightarrow m_j$ -even

Table 5.1:  $J$ 's relations for  $m_1 = m_3$ .

Next, there are cross relations in the above table. For example, as long  $m_1 = m_3$ , the definiton (5.1) and Eq. (5.11) state that for  $J^{\text{any}} = J, J^{\text{cr}}$

$$J_{0,0,1,1}^{\text{any}}(m_i, m_j) = J_{1,0,0,1}^{\text{any}}(m_j, m_i),$$

where, as above,  $m_1, m_2, m_3, m_4$  are kept fixed (just  $Q \rightarrow -Q$  change). On the other hand, Table 5.1 shows that  $J_{0,0,1,1}(m_i, m_j) = J_{0,0,1,1}^{\text{cr}}(m_j, m_i)$ ,  $J_{1,0,0,1}(m_i, m_j) = J_{1,0,0,1}^{\text{cr}}(m_j, m_i)$ ,

<sup>4</sup>The box integrals for diagrams with mixed  $\gamma$  and  $Z$  exchange in Fig. 4.8 (here  $m_1 \neq m_3$ ) possess analogous properties, which, in fact, cause another big cancellation within CP-odd contributions due to these diagrams.



which gives the equalities:

$$J_{0,0,1,1}(m_i, m_j) = J_{1,0,0,1}^{\text{cr}}(m_i, m_j), \quad J_{1,0,0,1}(m_i, m_j) = J_{0,0,1,1}^{\text{cr}}(m_i, m_j).$$

Using “**t**” and “**tx**” parametrization one can establish some additional relations, which we skip here. The above properties serve as good tests for numerical calculations.

## 5.4 Reduction of $J$ 's with negative index (uncrossed box)

Consider the uncrossed box skeleton, like, e.g., one of the first two in Fig. 5.1 and look at the integral  $J_{-1,1,1,1}$ . Note, that, since the “**s**” and “**t**” parameterizations differ from each other only by the integration variable shift, we can choose any of these two parameterizations. For this particular integral it is convenient to use the “**t**” one. Then, according to Eq. (5.8),

$$\begin{aligned} J_{-1,1,1,1} &\equiv \int d^n q \frac{d_1}{d_2 d_3 d_4} \\ &= \int d^n q' \frac{1}{d_2 d_3 d_4} \left( q'^2 + q' V_u + \frac{1}{4} V_u^2 - m_1^2 \right) \\ &= \int d^n q' \frac{1}{d_2 d_3 d_4} \left[ \frac{1}{2} (d_2 + d_4) - \frac{1}{4} T^2 + \frac{1}{2} (m_2^2 + m_4^2) + q' V_u + \frac{1}{4} V_u^2 - m_1^2 \right] \\ &= \frac{1}{2} (J_{0,0,1,1} + J_{0,1,1,0}) - \left[ \frac{1}{4} T^2 - \frac{1}{2} (m_2^2 + m_4^2) - \frac{1}{4} V_u^2 + m_1^2 \right] J_{0,1,1,1} \\ &\quad + V_u^\mu \int d^n q' \frac{q'_\mu}{d_2 d_3 d_4}. \end{aligned} \quad (5.12)$$

The scalar products of the momenta are given by (on-shell) Eq. (5.11), while the last (tensor) integral is to be evaluated in Section 5.6 below.

In the same fashion,  $J_{1,1,-1,1}$  can be rewritten as (in fact, one may substitute  $d_1 \leftrightarrow d_3$  or, equivalently,  $m_1 \leftrightarrow m_3$ ,  $V_u \leftrightarrow V_d$  in Eq. (5.12), which also leads to the index change  $\nu_1 \leftrightarrow \nu_3$  in the integrals on the RHS):

$$\begin{aligned} J_{1,1,-1,1} &= \frac{1}{2} (J_{1,0,0,1} + J_{1,1,0,0}) - \left[ \frac{1}{4} T^2 - \frac{1}{2} (m_2^2 + m_4^2) - \frac{1}{4} V_d^2 + m_3^2 \right] J_{1,1,0,1} \\ &\quad + V_d^\mu \int d^n q' \frac{q'_\mu}{d_1 d_2 d_4}. \end{aligned} \quad (5.13)$$

Next, using the “**s**”-parametrization (Fig. 5.1) we obtain:

$$\begin{aligned} J_{1,-1,1,1} &\equiv \int d^n q \frac{d_2}{d_1 d_3 d_4} \\ &= \int d^n q \frac{1}{d_1 d_3 d_4} \left( q^2 + q P_g + \frac{1}{4} P_g^2 - m_2^2 \right) \\ &= \int d^n q \frac{1}{d_1 d_3 d_4} \left[ \frac{1}{2} (d_1 + d_3) - \frac{1}{4} Q^2 + \frac{1}{2} (m_1^2 + m_3^2) + q P_g + \frac{1}{4} P_g^2 - m_2^2 \right] \\ &= \frac{1}{2} (J_{0,0,1,1} + J_{1,0,0,1}) - \left[ \frac{1}{4} Q^2 - \frac{1}{2} (m_1^2 + m_3^2) - \frac{1}{4} P_g^2 + m_2^2 \right] J_{1,0,1,1} \\ &\quad + P_g^\mu \int d^n q \frac{q_\mu}{d_1 d_3 d_4}, \end{aligned} \quad (5.14)$$

and, at last (just substitute  $d_2 \leftrightarrow d_4$  or, equivalently,  $m_2 \leftrightarrow m_4$ ,  $P_g \leftrightarrow P_t$  in Eq. (5.14), which also leads to  $\nu_2 \leftrightarrow \nu_4$  in the integrals on the RHS):

$$J_{1,1,1,-1} = \frac{1}{2} \left( J_{0,1,1,0} + J_{1,1,0,0} \right) - \left[ \frac{1}{4} Q^2 - \frac{1}{2} (m_1^2 + m_3^2) - \frac{1}{4} P_t^2 + m_4^2 \right] J_{1,1,1,0} + P_t^\mu \int d^n q \frac{q_\mu}{d_1 d_2 d_3}. \quad (5.15)$$

The tensor integral still remains on the RHS — it is evaluated in Section 5.6 below.

## 5.5 Reduction of $J$ 's with negative index (crossed box)

Let us now consider the crossed box, like, e.g., the third or fourth in Fig. 5.1. Again, let us look at  $J_{-1,1,1,1}$  first. A natural choice here is the “**tx**” parametrization, which (see Eq. (5.10)) is obtained from “**t**” by the  $V_{u,v} \rightarrow W_{u,v}$ ,  $T \rightarrow U$  substitution. Hence (cf. Eq. (5.12)):

$$J_{-1,1,1,1}^{\text{cr}} = \frac{1}{2} \left( J_{0,0,1,1}^{\text{cr}} + J_{0,1,1,0}^{\text{cr}} \right) - \left[ \frac{1}{4} U^2 - \frac{1}{2} (m_2^2 + m_4^2) - \frac{1}{4} W_u^2 + m_1^2 \right] J_{0,1,1,1}^{\text{cr}} + W_u^\mu \int d^n q' \frac{q'_\mu}{d_2 d_3 d_4}. \quad (5.16)$$

The scalar products are again given by Eq. (5.11), and the last (tensor) integral is to be done in Section 5.7 below. Similarly (cf. Eq. (5.13)):

$$J_{1,1,-1,1}^{\text{cr}} = \frac{1}{2} \left( J_{1,0,0,1}^{\text{cr}} + J_{1,1,0,0}^{\text{cr}} \right) - \left[ \frac{1}{4} U^2 - \frac{1}{2} (m_2^2 + m_4^2) - \frac{1}{4} W_d^2 + m_3^2 \right] J_{1,1,0,1}^{\text{cr}} + W_d^\mu \int d^n q' \frac{q'_\mu}{d_1 d_2 d_4}. \quad (5.17)$$

The “**sx**”-parametrization (Eq. (5.6)) is obtained from “**s**” by just  $P_t \rightarrow -P_t$ , so the appearance of the decomposition (cf. Eq. (5.14)):

$$J_{1,-1,1,1}^{\text{cr}} = \frac{1}{2} \left( J_{0,0,1,1}^{\text{cr}} + J_{1,0,0,1}^{\text{cr}} \right) - \left[ \frac{1}{4} Q^2 - \frac{1}{2} (m_1^2 + m_3^2) - \frac{1}{4} P_g^2 + m_2^2 \right] J_{1,0,1,1}^{\text{cr}} + P_g^\mu \int d^n q \frac{q_\mu}{d_1 d_3 d_4}, \quad (5.18)$$

is unchanged, while  $J_{1,1,1,-1}$  is changed to:

$$J_{1,1,1,-1}^{\text{cr}} = \frac{1}{2} \left( J_{0,1,1,0}^{\text{cr}} + J_{1,1,0,0}^{\text{cr}} \right) - \left[ \frac{1}{4} Q^2 - \frac{1}{2} (m_1^2 + m_3^2) - \frac{1}{4} P_t^2 + m_4^2 \right] J_{1,1,1,0}^{\text{cr}} - P_t^\mu \int d^n q \frac{q_\mu}{d_1 d_2 d_3}. \quad (5.19)$$

The tensor integrals on the RHS will be evaluated in Section 5.7.

## 5.6 “Three-point” tensor integrals (uncrossed box)

Let us evaluate the tensor integrals we just encountered. Due to the Lorentz covariance the first one can be written as (in the “**t**”-parametrization):

$$J_{0,1,1,1}^\mu \equiv \int d^n q' \frac{q'_\mu}{d_2 d_3 d_4} = C_1^T T^\mu + C_1^{V_d} V_d^\mu, \quad (5.20)$$

where the  $C$ 's are some Lorentz scalars<sup>5</sup>. To obtain these scalars, dot the latter equation by  $T$  and  $V_d$ , which gives the  $2 \times 2$  linear system:

$$\begin{aligned} T \cdot J &\equiv \int d^n q' \frac{q'T}{d_2 d_3 d_4} = C_1^T T^2 + C_1^{V_d} T V_d, \\ V_d \cdot J &\equiv \int d^n q' \frac{q'V_d}{d_2 d_3 d_4} = C_1^T T V_d + C_1^{V_d} V_d^2. \end{aligned} \quad (5.21)$$

Note, that the scalar products on the RHS are given by Eq. (5.11), while the integrals on the left can be further reduced with the help of Eq. (5.8). Indeed, substituting for  $q'T$  and  $q'V_d$  from the latter equalities, we get for the LHS:

$$\begin{aligned} T \cdot J &= \int d^n q' \frac{1}{d_2 d_3 d_4} \left[ \frac{1}{2}(d_2 - d_4) + \frac{1}{2}(m_2^2 - m_4^2) \right] \\ &= \frac{1}{2} (J_{0,0,1,1} - J_{0,1,1,0}) + \frac{1}{2} (m_2^2 - m_4^2) J_{0,1,1,1}, \\ V_d \cdot J &= \int d^n q' \frac{1}{d_2 d_3 d_4} \left[ d_3 - \frac{1}{2}(d_2 + d_4) + \frac{1}{4}(T^2 - V_d^2) + \frac{1}{2}(2m_3^2 - m_2^2 - m_4^2) \right] \\ &= J_{0,1,0,1} - \frac{1}{2} (J_{0,0,1,1} + J_{0,1,1,0}) + \left[ \frac{1}{4}(T^2 - V_d^2) + \frac{1}{2}(2m_3^2 - m_2^2 - m_4^2) \right] J_{0,1,1,1}. \end{aligned}$$

Thus, to complete the reduction one can just substitute the latter relations in the solution of the system (5.21):

$$C_1^T = \frac{V_d^2(T \cdot J) - T V_d(V_d \cdot J)}{T^2 V_d^2 - (T V_d)^2}, \quad C_1^{V_d} = \frac{T^2(V_d \cdot J) - T V_d(T \cdot J)}{T^2 V_d^2 - (T V_d)^2}.$$

Similarly, for the integral

$$J_{1,1,0,1}^\mu \equiv \int d^n q' \frac{q'_\mu}{d_1 d_2 d_4} = C_3^T T^\mu + C_3^{V_u} V_u^\mu \quad (5.22)$$

the linear system is:

$$\begin{aligned} T \cdot J &\equiv \int d^n q' \frac{q'T}{d_2 d_3 d_4} = C_3^T T^2 + C_3^{V_u} T V_u, \\ V_u \cdot J &\equiv \int d^n q' \frac{q'V_u}{d_2 d_3 d_4} = C_3^T T V_u + C_3^{V_u} V_u^2; \end{aligned} \quad (5.23)$$

the simplest way to obtain this system is to substitute  $d_3 \leftrightarrow d_1$  or, equivalently,  $m_3 \leftrightarrow m_1$ ,  $V_d \leftrightarrow V_u$  in Eqs. (5.20) and (5.21), which also amounts to  $\nu_3 \leftrightarrow \nu_1$  in the integrals on the LHS of the linear system. Consequently, the solution of the system (5.23) is given by:

$$C_3^T = \frac{V_u^2(T \cdot J) - T V_u(V_u \cdot J)}{T^2 V_u^2 - (T V_u)^2}, \quad C_3^{V_u} = \frac{T^2(V_u \cdot J) - T V_u(T \cdot J)}{T^2 V_u^2 - (T V_u)^2},$$

---

<sup>5</sup>In the “s”-parametrization we would have *three* independent momenta on the RHS of Eq. 5.20, that is why the “t” one is preferable here.

with

$$\begin{aligned}
T \cdot J &= \int d^n q' \frac{1}{d_1 d_2 d_4} \left[ \frac{1}{2} (d_2 - d_4) + \frac{1}{2} (m_2^2 - m_4^2) \right] \\
&= \frac{1}{2} (J_{1,0,0,1} - J_{1,1,0,0}) + \frac{1}{2} (m_2^2 - m_4^2) J_{1,1,0,1} , \\
V_u \cdot J &= \int d^n q' \frac{1}{d_1 d_2 d_4} \left[ d_1 - \frac{1}{2} (d_2 + d_4) + \frac{1}{4} (T^2 - V_u^2) + \frac{1}{2} (2m_1^2 - m_2^2 - m_4^2) \right] \\
&= J_{0,1,0,1} - \frac{1}{2} (J_{1,0,0,1} + J_{1,1,0,0}) + \left[ \frac{1}{4} (T^2 - V_u^2) + \frac{1}{2} (2m_1^2 - m_2^2 - m_4^2) \right] J_{1,1,0,1} .
\end{aligned}$$

The remaining two tensor integrals of this kind are easily reduced in the “s”-parametrization. That is, for the integral

$$J_{1,0,1,1}^\mu \equiv \int d^n q \frac{q^\mu}{d_1 d_3 d_4} = C_2^Q Q^\mu + C_2^{P_t} P_t^\mu \quad (5.24)$$

we have to solve the system:

$$\begin{aligned}
Q \cdot J &\equiv \int d^n q \frac{qQ}{d_1 d_3 d_4} = C_2^Q Q^2 + C_2^{P_t} Q P_t , \\
P_t \cdot J &\equiv \int d^n q \frac{q P_t}{d_1 d_3 d_4} = C_2^Q Q P_t + C_2^{P_t} P_t^2 .
\end{aligned} \quad (5.25)$$

With Eq. (5.4) the LHS can be expressed as:

$$\begin{aligned}
Q \cdot J &= \int d^n q \frac{1}{d_1 d_3 d_4} \left[ \frac{1}{2} (d_3 - d_1) + \frac{1}{2} (m_3^2 - m_1^2) \right] \\
&= \frac{1}{2} (J_{1,0,0,1} - J_{0,0,1,1}) + \frac{1}{2} (m_3^2 - m_1^2) J_{1,0,1,1} , \\
P_t \cdot J &= \int d^n q \frac{1}{d_1 d_3 d_4} \left[ d_4 - \frac{1}{2} (d_1 + d_3) + \frac{1}{4} (Q^2 - P_t^2) + \frac{1}{2} (2m_4^2 - m_1^2 - m_3^2) \right] \\
&= J_{1,0,1,0} - \frac{1}{2} (J_{0,0,1,1} + J_{1,0,0,1}) + \left[ \frac{1}{4} (Q^2 - P_t^2) + \frac{1}{2} (2m_4^2 - m_1^2 - m_3^2) \right] J_{1,0,1,1} ,
\end{aligned}$$

and the solution of (5.25) is given by:

$$C_2^Q = \frac{P_t^2 (Q \cdot J) - Q P_t (P_t \cdot J)}{Q^2 P_t^2 - (Q P_t)^2} , \quad C_2^{P_t} = \frac{Q^2 (P_t \cdot J) - Q P_t (Q \cdot J)}{Q^2 P_t^2 - (Q P_t)^2} .$$

Finally, the integral

$$J_{1,1,1,0}^\mu \equiv \int d^n q \frac{q^\mu}{d_1 d_2 d_3} = C_4^Q Q^\mu + C_4^{P_g} P_g^\mu \quad (5.26)$$

gives rise to the system:

$$\begin{aligned}
Q \cdot J &\equiv \int d^n q \frac{qQ}{d_1 d_2 d_3} = C_4^Q Q^2 + C_4^{P_g} Q P_g , \\
P_g \cdot J &\equiv \int d^n q \frac{q P_g}{d_1 d_2 d_3} = C_4^Q Q P_g + C_4^{P_g} P_g^2 ;
\end{aligned} \quad (5.27)$$

again, to get this system one may just substitute  $d_4 \leftrightarrow d_2$  or, equivalently,  $m_4 \leftrightarrow m_2$ ,  $P_t \leftrightarrow P_g$  in Eqs. (5.24) and (5.25), which also changes indices  $\nu_3 \leftrightarrow \nu_1$  in the integrals on the LHS of the linear system. The solution for the coefficients entering in Eqs. (5.27) is:

$$C_4^Q = \frac{P_g^2(Q \cdot J) - QP_g(P_g \cdot J)}{Q^2P_g^2 - (QP_g)^2}, \quad C_4^{P_g} = \frac{Q^2(P_g \cdot J) - QP_g(Q \cdot J)}{Q^2P_g^2 - (QP_g)^2},$$

with

$$\begin{aligned} Q \cdot J &= \int d^n q \frac{1}{d_1 d_2 d_3} \left[ \frac{1}{2}(d_3 - d_1) + \frac{1}{2}(m_3^2 - m_1^2) \right] \\ &= \frac{1}{2} \left( J_{1,1,0,0} - J_{0,1,1,0} \right) + \frac{1}{2} (m_3^2 - m_1^2) J_{1,1,1,0}, \\ P_g \cdot J &= \int d^n q \frac{1}{d_1 d_2 d_3} \left[ d_2 - \frac{1}{2}(d_1 + d_3) + \frac{1}{4}(Q^2 - P_g^2) + \frac{1}{2}(2m_2^2 - m_1^2 - m_3^2) \right] \\ &= J_{1,0,1,0} - \frac{1}{2} \left( J_{0,1,1,0} + J_{1,1,0,0} \right) + \left[ \frac{1}{4}(Q^2 - P_g^2) + \frac{1}{2}(2m_2^2 - m_1^2 - m_3^2) \right] J_{1,1,1,0}. \end{aligned}$$

Thus, any “three-point” integral with one tensor index (for uncrossed box) one can encounter in these calculations can be reduced to conventional  $J$ 's with positive indices. In the next section we do this reduction for similar integrals arising from crossed boxes.

## 5.7 “Three-point” tensor integrals (crossed box)

The reduction formulae for the “crossed” tensor integrals can be obtained from the “uncrossed” ones by using the variable substitutions which connect the crossed and uncrossed parametrizations. Indeed, employing the Lorentz-covariance in exactly the same way as in the previous Section, but in the “ $\mathbf{tx}$ ”-parametrization, one can write:

$$J_{0,1,1,1}^{\text{cr}\mu} \equiv \int d^n q' \frac{q'_\mu}{d_2 d_3 d_4} = C_1^U U^\mu + C_1^{W_d} W_d^\mu. \quad (5.28)$$

It is easy to see that the latter integral is obtained from (5.20) by the change:  $V_{u,v} \rightarrow W_{u,v}$ ,  $T \rightarrow U$  (from “ $\mathbf{t}$ ” to “ $\mathbf{tx}$ ”). Thus,

$$C_1^U = \frac{W_d^2(U \cdot J^{\text{cr}}) - UW_d(W_d \cdot J^{\text{cr}})}{U^2W_d^2 - (UW_d)^2}, \quad C_1^{W_d} = \frac{U^2(W_d \cdot J^{\text{cr}}) - UW_d(U \cdot J)^{\text{cr}}}{U^2W_d^2 - (UW_d)^2},$$

with:

$$\begin{aligned} U \cdot J^{\text{cr}} &= \frac{1}{2} \left( J_{0,0,1,1}^{\text{cr}} - J_{0,1,1,0}^{\text{cr}} \right) + \frac{1}{2} (m_2^2 - m_4^2) J_{0,1,1,1}^{\text{cr}}, \\ W_d \cdot J^{\text{cr}} &= J_{0,1,0,1}^{\text{cr}} - \frac{1}{2} \left( J_{0,0,1,1}^{\text{cr}} + J_{0,1,1,0}^{\text{cr}} \right) + \left[ \frac{1}{4}(U^2 - W_d^2) + \frac{1}{2}(2m_3^2 - m_2^2 - m_4^2) \right] J_{0,1,1,1}^{\text{cr}}. \end{aligned}$$

Similarly, to obtain the result for

$$J_{1,1,0,1}^{\text{cr}\mu} \equiv \int d^n q' \frac{q'_\mu}{d_1 d_2 d_4} = C_3^U U^\mu + C_3^{W_u} W_u^\mu, \quad (5.29)$$

one performs the same substitution  $V_{u,v} \rightarrow W_{u,v}$ ,  $T \rightarrow U$  in the expressions for the integral (5.22), obtaining

$$C_3^U = \frac{W_u^2(U \cdot J^{\text{cr}}) - UW_u(W_u \cdot J^{\text{cr}})}{U^2W_u^2 - (UW_u)^2}, \quad C_3^{W_u} = \frac{U^2(W_u \cdot J^{\text{cr}}) - UW_u(U \cdot J^{\text{cr}})}{U^2W_u^2 - (UW_u)^2},$$

where

$$\begin{aligned} U \cdot J^{\text{cr}} &= \frac{1}{2} \left( J_{1,0,0,1}^{\text{cr}} - J_{1,1,0,0}^{\text{cr}} \right) + \frac{1}{2} (m_2^2 - m_4^2) J_{1,1,0,1}^{\text{cr}}, \\ W_u \cdot J^{\text{cr}} &= J_{0,1,0,1}^{\text{cr}} - \frac{1}{2} \left( J_{1,0,0,1}^{\text{cr}} + J_{1,1,0,0}^{\text{cr}} \right) + \left[ \frac{1}{4} (U^2 - W_u^2) + \frac{1}{2} (2m_1^2 - m_2^2 - m_4^2) \right] J_{1,1,0,1}^{\text{cr}}. \end{aligned}$$

The last two integrals shall be done in the “**sx**”-parametrization. If we expand the “crossed” integral as

$$J_{1,0,1,1}^{\text{cr}\mu} \equiv \int d^n q \frac{q_\mu}{d_1 d_3 d_4} = \tilde{C}_2^Q Q^\mu + \tilde{C}_2^{P_t} P_t^\mu \quad (5.30)$$

the appearance of the linear system for the coefficients  $\tilde{C}_2^Q$  and  $\tilde{C}_2^{P_t}$  is the same as that of (5.25), and, therefore, the solution has the same form:

$$\tilde{C}_2^Q = \frac{P_t^2(Q \cdot J^{\text{cr}}) - QP_t(P_t \cdot J^{\text{cr}})}{Q^2P_t^2 - (QP_t)^2}, \quad \tilde{C}_2^{P_t} = \frac{Q^2(P_t \cdot J^{\text{cr}}) - QP_t(Q \cdot J^{\text{cr}})}{Q^2P_t^2 - (QP_t)^2},$$

while the scalar products with integrals are changed according to the  $P_t \rightarrow -P_t$  rule (which changes “**s**” to “**sx**”):

$$\begin{aligned} Q \cdot J^{\text{cr}} &= \frac{1}{2} \left( J_{1,0,0,1}^{\text{cr}} - J_{0,0,1,1}^{\text{cr}} \right) + \frac{1}{2} (m_3^2 - m_1^2) J_{1,0,1,1}^{\text{cr}}, \\ P_t \cdot J^{\text{cr}} &= -J_{1,0,1,0}^{\text{cr}} + \frac{1}{2} \left( J_{0,0,1,1}^{\text{cr}} + J_{1,0,0,1}^{\text{cr}} \right) - \left[ \frac{1}{4} (Q^2 - P_t^2) + \frac{1}{2} (2m_4^2 - m_1^2 - m_3^2) \right] J_{1,0,1,1}^{\text{cr}}. \end{aligned}$$

Finally, since the integral

$$J_{1,1,1,0}^{\text{cr}\mu} \equiv \int d^n q \frac{q_\mu}{d_1 d_2 d_3} = C_4^Q Q^\mu + C_4^{P_g} P_g^\mu \quad (5.31)$$

does not depend on  $P_t$ , it numerically equals the  $J_{1,1,1,0}^\mu$  in (5.26), and one may use the reduction formulae given for the latter integral in Section 5.6. Moreover, there is no need to substitute the “**cr**” superscript to the latter formulae, since, as we already mentioned, for  $\nu_4 = 0$  the crossed and uncrossed integrals are always equal:  $J_{\nu_1, \nu_2, \nu_3, 0}^{\text{cr}} \equiv J_{\nu_1, \nu_2, \nu_3, 0}$ .

## 5.8 “Three-point” $J$ with one negative index

Consider the integral:

$$I = \int d^n q \frac{d_a}{d_b d_c} \equiv \int d^n q \frac{d_a \left( q + \frac{1}{2}A \right)}{d_b \left( q + \frac{1}{2}B \right) d_c \left( q + \frac{1}{2}C \right)}, \quad (5.32)$$

where the indices  $a, b, c$  refer to different inner loop lines (1, 2, 3, or 4, see Fig. 5.1), and it is implied that one of the parametrizations from Section 5.2 is used (“**s**”, “**sx**”, “**t**” or “**tx**”). It

means that  $A, B$  and  $C$  denote some of the momenta  $Q, T, U$  or  $P, V, W$  from Fig. 5.1 up to a sign, as (depending on which parametrization is chosen) dictated by one of the relations: (5.3), (5.5), (5.7), or (5.9).

To reduce this integral to a set of standard ones, let us first introduce two new momenta:

$$\begin{aligned} \alpha &= \frac{1}{2}(B + C), \quad \beta = \frac{1}{2}(B - C), \\ \text{so that: } B &= \alpha + \beta, \quad C = \alpha - \beta, \end{aligned} \quad (5.33)$$

and

$$I = \int d^n q \frac{d_a(q + \frac{1}{2}A)}{d_b(q + \frac{1}{2}(\alpha + \beta)) d_c(q + \frac{1}{2}(\alpha - \beta))}.$$

Then shift the integration variables  $q \rightarrow q + \frac{1}{2}\alpha = k$ :

$$I = \int d^n k \frac{d_a(k + \frac{1}{2}(A - \alpha))}{d_b(k + \frac{1}{2}\beta) d_c(k - \frac{1}{2}\beta)}.$$

Now, let us expand  $d_a$  in the numerator:

$$I = \int d^n k \frac{k^2 + k(A - \alpha) + \frac{1}{4}(A - \alpha)^2 - m_a^2}{\tilde{d}_b \tilde{d}_c}, \quad (5.34)$$

where for brevity we write  $\tilde{d}_b$  and  $\tilde{d}_c$  instead of  $d_b(k + \frac{1}{2}\beta)$  and  $d_c(k - \frac{1}{2}\beta)$ , respectively.

The first term in the numerator can be expressed as follows:

$$k^2 = \frac{1}{2}(\tilde{d}_b + \tilde{d}_c) + \frac{1}{2}(m_b^2 + m_c^2) - \frac{1}{4}\beta^2,$$

hence, if one changes the integration variable back to  $q$  on the RHS:

$$\int d^n k \frac{k^2}{\tilde{d}_b \tilde{d}_c} = \frac{1}{2}(J_c + J_b) + \left( \frac{1}{2}(m_b^2 + m_c^2) - \frac{1}{4}\beta^2 \right) J_{bc}, \quad (5.35)$$

where the subscript of  $J_{jk\dots}$  indicates "1" at the position number  $j, k \dots$ , the rest are zeros.

Next, the term linear in  $k$  can be evaluated as follows. Due to Lorentz covariance

$$\int d^n k \frac{k^\mu}{d_b(k + \frac{1}{2}\beta) d_c(k - \frac{1}{2}\beta)} = W \beta^\mu, \quad (5.36)$$

where  $W$  is some scalar function of momenta, masses and dimension. Dotting Eq. (5.36) by  $\beta_\mu$ , and expressing

$$k\beta = \frac{1}{2}(\tilde{d}_b - \tilde{d}_c + m_b^2 - m_c^2),$$

one gets:

$$W = \frac{1}{\beta^2} \int d^n k \frac{k\beta}{\tilde{d}_b \tilde{d}_c} = \frac{1}{2\beta^2} (J_c - J_b + (m_b^2 - m_c^2) J_{bc})$$

(assuming again that the variable is shifted back to  $q$ ). Therefore

$$\int d^n k \frac{k^\mu}{\tilde{d}_b \tilde{d}_c} = \frac{\beta^\mu}{2\beta^2} (J_c - J_b) + \frac{\beta^\mu}{2\beta^2} (m_b^2 - m_c^2) J_{bc}$$

and, hence:

$$\int d^n k \frac{k(A-\alpha)}{\tilde{d}_b \tilde{d}_c} = \frac{(A-\alpha)\beta}{2\beta^2} (J_c - J_b) + \frac{(A-\alpha)\beta}{2\beta^2} (m_b^2 - m_c^2) J_{bc} .$$

Finally, the last two terms in the numerator of Eq. (5.34) trivially result in a contribution proportional to  $J_{bc}$ .

Collecting all the above contributions, one gets:

$$\begin{aligned} I &= \frac{1}{2}(J_c + J_b) + \left( \frac{1}{2}(m_b^2 + m_c^2) - \frac{1}{4}\beta^2 \right) J_{bc} + \frac{(A-\alpha)\beta}{2\beta^2} (J_c - J_b) + \frac{(A-\alpha)\beta}{2\beta^2} (m_b^2 - m_c^2) J_{bc} \\ &\quad + \left( \frac{1}{4}(A-\alpha)^2 - m_a^2 \right) J_{bc} \\ &= \frac{1}{2} \left( 1 - \frac{(A-\alpha)\beta}{\beta^2} \right) J_b + \frac{1}{2} \left( 1 + \frac{(A-\alpha)\beta}{\beta^2} \right) J_c \\ &\quad + \frac{1}{2} \left\{ (m_b^2 + m_c^2 - 2m_a^2) + \frac{(A-\alpha)\beta}{\beta^2} (m_b^2 - m_c^2) + \frac{1}{2} [(A-\alpha)^2 - \beta^2] \right\} J_{bc} . \end{aligned} \quad (5.37)$$

As usual, regularization is implicitly assumed where necessary.

It is also useful to rewrite Eq. (5.37) solely in terms of  $A, B, C$ . Using (5.33) one gets:

$$\frac{(A-\alpha)\beta}{\beta^2} = \frac{(2A-B-C)(B-C)}{(B-C)^2}, \quad (A-\alpha)^2 - \beta^2 = (A-B)(A-C),$$

and

$$1 \pm \frac{(A-\alpha)\beta}{\beta^2} = \frac{(B-C)[B-C \pm (2A-B-C)]}{(B-C)^2} ;$$

the last expression on the RHS is equal to

$$\begin{aligned} &2 \frac{(B-C)(A-C)}{(B-C)^2} \quad \text{in case of "+" , and} \\ &2 \frac{(B-C)(B-A)}{(B-C)^2} \quad \text{in case of "-" .} \end{aligned}$$

Thus:

$$\begin{aligned} I &= \frac{(B-C)(B-A)}{(B-C)^2} J_b + \frac{(B-C)(A-C)}{(B-C)^2} J_c \\ &\quad + \frac{1}{2} \left\{ (m_b^2 + m_c^2 - 2m_a^2) + \frac{(B-C)(2A-B-C)}{(B-C)^2} (m_b^2 - m_c^2) \right. \\ &\quad \left. + \frac{1}{2}(A-B)(A-C) \right\} J_{bc} . \end{aligned} \quad (5.38)$$

Further rearrangement is hardly needed.



Let us now work out some particular cases of interest. Consider the integral

$$J(-1, 0, 1, 1) \equiv \int d^n q \frac{d_1}{d_3 d_4} \quad (5.39)$$

in the "s"-parametrization, so  $d$ 's are given by Eq. (5.3). Comparing it with the general formula (5.32), we establish the correspondence (below  $P \equiv P_t$ ):

$$\begin{aligned} a = 1, \quad A = -Q, \quad b = 3, \quad B = Q, \quad c = 4, \quad C = P; \\ B - C = Q - P, \quad B - A = 2Q, \\ A - C = -(Q + P), \quad 2A - B - C = -3Q - P. \end{aligned}$$

Then Eq. (5.38) gives:

$$\begin{aligned} J(-1, 0, 1, 1) = & 2 \frac{(Q-P)Q}{(Q-P)^2} J(0, 0, 1, 0) - \frac{(Q-P)(Q+P)}{(Q-P)^2} J(0, 0, 0, 1) \\ & + \frac{1}{2} \left\{ m_3^2 + m_4^2 - 2m_1^2 - \frac{(Q-P)(3Q+P)}{(Q-P)^2} (m_3^2 - m_4^2) \right. \\ & \left. + Q(Q+P) \right\} J(0, 0, 1, 1) \end{aligned} \quad (5.40)$$

Another integral,

$$J(1, 0, -1, 1) \equiv \int d^n q \frac{d_3}{d_1 d_4}, \quad (5.41)$$

is obtained from (5.39)–(5.40) by the substitution  $d_1 \leftrightarrow d_3$ , which is equivalent to  $Q \rightarrow -Q$  and  $m_1 \leftrightarrow m_3$ . Thus,

$$\begin{aligned} J(1, 0, -1, 1) = & 2 \frac{(Q+P)Q}{(Q+P)^2} J(1, 0, 0, 0) - \frac{(Q+P)(Q-P)}{(Q+P)^2} J(0, 0, 0, 1) \\ & + \frac{1}{2} \left\{ m_1^2 + m_4^2 - 2m_3^2 - \frac{(Q+P)(3Q-P)}{(Q+P)^2} (m_1^2 - m_4^2) \right. \\ & \left. + Q(Q-P) \right\} J(1, 0, 0, 1). \end{aligned} \quad (5.42)$$

Similarly, for the integral

$$J(1, 0, 1, -1) \equiv \int d^n q \frac{d_4}{d_1 d_3} \quad (5.43)$$

the correspondence with Eq. (5.32) gives:

$$\begin{aligned} a = 4, \quad A = P, \quad b = 1, \quad B = -Q, \quad c = 3, \quad C = Q; \\ B - C = -2Q, \quad B - A = -(Q + P), \\ A - C = P - Q, \quad 2A - B - C = 2P; \end{aligned}$$

which leads to:

$$\begin{aligned} J(1, 0, 1, -1) = & \frac{Q(P+Q)}{2Q^2} J(1, 0, 0, 0) - \frac{Q(P-Q)}{2Q^2} J(0, 0, 1, 0) \\ & + \frac{1}{2} \left\{ m_1^2 + m_3^2 - 2m_4^2 - \frac{QP}{Q^2} (m_1^2 - m_3^2) \right. \\ & \left. + \frac{1}{2} (P+Q)(P-Q) \right\} J(1, 0, 1, 0). \end{aligned} \quad (5.44)$$

Other "three-point" integrals of this kind can be evaluated in the same manner employing Eq. (5.32), however they were not encountered in algebraic calculations in the heavy slepton limit.

## 5.9 $J$ with two Lorentz indices

Finally, let us consider the tensor integral with two Lorentz indices: integrals with three and more indices do not arise in the calculation of the observable (2.17). To simplify the formulae, we demonstrate the reduction procedure on the integral with three propagators (which comes both from boxes and from triangle loops) in the "s"-parametrization (see Sec. 5.2).

It is easy to see that the only case where the two-index tensor structure cannot be factored out of the integration operation is represented by the following integral:

$$J^{\mu_1\mu_2} \equiv \int d^n q \frac{q^{\mu_1} q^{\mu_2}}{d_1 d_3 d_4}, \quad (5.45)$$

which, by Lorentz invariance can always be expanded as (denoting  $P \equiv P_t$ ):

$$J^{\mu_1\mu_2} = g^{\mu_1\mu_2} D_{00} + Q^{\mu_1} Q^{\mu_2} D_{QQ} + P^{\mu_1} P^{\mu_2} D_{PP} + (P^{\mu_1} Q^{\mu_2} + Q^{\mu_1} P^{\mu_2}) D_{PQ}. \quad (5.46)$$

Now, contracting the latter equality with  $g_{\mu_1\mu_2}$  we get:

$$\int d^n q \frac{q^2}{d_1 d_3 d_4} = n D_{00} + Q^2 D_{QQ} + P^2 D_{PP} + 2(P \cdot Q) D_{PQ}; \quad (5.47)$$

contracting with  $Q_{\mu_1} Q_{\mu_2}$  gives:

$$\int d^n q \frac{(q \cdot Q)^2}{d_1 d_3 d_4} = Q^2 D_{00} + (Q^2)^2 D_{QQ} + (Q \cdot P)^2 D_{PP} + 2(P \cdot Q) Q^2 D_{PQ}; \quad (5.48)$$

contracting with  $P_{\mu_1} P_{\mu_2}$  gives:

$$\int d^n q \frac{(q \cdot P)^2}{d_1 d_3 d_4} = P^2 D_{00} + (P \cdot Q)^2 D_{QQ} + (P^2)^2 D_{PP} + 2P^2 (P \cdot Q) D_{PQ}; \quad (5.49)$$

and, finally, contracting with  $(P_{\mu_1} Q_{\mu_2} + Q_{\mu_1} P_{\mu_2})$  and canceling overall factor of two we get:

$$\begin{aligned} \int d^n q \frac{(q \cdot P)(q \cdot Q)}{d_1 d_3 d_4} &= (P \cdot Q) D_{00} + (P \cdot Q) Q^2 D_{QQ} + (P \cdot Q) P^2 D_{PP} \\ &\quad + [P^2 Q^2 + (Q \cdot P)^2] D_{PQ}. \end{aligned} \quad (5.50)$$

The Equations (5.47)–(5.50) form a linear system for four scalar variables:  $D_{00}$ ,  $D_{QQ}$ ,  $D_{PP}$ , and  $D_{PQ}$ . It is easy to check that the solution exist (e.g., the determinant is non-zero), and hence these four quantities are uniquely defined as linear functions of the *scalar* integrals that stand in the LHS of the equations. The latter integrals are of the type that we have evaluated in previous sections. Thus, the initial tensor integral (5.45) got reduced to the basic  $J$ 's with positive indices. It is easy to see that this also holds for all other loop momenta parametrizations defined in Section 5.2.

The integral with four propagators in the denominator is handled in completely analogous way: the linear system just becomes bigger (as there are more independent Lorentz tensors in the box).

This Section completes the demonstration of the integral reduction: as one can see, all the integrals encountered in calculations of the 1-loop observable (2.17) got reduced to  $J$ 's with positive indices. The latter can be computed numerically.

Since the considered 1-loop observable is finite, the final result does not depend on the regularization. This was further confirmed by cancellation of the divergent integral parts in the final result.



## Chapter 6

# Box contributions to CP-odd observables

### 6.1 Loop contribution overview

In Chapter 3 we have demonstrated that the tree-level cross section of the process (2.1) is CP even, even if the incoming  $e^+e^-$  beams are polarized. This makes it evident that many of the one-loop correction to the unpolarized cross-section  $d\sigma_0$  (cf. Eq. (2.13)) are actually being canceled in the CP-odd part of the 1-loop cross-section:  $d\sigma_0^{\text{odd}}|_{1\text{ loop}}$ , the numerator of the observable (2.17).

Indeed, the external wave function renormalization is multiplicative, so the propagator corrections result just in a propagator mass shift.<sup>1</sup> Therefore we do not need to calculate the two-point functions and, hence, neither Faddeev–Popov ghosts nor coloured particles will be involved. Thus, there are only two types of one-loop corrections that may contribute to  $d\sigma_0^{\text{odd}}$  (Eq. 2.16): the box diagrams and the tree diagrams from Fig. 3.1 with a triangle loop instead of one of the vertices. Both types of diagrams have been classified in Chapter 4. Before we take a closer look at the box diagrams (and later at the full 1-loop contribution), it is necessary to say a couple of words about the ultraviolet and infrared behavior of  $d\sigma_0^{\text{odd}}$  at the one-loop order.

As we mention in the end of Chapter 3,  $d\sigma_0^{\text{odd}}$  must be UV finite, since it vanishes at tree level: otherwise the counterterms required would mirror the tree level CP-odd contribution. So, no infinite (UV-divergent) counterterms are required. In fact, one can also see that any *finite* counterterm just results in corrections to the tree level vertices in Fig. 3.1. For example, in the  $Z$ -exchange term  $X_0(ZZ)$ , Eq. (3.17), only  $g_{v,a}$  and  $G_{v,a}$  (defined by Eqs. (C.9), (3.9) and Eqs. (C.15), (3.6), respectively) may get modified. Then, since the hermiticity property Eq. (C.16) should always hold (which is essential for C-transformation rules (3.19) to be valid), one can just duplicate the analysis of the Section 3.3 to see that the result will still be CP-even: no contributions to  $d\sigma_0^{\text{odd}}$  will arise. In exactly the same way one can check that the unpolarized cross section with sneutrino exchange will also be unaffected by potential

---

<sup>1</sup>It is a bit more tricky if one sticks to precise one-loop order and does not allow for the Dyson resummation in the propagators. Then each of the tree graphs (Fig. 3.1) acquires different functional (CP-even) multiplier. It is actually the structure of the tree-level result [27] that ensures in this case that CP-odd terms cannot arise. We do not demonstrate it here as we discard the sneutrino exchange graph, and, therefore, will get a multiplicative correction anyway.

UV-stabilizing counterterms.

These arguments also apply to finite counterterms which may be required to restore the symmetries of  $d\sigma_0^{\text{odd}}$  violated by regularization<sup>2</sup> in the so-called algebraic renormalization approach [30]. So, at least for the unpolarized cross section, one should not worry about the renormalization scheme (we assume that the on-shell normalization conditions are used) and the standard dimensional regularization will be adequate at the one loop order: all divergent pieces must cancel in  $d\sigma_0^{\text{odd}}$ .

The situation with infrared (IR) finiteness is slightly more complicated: there are many loops with massless particles inside. However, according to [30], all the IR singularities that appear at any loop order in our amplitude are of the standard type, namely, they arise due to the soft photons and cancel when real bremsstrahlung is accounted for. On the other hand, the bremsstrahlung photon emission from the tree diagram results in just an overall factor for the corresponding amplitude. Since the tree amplitude is CP-even, we conclude that  $d\sigma_0^{\text{odd}}$  is free of IR singularities.

Each possible box diagram (see Section 4.2) turns out to be UV-finite just by power counting. Since we assume heavy sleptons, any box with a slepton line can be neglected. Thus, in such approximation the only box diagrams that may contribute to Eq. (2.17) are those drawn in Fig. 4.8, Section 4.3. The contribution of these box graphs to  $d\sigma_0^{\text{odd}}$  will be evaluated in Section 6.2 below. Analytical results for the coefficients of the box type Passarino–Veltman-like functions presented in the next section<sup>3</sup> ensure that the CP-odd contribution from box diagrams can not be completely cancelled by graphs with triangle loop corrections and, hence, the CP-violation is indeed present in the unpolarized cross section. Further, in Section 6.3 we present some plots for the full 1-loop contribution<sup>4</sup> to the CP-odd observable (2.17). At last, in Section 6.4 we shortly discuss how the chargino decay can possibly affect the latter observable.

## 6.2 Analysis of box contributions

Loop amplitudes are conveniently evaluated in terms of Passarino–Veltman functions [51]. In [55] the cross section of the process (2.1) was parameterized in terms of those functions and calculated in various parameter points. However, the latter results were obtained assuming a CP-invariant theory (real couplings) and (to make the results compact) the reduction to scalar Passarino–Veltman functions was not done. Since only the scalar functions can be considered independent (differ from each other by singularity pattern) we performed this reduction in our formulae. Namely, using the relations we derived in Chapter 5 all integrals encountered in current calculations were reduced to a basic set of scalar (Passarino–Veltman) integrals.

At one loop order the cross section is defined by the conventional formula:

$$\frac{d\sigma}{d\Omega} = \frac{\beta}{64\pi^2 s} |\mathcal{M}^2|_{1\text{loop}}, \quad \beta \equiv \frac{|\mathbf{p}_{\text{out}}|}{|\mathbf{p}_{\text{in}}|}, \quad (6.1)$$

<sup>2</sup>There are, however, no such simple arguments for *polarized* amplitudes, as one of the potential CP-odd terms in this case is canceled due to the tree level SUSY relation between chargino and sneutrino couplings [27]. The symmetry-restoring counterterms may, in general, violate this relation and therefore can give an additional CP-odd term. We shall not discuss it here.

<sup>3</sup>These results were first presented in [35].

<sup>4</sup>Obtained in collaboration with K. Rolbiecki and J. Kalinowski: see [36].

where the “amplitude squared” involves both tree- and 1-loop-amplitude of the process:

$$|\mathcal{M}^2|_{1\text{loop}} = \mathcal{M}_{\text{tree}}^* \mathcal{M}_{1\text{loop}} + \mathcal{M}_{\text{tree}} \mathcal{M}_{1\text{loop}}^* .$$

Since in numerical studies we assumed heavy sleptons, the tree amplitude  $\mathcal{M}_{\text{tree}}$  contained only the  $s$ -channel  $Z$ -exchange graph of Fig. 3.1. Direct calculations show that the CP-odd part of  $|\mathcal{M}^2|_{1\text{loop}}$  acquires four-point (“box”) integral contributions. In particular, for the  $Z$ -exchange (uncrossed and crossed) box diagrams of Fig. 4.8, after reduction to scalar integrals one obtains (the subscript “D” refers to terms proportional to genuine box diagram functions, as defined below):

$$\begin{aligned} |\mathcal{M}^2|_{\substack{\text{CP-odd,} \\ \text{Z-box, D}}} &= \frac{1}{(2\pi)^4} 2 \operatorname{Re} \left[ \frac{ig^6 m_i m_j}{(4 \cos \theta_W)^6} (G_{Aij} G_{Vji} - G_{Aji} G_{Vij}) \right. \\ &\quad \times \left\{ g_A (g_A^2 + 3g_V^2) m_Z^2 (G_{Vii} I_{i;ji} + G_{Vjj} I_{j;ji}) \right. \\ &\quad + g_V (3g_A^2 + g_V^2) [(2m_i^2 - m_Z^2 - 2t) G_{Aii} I_{i;ji} \\ &\quad + (2m_j^2 - m_Z^2 - 2t) G_{Ajj} I_{j;ji}] \\ &\quad + g_A (g_A^2 + 3g_V^2) m_Z^2 (G_{Vii} I_{i;ji}^{\text{cr}} + G_{Vjj} I_{j;ji}^{\text{cr}}) \\ &\quad - g_V (3g_A^2 + g_V^2) [(2m_i^2 - m_Z^2 - 2u) G_{Aii} I_{i;ji}^{\text{cr}} \\ &\quad \left. \left. + (2m_j^2 - m_Z^2 - 2u) G_{Ajj} I_{j;ji}^{\text{cr}}] \right\} \right]. \end{aligned} \quad (6.2)$$

Here, as above,  $m_i, m_j$  are the chargino masses ( $i, j = 1, 2$ ); the other couplings are defined in Chapter 3. The origin of the factors is as follows: from the tree diagram there is a coupling  $g_V$  or  $g_A$  at the  $Zee$  vertex, and a  $G_{Vji}$  or  $G_{Aji}$  at the  $Z\chi_i\chi_j$  vertex, whereas the box diagrams contribute two  $Zee$  couplings ( $g_V^2, g_A^2$  or  $g_V g_A$ ), and two  $Z\chi\chi$  vertices, one of which will be diagonal in mass index ( $G_{Vii}, G_{Aii}, G_{Vjj}$  or  $G_{Ajj}$ ), and one will be non-diagonal ( $G_{Vij}, G_{Aij}, G_{Vji}$  or  $G_{Aji}$ ). The two non-diagonal  $Z\chi\chi$  couplings factor out as the combination

$$G_{Aij} G_{Vji} - G_{Aji} G_{Vij} = 2i \operatorname{Im} (G_{Aij} G_{Vji}) . \quad (6.3)$$

This quantity is shown in Fig. 6.1, for the set of parameters:

$$|\mu| = 300 \text{ GeV}, \quad M_2 = 200 \text{ GeV}. \quad (6.4)$$

We note that the quantity (6.3) increases with decreasing values of  $\tan \beta$ .

The integrals  $I$  and  $I^{\text{cr}}$  of Eq. (6.2) are the Passarino–Veltman-like scalar four-point functions which correspond to “normal” and “crossed” box diagrams in Fig. 4.8, respectively. In the notations of Chapter 5 they are:

$$I_{k;ij} \equiv J_{1,1,1,1}(i, j), \quad I_{k;ij}^{\text{cr}} \equiv J_{1,1,1,1}^{\text{cr}}(i, j),$$

with  $m_1 = m_3 = m_Z, m_2 = m_e = 0$  (we used the zero electron-mass approximation), and  $m_4 = m_k$  (the mass of the chargino  $\tilde{\chi}_k, k = 1, 2$  at the right vertical propagator of the box loop). Note that according to Table 5.1:

$$J_{1,1,1,1}^{\text{cr}}(m_i, m_j) \stackrel{t \leftrightarrow u}{=} J_{1,1,1,1}(m_i, m_j).$$

In fact, the only diagrams from Figure 4.8 that actually bring  $J_{1,1,1,1}$  (or  $J_{1,1,1,1}^{\text{cr}}$ ) contribution to the observable (2.17) are the box diagrams with two  $Z$ - or two  $W$ -boson propagators

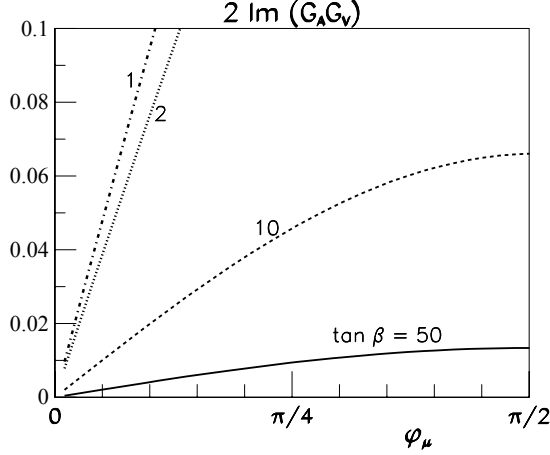


Figure 6.1: The couplings of Eq. (6.3) vs.  $\phi_\mu$  for various values of  $\tan\beta$ .

(both un-crossed and crossed). It turned out that the remaining diagrams from Figure 4.8 can bring only integrals with three (“triangle”-type) and less propagators in denominator. Indeed, the box diagram with two photon propagators (Fig. 4.8) obviously vanishes if the final charginos are different: this is just because the  $\gamma\tilde{\chi}_i\tilde{\chi}_j$  coupling is zero for  $m_i \neq m_j$  (by QED-like Ward identities: see, e.g., [37]; see also Appendix B). Further, it turned out that the CP-odd  $J_{1,1,1,1}$  coefficients arising from boxes with one photon and one Z-boson propagator add up to zero when all such diagrams are included. Note, however, that other  $J$ -integrals from the latter diagrams still contribute to the CP-odd part of the cross-sections. We do not write down the latter contributions here, as they shall be considered together with triangle diagrams. Besides, the expressions are very long and best handled numerically (see, e.g., Section 6.3 below).

The integrals  $I$  from Eq. (6.2) above are simply related to the conventional Passarino-Veltman function  $D$ :

$$\begin{aligned} I_{k;ij} &\equiv D(p_1, p_2, -k_2, -k_1, m_Z, 0, m_Z, m_{\chi_k}) \\ I_{k;ij}^{\text{cr}} &\equiv D(p_1, p_2, -k_1, -k_2, m_Z, 0, m_Z, m_{\chi_k}), \end{aligned}$$

where  $D$  is defined in [51] as

$$\begin{aligned} &D(l_1, l_2, l_3, l_4, m_1, m_2, m_3, m_4) \\ &\equiv \int d^4q \{ (q^2 - m_1^2)[(q + l_1)^2 - m_2^2][(q + l_1 + l_2)^2 - m_3^2][(q + l_1 + l_2 + l_3)^2 - m_4^2] \}^{-1}. \end{aligned} \quad (6.5)$$

Analogous, though more cumbersome, pieces follow from the box diagram with  $W$ -exchange (as we just mentioned, the  $D$ -pieces of the  $\gamma Z$ -exchange box diagrams cancel) and one can check that all these four-point integral contributions do not cancel each other. Besides,



two- and three-point integrals (denoted  $B$  and  $C$  in [51]) also appear after reduction of tensor box integrals stemming from the diagrams in Fig. 4.8. What is essential, is that while the graphs with triangle vertex corrections may contribute to  $B$  and  $C$  (and, possibly,  $A$  — the one-point) functions to  $d\sigma_0^{\text{odd}}$ , the  $D$  function can never appear in triangle diagrams. As the function  $D$  cannot be constructed out of  $A$ ,  $B$ ,  $C$  integrals and rational functions, *we may conclude that  $d\sigma_0^{\text{odd}}$  is non-zero at the one-loop order.*

Even assuming heavy sleptons the total box diagram contribution to  $d\sigma_0^{\text{odd}}$  is too lengthy<sup>5</sup> to provide here the complete formulae. Instead, to give an idea about the orders of magnitude, we shall provide some plots. We stress once more that the triangle loop corrections to the tree-level vertices are not accounted for in this Section, therefore the numbers given in this Section are purely illustrative. A similar plot for the full 1-loop observable is provided in Section 6.3. Below, the ratio (2.17) (with the amplitude  $\mathcal{M}_{1\text{ loop}}$  built solely of the diagrams in Fig. 4.8) is plotted as a function of the CP-violating phase  $\phi_\mu$ , which is the phase of the higgsino mass parameter  $\mu$ , (see Eq. (C.13)). For simplicity the U(1) gaugino mass parameter appearing in the neutralino mass matrix is taken to be real in the plots below:  $M_1 = 250$  GeV. The absolute values used for the remaining chargino and neutralino mass matrix parameters are given by Eq. (6.4).

Figure 6.2 shows the asymmetry resulting from the box diagrams (for the numerical work,

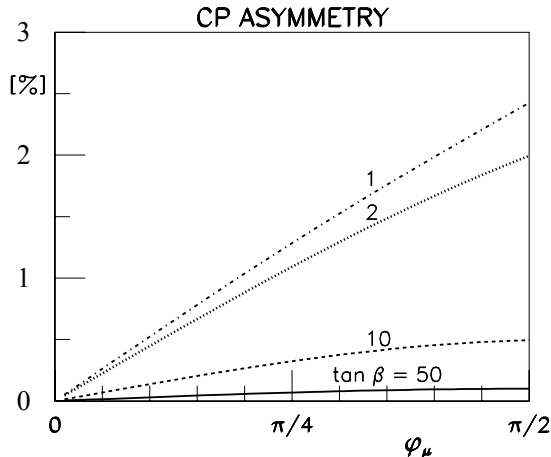


Figure 6.2: The ratio (2.17) at various values of  $\phi_\mu$  and  $\tan\beta$ . The polar scattering angle is  $\theta = \pi/3$  while  $\sqrt{s} = 600$  GeV.

we used the `LoopTools` [53, 54] package), as a function of  $\phi_\mu$ , for  $\sqrt{s} = 600$  GeV,  $\cos\theta = 0.5$  and a few values of  $\tan\beta$ . As anticipated, for  $|\phi_\mu| \ll 1$ , the effect is linear in  $\phi_\mu$ . Also, we note that the shape of these curves (i.e., dependence on  $\phi_\mu$  and  $\tan\beta$ ) is essentially given by the coupling constants (6.3) and shown in Fig. 6.1.

<sup>5</sup>For many algebraic manipulations REDUCE and MATLAB packages were used.

When the energy increases, the effect is reduced, as illustrated in Fig. 6.3, where we show

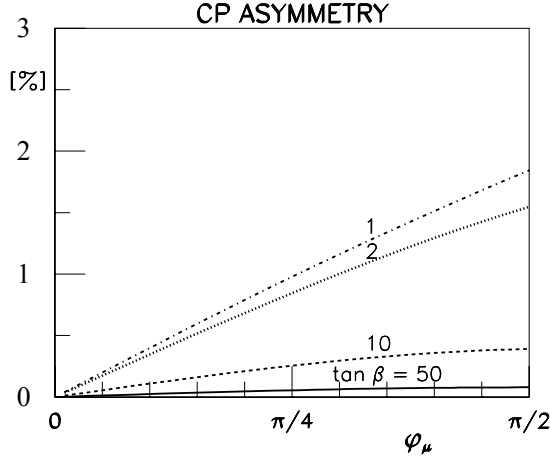


Figure 6.3: Same parameters as in Fig. 6.2, except  $\sqrt{s} = 800$  GeV.

similar plots for  $\sqrt{s} = 800$  GeV. The CP violation is related to the fact that the two charginos will have different velocities (due to different masses). At high energies, the difference in masses plays a lesser role.

The asymmetry demonstrates a smooth behaviour with respect to the polar angle (see Fig. 6.4).

Since the effect somehow is due to the fact that the two chargino mass states are different, one might think that it would vanish in the limit of equal chargino masses. This is not the case. First of all, because of the finite  $W$  mass, there is a minimum splitting among the two chargino masses. The splitting would only vanish in the limit of  $\mu M_2$  being real and negative, in which case there is no CP violation. Secondly, these coupling constants do not correlate very well with the mass difference,  $\Delta m = m_{\chi_2} - m_{\chi_1}$ . This is illustrated in Fig. 6.5, where we show the quantity (6.3) vs.  $\Delta m$ , for the cases of fixed  $M_2$  and fixed  $|\mu|$ , scanning over the other, and two values of  $\tan \beta$ .

Since triangle diagrams have not been accounted for in this section, the results given in Figs. 6.2–6.4 are not to be seen as quantitative results, they are of a purely illustrative character. However, since the kinematic structure of the triangle diagrams is different from that of the box diagrams, when included, these can not cancel the contributions of the box diagrams. Thus, we conclude that the CP-violating asymmetry in the unpolarized cross section is non-zero. Furthermore, as we show in the next Section, the effect, which depends on the phases of both  $\mu$  and  $M_1$ , is not dramatically altered by inclusion of the triangle loop corrections.

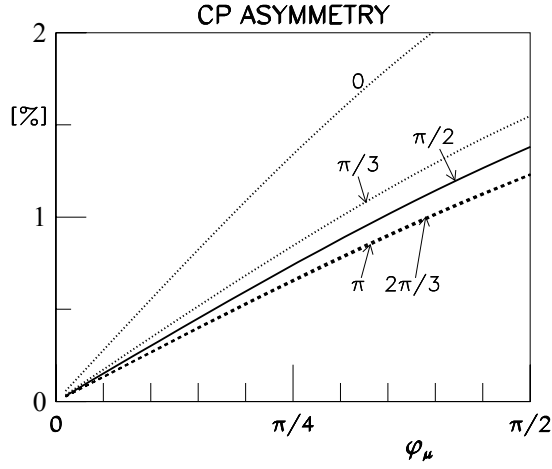


Figure 6.4: The ratio (2.17) for various values of the polar angle  $\theta$ . The other parameters are fixed as  $\tan\beta = 5$ ,  $\sqrt{s} = 800$  GeV.

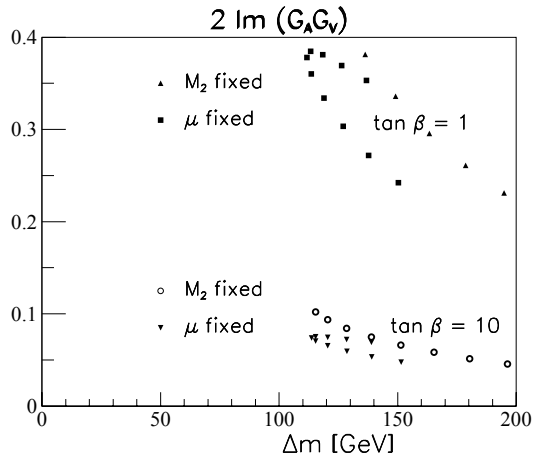


Figure 6.5: The couplings of Eq. (6.3) vs.  $\Delta m$ , for two values of  $\tan\beta$ . Some points are obtained with fixed  $|\mu| = 300$  GeV and varying  $M_2$ , others are obtained with fixed  $M_2 = 200$  GeV and varying  $|\mu|$ . In all cases  $\phi_\mu = \pi/2$ .

### 6.3 Full 1 loop CP-odd contribution

To obtain the complete one-loop result for the observable (2.15), one also needs to compute the (triangle) loop corrections for each of the tree-level vertices appearing in diagrams Fig. 3.1 (apart from the one with the Higgs coupling, which is negligible) assuming, of course, that higgsino and U(1) gaugino mass parameters are complex. Such a calculation involves 40–60 diagrams (depending on how one counts [55]), and the heavy-sneutrino limit does not lead to any obvious simplification. This calculation have been done in collaboration with K. Rolbieceki and J. Kalinowski (see [36]), exploring the code written by these authors (see, e.g., [34] and references therein).

In contrast to the box diagrams, individual triangle diagrams are divergent. However, as was argued above, since there is no contribution to the asymmetry (2.15) at the tree level, they have to combine to a finite quantity.

As was expected, the full result turns out to be of the same order as the “box-only estimates”. In Figure 6.6 the box-only and full one-loop values of the observable (2.17) are

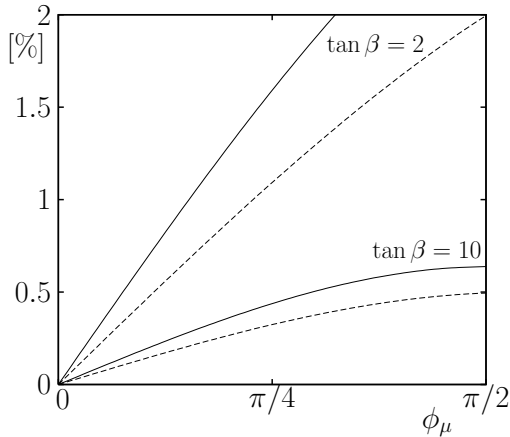


Figure 6.6: Box-only contribution (dashed lines) vs. full one-loop result (full lines) in the heavy sfermions limit for  $\tan\beta = 2$  and 10.

plotted as functions of the higgsino phase  $\phi_\mu$  for  $\tan\beta = 2$  and 10. The other parameters are taken as:  $\sqrt{s} = 600$  GeV, the polar scattering angle  $\theta = \pi/3$ , the higgsino mass parameter  $\mu = |\mu|e^{i\phi_\mu}$ ,  $|\mu| = 300$  GeV, the SU(2) gaugino mass parameter  $M_2 = 200$  GeV, the U(1) gaugino mass parameter (taken to be real)  $M_1 = 250$  GeV. The common SUSY breaking mass of the scalars (for the full one-loop calculation) is 1 TeV.

The qualitative agreement between the complete 1 loop result and the gauge box contribution alone can be (at least, partially) explained. Indeed, a closer look at the expression for the Z-boson exchange contribution (Eq. (6.2) gives the D-function part) shows, that only the imaginary part of the box integral can affect the observable. Since in the heavy slepton limit the position of the threshold singularity is high, the integral remains real in the kinematical region we consider.

The selectron exchange box diagram (Fig. 6.7) provides a nice illustration: when one raises

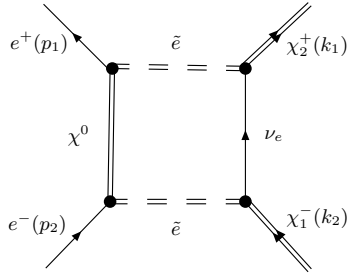


Figure 6.7: Selectron exchange box diagram.

the c.m. energy above the selectron pair production threshold the selectron box diagram develops an absorptive part and its contribution to the asymmetry (2.17) is non-zero, see Fig. 6.8 (the selectron mass is 403 GeV).

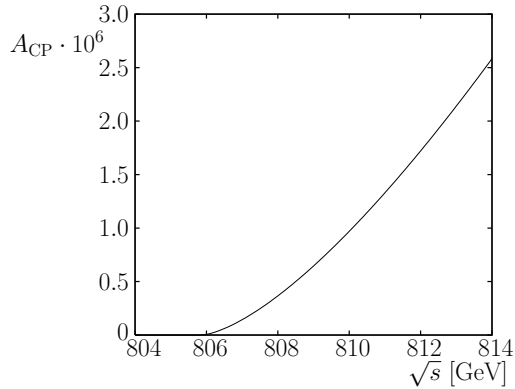


Figure 6.8: The contribution of the selectron exchange box diagram to the observable (2.17) (here denoted as  $A_{CP}$ ). The selectron mass is 403 GeV.

Similar statements can be made about most of the diagrams contributing to (2.17) at the one-loop order. That it why one could initially expect that the box diagrams alone will provide the major part of the contribution. Figure 6.8 confirms this.

It is important to note, however, that the above argument also indicates that in a scenario with lighter sparticles, other diagrams with vertex and self-energy corrections cannot be neglected. This is demonstrated in [34], where the authors, in particular, show that for the case of CP-violating origin in the top squark sector the box diagrams do not contribute and the CP asymmetry receives contributions only from vertex and self-energy diagrams. This is, however, a different sector of phenomenological parameters that we do not consider here.

## 6.4 Interference with chargino decay

Since charginos are not stable particles and decay finally to leptons/quarks and the LSP, in a realistic experiment one has to take into account also chargino decays. On the other hand it has been shown that in chargino decays it is also possible to obtain CP-violating effects at one-loop level [56]. Therefore one can worry if CP-violating effects in the decay would not cancel similar effects in the chargino production. However, a consideration similar to one presented in Section 6.2 helps here. As we demonstrated in that section, at the one-loop level the observable (2.17) among other pieces contains the  $D$ -function integral, which has very specific singularities in the complex space of kinematical variables. As long as this integral is not present in the chargino decay cross-sections, the analyticity dictates that the CP-violating effect we describe in this Thesis will be present, although, of course, it can be reduced (or enhanced) in some kinematical regions.

Indeed, to cancel such a contribution at *any* kinematical point, one needs a corresponding analytical contribution from the final particle decay. Thus, the only possible way is the box diagram (e.g., the  $Z$ - or  $W$ - exchange box as in Fig. 4.8) attached to one of the chargino external legs. But even if the mass splitting between charginos is larger than  $2m_Z$ , the kinematic configuration of the box diagram in the decay is completely different from the one in the production, so the cancellation of different CP-odd contributions is in general not possible.

To illustrate this statement, one can consider some specific cases. For example, the presence of CP-violation in chargino production becomes obvious if the mass splitting is smaller than  $2m_Z$  and no CP asymmetry arises in the decay due to double  $Z$  exchange diagram. Moreover, it was shown in [34] that it is even possible to arrange parameters in such a way that no 2-body decay channels remain open for charginos and therefore no CP-odd contribution due to chargino decays enter in the full production and decay process, but still allowing for CP-violating contributions to the observable (2.17).

## Chapter 7

# Conclusions

We considered the chargino creation process

$$e^+ + e^- \rightarrow \tilde{\chi}_i^+ + \tilde{\chi}_j^-$$

in the frame of most general phenomenological MSSM. We demonstrated that for this process it is possible to identify the CP-violating observable (2.15), which is sensitive to specific SUSY model parameters and, at the same time, does not depend on the spin/polarization of the initial beams. This observable, while vanishing at the tree level, gets its first contribution from 1 loop graphs and thus UV-finite. By analytical computation of the main contribution to this observable (1-loop box diagrams) in properly selected points of the parameter space, we demonstrated that the CP-violation effect is indeed non-zero, provided the higgsino mass parameter  $\mu$  is complex. Further, we verified the results by numerical computation of the full 1-loop approximation of the CP-asymmetry in the cross-section.

All calculations have been performed within the simplest version of unconstrained MSSM making no assumptions about the symmetry breaking mechanisms [32], neither do we impose any constraints on the CP-violating phases. To reduce the amount of diagrams, we did assume conservation of the lepton flavor and R-parity. Further to this, when doing the numerical simulations we selected the parameter points where all the sleptons are heavy. However, from the mere structure of the observable (2.15) and the obtained results (Chapter 6) one can see that it is easy to relax all these constraints. It is safe to state that even in the most general case the considered observable will not vanish, although it will acquire contributions from a much richer class of diagrams and may, of course, also be damped kinematically at some domains of the parameter space.

To test these theoretical predictions by an experiment, one first needs to confirm the existence of the supersymmetric particles (charginos  $\tilde{\chi}_i$ ). By the time of writing this Thesis, no SUSY particles were yet discovered. Further, one would need a machine capable of producing electron-positron beams with energies sufficient to pass the chargino creation threshold<sup>1</sup>. And, even when all these criteria are met, we still have to admit that from an experimentalist point of view, the chargino creation process analyzed in this Thesis is not an easy process to study. In one of the most commonly considered (today) scenarios where the lightest neutralino  $\tilde{\chi}_0$  is the Lightest Supersymmetric Particle (LSP), each chargino will typically decay to a charged lepton and a neutrino, plus the LSP, thus giving two invisible particles. At the same time, to

---

<sup>1</sup>More precisely, one needs the energies at which some of the box integrals analyzed in Chapter 6 develop the absorptive part; see the discussion in Section 6.3

measure the observable (2.15), one will obviously need to distinguish the outgoing particles (lepton, neutrino, and, perhaps, decay products of the unstable neutralino) created in the decay of charginos of different masses: see, e.g., (Eq. 2.16). So, it may turn out that the neutralino sector will be involved, which complicates the picture even further<sup>2</sup>.

The magnitude of CP-violation in hypothetical electron-positron collision experiment can also be affected not only by the “observable” (2.15), but also by many additional factors. As a simplest example, at the one-loop level, CP violation is also induced in the decay  $\tilde{\chi}_i^\pm \rightarrow \tilde{\chi}_1^0 W^\pm$  [26]. The CP violation resulting from the latter decay has a strong dependence on the phase of the soft-SUSY-breaking trilinear parameter  $A$ , in particular that involving the third-generation quarks and leptons.

In fact, if the heavier chargino is considerably heavier than the lighter one, it might be easier to observe CP-violation in the production of equal-mass charginos, using polarized beams [60], however the one-loop corrections to polarized amplitudes of this process require a separate study.

A straightforward way to probe for complex phases of the model (such as those of the higgsino mass parameter  $\mu$ ) would be to complete a whole model calculation of the process, including all final particles decay, and then test the results for the sensitivity to various input parameters. After this is done, the resulting cross-sections can be compared to experiment. For the chargino production discussed in this Thesis this task is too huge until some more parameters of the theory (such as  $\tan\beta$ ) are more strictly bounded by experimental observations.

However, apart from the theoretical interest, the results presented above have certain practical value. As we repeatedly emphasize, one of the main results presented in this Thesis (published in [35]) is the fact that CP-violation induced by SUSY model structure can potentially be tested in  $e^+e^-$  collisions *without* observing the polarization of the initial beams. Apart from the simplifications that this fact brings into the calculations of the cross-sections, it potentially increases the *number of CP-violating events* that can be produced in this (yet hypothetical) collision experiment. The International Linear Collider project [22] may make such experiments possible. In this respect it is interesting to outline further ways to explore the discussed effect.

The first thing that comes to mind is the kinematical analysis: it would be very interesting to have a full overview of the regions of parameter space where the effect is possible to detect, and, as we just mentioned, the analysis of the sensitivity to various SUSY model parameters. In Chapter 6 (see also [35] and [36]) we presented a brief study of the magnitude of the CP-violation varying  $\text{Arg}\{\mu\}$ ,  $\tan\beta$ , and the beam energy, while the other theory parameters (like  $|\mu|$ ,  $M_2$ ,  $M_1$ , etc.) were normally kept fixed. However, even when considering the chargino sector alone, the couplings have non-trivial connections, which is illustrated by, e.g., Fig. 6.5. Such connections will, of course, have a strong effect on the overall sensitivity to the theory parameters, especially in case if one further consider variations of parameters in the neutralino sector (including Neutralino phases: U(1) gaugino mass parameter) and other couplings.

Next, all the numerical analysis sketched above was performed under the assumption that all sleptons are heavy, which allowed as to neglect a large class of diagrams in Chapter 4. Even partial relaxation of this assumption will bring new parameters into play, and, again,

---

<sup>2</sup>A short review of CP violation in neutralino pair production (polarized beams) can be found in [57] and references therein. Further possibilities to study a suitable asymmetry in neutralino production, where one neutralino subsequently decays to a  $\tilde{\tau}$  and a  $\tau$  are discussed in [58] and [59].



affect the observables. The same can be said about allowing for R-parity and/or lepton flavor violation.

It may also turn out that the polarization-*dependent* observables briefly discussed in Chapter 2 will be easier to study experimentally. The 1 loop calculations described above will then have to be complemented by inclusion of the spin projection operators which will bring additional terms (linear and bilinear in polarization — see Chapter 2) into the CP-violating observables.



# Appendix A

## The Fiertz transformation

Here we present the general Fiertz transformations that has been used for calculations of the tree-level results. The derivation of these formulae for some special cases is sketched in, e.g., [61]; below we use the general case communicated to us by Prof. V. Vereshagin. As one will see from the example provided below, by applying these transformations to the tree amplitudes one is able to avoid computations that contain the charge conjugation matrix  $C$  explicitly. This, in turn, allows to maintain explicit Lorentz-invariance in the computation of traces at the tree level. For the loop graphs, however, this method turned out to be less efficient, that is why a special type of Feynman rules described in Appendix C.1 was used in loop calculations instead.

### A.1 General Fiertz transformation

Using the properties of Dirac matrices  $\gamma_\mu, \gamma_5$  it is possible to show that any  $4 \times 4$  matrix  $M$  can be decomposed as

$$M = \frac{1}{4} \left( C_S \cdot I + C_P \cdot i\gamma_5 + C_V \cdot \gamma_\alpha + C_A^\alpha \cdot \gamma_\alpha \gamma_5 + C_T^{\alpha\beta} \cdot \sigma_{\alpha\beta} \right), \quad (\text{A.1})$$

where  $I$  is the identity matrix, the summation over the repeated Lorentz indices  $\alpha, \beta$  is implied, and the definitions<sup>1</sup>

$$\gamma_5 \equiv -i\gamma^0\gamma^1\gamma^2\gamma^3, \quad \sigma_{\alpha\beta} \equiv -\frac{i}{4}[\gamma_\alpha, \gamma_\beta]$$

are chosen to ensure the following trace (“normalization”) conditions:

$$\frac{1}{4} \text{Tr} \{ (\gamma_5)^2 \} = 1, \quad \text{Tr} \{ \sigma_{\alpha\beta} \sigma^{\tilde{\alpha}\tilde{\beta}} \} = g_\alpha^{\tilde{\alpha}} g_\beta^{\tilde{\beta}} - g_\alpha^{\tilde{\beta}} g_\beta^{\tilde{\alpha}}. \quad (\text{A.2})$$

The coefficients  $C_{\dots}$  (which can carry Lorentz, but not matrix indices) are then obtained as traces:

$$\begin{aligned} C_S &= \text{Tr} \{ M \}, & C_P &= -\text{Tr} \{ M(i\gamma_5) \}, & C_V^\alpha &= \text{Tr} \{ M\gamma^\alpha \}, \\ C_A^\alpha &= -\text{Tr} \{ M\gamma^\alpha \gamma_5 \}, & C_T^{\alpha\beta} &= 2 \text{Tr} \{ M\sigma^{\alpha\beta} \}. \end{aligned} \quad (\text{A.3})$$

---

<sup>1</sup>Here we use a non-traditional convention for the Dirac matrices in order to preserve a convenient normalization. Note however that  $\gamma_5$  differs from one defined in [62] only by a sign.

Note that the actual (sign) convention used to define  $\gamma_5$  and  $\sigma_{\alpha\beta}$  via  $\gamma$ -matrices is not that important here: the Eqs. (A.1) and (A.3) are consistent as long as the “normalization” (A.2) is maintained.

To avoid confusions we shall perhaps make another note. Namely: due to anti-symmetry of  $\sigma_{\alpha\beta}$  there are only 6 linearly independent  $\sigma$ -matrices. Therefore, there are in total 16 linearly independent matrices in the expansion (A.1): this is sufficient to decompose any  $4 \times 4$  matrix  $M$ . Still, to make the notations Lorentz-invariant, we have chosen to use all the 12 non-zero  $\sigma$ -matrices (and thus 22 matrices in total) in the decomposition (A.1). This is compensated by appropriate coefficient for  $C_T^{\alpha\beta}$  in Eq. (A.3), which is 2, and not 4 as it would be if we, for example, would use only  $\sigma^{\alpha\beta}$  with  $\alpha < \beta$ .

To proceed further, let us introduce more general notations. The (complete) set of Dirac matrices employed in Eq. (A.1) will be denoted as

$$\Gamma_{\ddot{Y}} \equiv \left\{ I, i\gamma_5, \gamma^\alpha, \gamma^\alpha\gamma_5, \sigma^{\alpha\beta} \right\} ; \quad (\text{A.4})$$

here the index  $Y$  runs through the 5 matrix types ( $S, P, V, A, T$ ), while the “dots” ( $\ddot{\cdot}$ ) stand for a Lorentz “hyper-index”: e.g., they are reserved for appropriate amount of Lorentz indices (e.g., none, one, or two). If we now define the “weight” factors as

$$\Delta_Y \equiv \{1, -1, 1, -1, 2\} , \quad (\text{A.5})$$

then the Eq. (A.3) takes the following form

$$C_{\ddot{Y}} = \Delta_Y \text{Tr} \{ M \Gamma_{\ddot{Y}} \} .$$

Substituting the latter to the expansion (A.1) we finally get:

$$M = \frac{1}{4} \sum_Y \Delta_Y \text{Tr} \{ M \Gamma_{\ddot{Y}} \} \Gamma_{Y\dots} , \quad (\text{A.6})$$

where, again, the “dots” denotes a Lorentz (hyper-) index, and we, of course, made sure that all Lorentz indices are contracted.

So far we have been hiding the ( $4 \times 4$ ) matrix indices; by showing them explicitly in the expansion (A.6) we get:

$$M_{kr} = \frac{1}{4} \sum_Y \Delta_Y M_{ij} (\Gamma_{\ddot{Y}})_{ji} (\Gamma_{Y\dots})_{kr} ;$$

as usual, the summation over the repeated indices (both: Lorentz and matrix ones) is implied. Switching the order of (scalar!) factors and dividing out the matrix  $M$  we obtain the following equality:

$$\left[ \delta_{ik}\delta_{jr} - \frac{1}{4} \sum_Y \Delta_Y (\Gamma_{\ddot{Y}})_{ji} (\Gamma_{Y\dots})_{kr} \right] M_{ij} = 0$$

which, by construction, holds for any matrix  $M$ . In other words, the following identity holds:

$$\delta_{ik}\delta_{jr} = \frac{1}{4} \sum_Y \Delta_Y (\Gamma_{\ddot{Y}})_{ji} (\Gamma_{Y\dots})_{kr} . \quad (\text{A.7})$$

This is, of course, nothing else but the completeness condition for the set of  $4 \times 4$  Dirac matrices  $\Gamma_Y$ .

Let us multiply Eq. (A.7) by two *arbitrary*  $4 \times 4$  matrices  $A_{in}$  and  $B_{mj}$  : each of them is allowed to carry any additional (e.g., Lorentz) indices — only their matrix structure is important for us. Contracting the repeated matrix indices we obtain:

$$A_{kn}B_{mr} = \frac{1}{4} \sum_Y \Delta_Y B_{mj} (\Gamma_Y^{\dots})_{ji} A_{in} (\Gamma_Y \dots)_{kr} .$$

At last, let us multiply the last equality by 4 arbitrary Dirac spinors  $(u_1)_k, (u_2)_n, (u_3)_m, (u_4)_r$  (each of them can be  $u, \bar{u}, v, \text{ or } \bar{v}$ ), thus contracting the 4 remaining free matrix indices:

$$[ u_1 A u_2 ] [ u_3 B u_4 ] = \frac{1}{4} \sum_Y \Delta_Y [ u_1 (\Gamma_Y \dots) u_4 ] [ u_3 (B \Gamma_Y^{\dots} A) u_2 ] . \quad (\text{A.8})$$

From the practical point of view it is important that the spinors  $u_2$  and  $u_4$  got effectively interchanged on the RHS. The price for this is, of course, the extra  $\Gamma_Y$  (Dirac) matrices that enter the expression, and the sum over Lorentz (hyper-)index (“ $\dots$ ”). However, as we will see in the next section, the expression on the RHS can often be simplified. Eq. (A.8), together with definitions (A.4) and (A.5) describe the general Fiertz transformation rule that we wanted to derive.

## A.2 Cross-channel s-neutrino exchange via Fiertz

To demonstrate the usefulness of the Fiertz transformation derived above we sketch here the calculation of the  $t$ -channel sneutrino exchange graph (Fig. A.1) contributing to the process (2.1) at tree level. The relevant Lagrangian terms (vertices) can be read off from Appendix C,

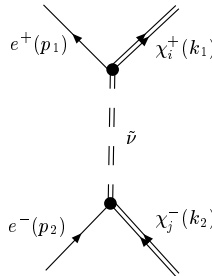


Figure A.1: Tree level sneutrino exchange.

Eq. (C.19).

To simplify the formulae we will drop the propagator, as well as all the vertex factors but the Dirac matrices and the charge conjugation matrix  $C$ . Then the amplitude of the graph in Fig. A.1 reads (remember that the positive chargino is treated as a *particle*, rather than antiparticle):

$$\mathcal{M}(\tilde{\nu}) \sim [\bar{v}(p_1)(1 + \gamma^5)C^{-1}\bar{u}(k_1)] \cdot [v(k_2)C(1 - \gamma^5)u(p_2)] . \quad (\text{A.9})$$

This form is obviously inconvenient, since it contains  $C$ -matrix explicitly, therefore one may want to employ the spinor properties:  $C^{-1}\bar{u} = v$ ;  $vC = -\bar{u}$ . However, the problem will then arise in calculations of the *interference* terms in the cross-section: Eq. (3.13) in Sec. 3.2. For example, the  $\gamma$ -exchange graph (Fig. A.2) is proportional to

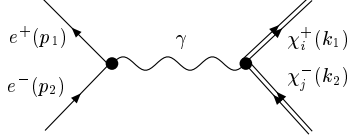


Figure A.2: Tree level photon exchange.

$$\mathcal{M}(\gamma) \sim [\bar{v}(p_1)\gamma^\mu u(p_2)] \cdot [\bar{u}(k_1)\gamma_\mu v(k_2)] . \quad (\text{A.10})$$

Thus, one can easily see that in the  $\gamma\tilde{\nu}$  interference term

$$X(\gamma\tilde{\nu}) \equiv \sum_{\tilde{\chi} \text{ spins}} [\mathcal{M}^*(\gamma)\mathcal{M}(\tilde{\nu}) + \mathcal{M}(\gamma)\mathcal{M}^*(\tilde{\nu})]$$

the traces will run over awkward spinor combinations like  $u(k_1)v(k_1)$  and will involve non-convenient matrix transpositions. To solve it, one will actually need to explicitly carry the  $C$ -matrix throughout the traces, or, even worse, stick to a specific representation of the Dirac matrices. In either way the calculations will become lengthy.

Instead, one may apply the Fiertz transformation to the expression (A.9). Denoting

$$A = (1 + \gamma_5) , \quad B = (1 - \gamma_5) ,$$

and using the Equation (A.8) we get:

$$\begin{aligned} \mathcal{M}(\tilde{\nu}) &\sim [\bar{v}(p_1) A C^{-1}\bar{u}(k_1)] \cdot [v(k_2)C B u(p_2)] \\ &= \frac{1}{4} \sum_Y \Delta_Y [\bar{v}(p_1) (\Gamma_Y \dots) u(p_2)] [v(k_2)C (B\Gamma_Y \dots A) C^{-1}\bar{u}(k_1)] . \end{aligned} \quad (\text{A.11})$$

It is easy to check, that the only products  $(B\Gamma_Y \dots A)$  that survive in the last expression are:

$$B\gamma_\alpha A = B\gamma_\alpha\gamma_5 A = 2\gamma_\alpha(1 + \gamma_5) .$$

So, with the values of  $\Delta_Y$  for  $Y = \gamma_\alpha, \gamma_\alpha\gamma_5$  given by Eq. (A.5), the RHS of the Eq. (A.11) is equal to:

$$\frac{1}{2} [\bar{v}(p_1)\gamma_\alpha(1 - \gamma_5)u(p_2)] [v(k_2)C\gamma^\alpha(1 + \gamma_5)C^{-1}\bar{u}(k_1)] . \quad (\text{A.12})$$

Finally, using the  $C$ -matrix “transposing” properties (that hold in *any* representation of Dirac matrices):

$$C\gamma^\alpha C^{-1} = -[\gamma^\alpha]^T , \quad C\gamma^\alpha\gamma_5 C^{-1} = [\gamma^\alpha\gamma_5]^T$$

one can rewrite Eq. A.12 as:

$$-\frac{1}{2} [\bar{v}(p_1)\gamma_\alpha(1 - \gamma_5)u(p_2)] [\bar{u}(k_1)\gamma^\alpha(1 - \gamma_5)v(k_2)] . \quad (\text{A.13})$$

The latter result for s-neutrino exchange graph has exactly the same spinor content and order as the amplitudes of  $\gamma$ - and  $Z$ -exchange graphs (cf., e.g., Eq. (A.10)). Therefore all the traces appearing in the tree-level cross section can now be handled in the conventional way.

The Fiertz transformation can obviously be applied to the amplitude at any loop order. However, as we mentioned in the beginning of this Chapter, there is a more general method allowing to remove the  $C$ -matrix at the level of Feynman vertices. The latter method (which was actually used to calculate 1 loop graphs) is described in Appendix C.1.





## Appendix B

# $U(1)$ Ward identities and the $\gamma f_i \bar{f}_j$ coupling

Here we sketch the derivation of the Ward-Takahashi identities that prohibit the photon from coupling to two different-mass charginos<sup>1</sup>. We apply a slightly modified version of the analysis used in the book by Pokorski [64] to obtain Ward-Takahashi identities for Quantum Electrodynamics.

Let us denote the chargino fields obtained after the chargino mass matrix diagonalization by  $\Psi_1$  and  $\Psi_2$ , and write down the generating functional for the full Green's functions in the form:

$$W[J, \alpha_1, \bar{\alpha}_1, \alpha_2, \bar{\alpha}_2] = \int \mathcal{D}(A_\mu \bar{\Psi}_1 \Psi_1 \bar{\Psi}_2 \Psi_2 \dots) \exp(iS_{\text{eff}}), \quad (\text{B.1})$$

with the action

$$S_{\text{eff}} = \int d^4x [\mathcal{L}(A_\mu, \Psi_i, \dots) + J_\mu A^\mu + \bar{\alpha}_1 \Psi_1 + \bar{\Psi}_1 \alpha_1 + \bar{\alpha}_2 \Psi_2 + \bar{\Psi}_2 \alpha_2].$$

Here  $J_\mu$  is the vector source for the photon field  $A_\mu$ , the  $\alpha$ 's are Grassmann sources for charginos, and the ellipsis denotes the other fields present in the MSSM. Since physical charginos have equal charge, in any covariant gauge the Lagrangian density can be expressed via the renormalized (physical) fields and charges (the subscripts “b” stand for “bare”):

$$A_b^\mu = (Z_3)^{\frac{1}{2}} A_\mu, \quad \Psi_{k_b} = (Z_{2,k})^{\frac{1}{2}} \Psi_k, \quad (k = 1, 2), \quad e_b = \frac{Z_{1,k}}{Z_{2,k}(Z_3)^{\frac{1}{2}}} e, \quad m_b = \frac{Z_{0,k}}{Z_{2,k}} m$$

as

$$-\frac{1}{4} Z_3 F_{\mu\nu} F^{\mu\nu} + \sum_{k=1,2} \left[ Z_{2,k} \bar{\Psi}_k \left( i \not{\partial} - e \frac{Z_{1,k}}{Z_{2,k}} \not{A} \right) \Psi_k - Z_{0,k} m_k \bar{\Psi}_k \Psi_k \right] - \frac{1}{2a} (\partial_\mu A^\mu)^2 + \dots,$$

where the  $Z$ 's are renormalization constants,  $e$  and  $m_k$  are renormalized charge and chargino masses, respectively, and  $a$  is the gauge fixing constant<sup>2</sup>.

<sup>1</sup>The fact that the photon can not couple to two fermions with different masses is mentioned, e.g., in the article by t' Hooft [50], but we are not aware of any reference for the detailed proof. Perhaps we shall also stress that the WI we are going to derive hold also *off shell*. The reason for this is that the conserved current we deal with here is the QED(-like) current, and not the SUSY current. For relevant discussion see, e.g., [63].

<sup>2</sup>More precisely, one of them: we do not need to show the remaining gauge fixing terms. The QED-like term we have shown does not require counterterms — this can be easily demonstrated with the help of the Ward identities we are going to derive in the same way as one does it in QED. For brevity we skip this part, relevant derivation can be found in, e.g., [64].

The first step is to make an infinitesimal gauge transformation

$$\Psi'_k = \exp(-i\bar{e}_k\Theta)\Psi_k \equiv (1 - i\bar{e}_k\Theta)\Psi_k + O(\Theta^2), \quad A'_\mu = A_\mu + \partial_\mu\Theta, \quad \bar{e}_k \equiv e \frac{Z_{1,k}}{Z_{2,k}} \quad (\text{B.2})$$

under the functional integral (B.1). The change of variables can not affect the value of the integral, so, in particular,

$$\left. \frac{\delta W}{\delta\Theta(y)} \right|_{\Theta=0} = 0. \quad (\text{B.3})$$

Since, by the very construction, the MSSM is invariant under  $U(1)$  gauge transformations, the measure  $\mathcal{D}$  in the path integral is also gauge invariant, and the only gauge dependent terms in the generating functional are those with sources and, of course, the gauge fixing term. Thereby, up to the  $O(\Theta^2)$  terms, the change in  $W$  caused by the gauge transformation (B.2) is:

$$\begin{aligned} \delta W &= i \int d^4x \int \mathcal{D}(A_\mu \bar{\Psi}_1 \Psi_1 \bar{\Psi}_2 \Psi_2 \dots) \exp(iS_{\text{eff}}) \\ &\times \left\{ J_\mu(x) \partial^\mu \Theta(x) - i \sum_{k=1,2} \bar{e}_k \Theta(x) \left[ \bar{\alpha}_k(x) \Psi_k(x) - \bar{\Psi}_k(x) \alpha_k(x) \right] - \frac{1}{a} \partial_\mu A^\mu(x) \partial^2 \Theta(x) \right\}. \end{aligned}$$

After we integrate it by parts and neglect surface terms, the last line becomes:

$$\Theta \left\{ -\frac{1}{a} \partial^2 \partial_\mu A^\mu - \partial^\mu J_\mu - i \sum_{k=1,2} \bar{e}_k \left[ \bar{\alpha}_k \Psi_k - \bar{\Psi}_k \alpha_k \right] \right\},$$

and, thus, (B.3) requires

$$\begin{aligned} &\int \mathcal{D}(A_\mu \bar{\Psi}_1 \Psi_1 \bar{\Psi}_2 \Psi_2 \dots) \exp(iS_{\text{eff}}) \\ &\times \left\{ \frac{1}{a} \partial^2 \partial_\mu A^\mu(y) + \partial^\mu J_\mu(y) + i \sum_{k=1,2} \bar{e}_k \left[ \bar{\alpha}_k(y) \Psi_k(y) - \bar{\Psi}_k(y) \alpha_k(y) \right] \right\} = 0. \quad (\text{B.4}) \end{aligned}$$

By its very definition, the path integral of a field's derivative is the derivative of the Green's function, so (B.4) states that

$$\frac{1}{a} \partial^2 \partial_\mu \frac{1}{i} \frac{\delta W}{\delta J_\mu(y)} + \partial^\mu J_\mu(y) W + \sum_{k=1,2} \bar{e}_k \left[ \bar{\alpha}_k(y) \frac{\overrightarrow{\delta}}{\delta \bar{\alpha}_k(y)} W - W \frac{\overleftarrow{\delta}}{\delta \alpha_k(y)} \alpha_k(y) \right] = 0;$$

in the following we prefer to use left derivatives only, so the last expression reads:

$$\frac{1}{a} \partial^2 \partial_\mu \frac{1}{i} \frac{\delta W}{\delta J_\mu(y)} + \partial^\mu J_\mu(y) W + \sum_{k=1,2} \bar{e}_k \left[ \bar{\alpha}_k(y) \frac{\delta W}{\delta \bar{\alpha}_k(y)} + \frac{\delta W}{\delta \alpha_k(y)} \alpha_k(y) \right] = 0.$$

Substituting  $W = \exp(iZ)$ , where  $Z$  is the generating functional for the connected Green's functions, we get:

$$\frac{1}{a} \partial^2 \partial_\mu \frac{\delta Z}{\delta J_\mu(y)} + \partial^\mu J_\mu(y) + i \sum_{k=1,2} \bar{e}_k \left[ \bar{\alpha}_k(y) \frac{\delta Z}{\delta \bar{\alpha}_k(y)} + \frac{\delta Z}{\delta \alpha_k(y)} \alpha_k(y) \right] = 0; \quad (\text{B.5})$$

it is these  $U(1)$  Ward identities that we are going to explore.

Differentiating (B.5) w.r.t.  $\frac{\delta}{\delta\bar{\alpha}_m(x)}\frac{\delta}{\delta\alpha_n(z)} \equiv -\frac{\delta}{\delta\alpha_n(z)}\frac{\delta}{\delta\bar{\alpha}_m(x)}$  and setting  $J = \bar{\alpha} = \alpha = 0$ , we obtain:

$$\frac{1}{a}\partial_{(y)}^2\partial_{\mu}^{(y)}\frac{\delta^3 Z}{\delta\bar{\alpha}_m(x)\delta\alpha_n(z)\delta J_{\mu}(y)} = i\bar{e}_m\delta(y-x)\frac{\delta^2 Z}{\delta\alpha_n(z)\delta\bar{\alpha}_m(y)} + i\bar{e}_n\delta(y-z)\frac{\delta^2 Z}{\delta\bar{\alpha}_m(x)\delta\alpha_n(y)}.$$

Finally, recalling that

$$\begin{aligned} \langle 0|T\Psi_m(x)\bar{\Psi}_n(y)|0\rangle &= i\frac{\delta^2 Z}{\delta\bar{\alpha}_m(x)\delta\alpha_n(y)}\Big|_{J=\bar{\alpha}=\alpha=0} \\ \langle 0|TA^{\mu}(y)\Psi_m(x)\bar{\Psi}_n(z)|0\rangle &= \frac{\delta^3 Z}{\delta J_{\mu}(y)\delta\bar{\alpha}_m(x)\delta\alpha_n(z)}\Big|_{J=\bar{\alpha}=\alpha=0}, \end{aligned}$$

we rewrite the identity as:

$$\begin{aligned} &-\frac{1}{a}\partial_{(y)}^2\partial_{\mu}^{(y)}\langle 0|TA^{\mu}(y)\Psi_m(x)\bar{\Psi}_n(z)|0\rangle \\ &= \bar{e}_m\delta(y-x)\langle 0|T\Psi_m(y)\bar{\Psi}_n(z)|0\rangle - \bar{e}_n\delta(y-z)\langle 0|T\Psi_m(x)\bar{\Psi}_n(y)|0\rangle. \end{aligned} \quad (\text{B.6})$$

For  $m = n$  one can easily recognize the Ward identities analogous to those in QED, which, of course, also hold in the MSSM. On the other hand, for  $m \neq n$  the right-hand side of Eq. (B.6) is zero, because the physical charginos do not mix — they are exactly the mass states obtained *after* the mass matrix diagonalization. So, the connected Green's function of the photon and two different mass chargino fields is zero to all loop orders. That is what had to be proven.

The renormalization prescriptions are typically imposed on 1PI Green's functions, so, for the sake of completeness, we shall derive also the identities analogous to (B.6) involving the so-called effective action — the generating functional for 1PI Green's functions.

The arguments of the effective action  $\Gamma$  are the *classical* fields  $\bar{\psi}$ ,  $\psi$  and  $\mathcal{A}_{\mu}$ , and  $\Gamma$  is defined as the Legendre transform

$$\Gamma[\mathcal{A}_{\mu}, \psi, \bar{\psi}] = Z[J, \alpha_k, \bar{\alpha}_k] - \int d^4x \left\{ J_{\mu}(x)\mathcal{A}^{\mu}(x) + \sum_{k=1,2} \left[ \bar{\alpha}_k\psi_k + \bar{\psi}_k\alpha_k \right] \right\}, \quad (\text{B.7})$$

so that

$$\mathcal{A}_{\mu} = \frac{\delta Z}{\delta J_{\mu}}, \quad \psi_k = \frac{\delta Z}{\delta\bar{\alpha}_k}, \quad \bar{\psi}_k = -\frac{\delta Z}{\delta\alpha_k}; \quad J_{\mu} = -\frac{\delta\Gamma}{\delta\mathcal{A}^{\mu}}, \quad \bar{\alpha}_k = \frac{\delta\Gamma}{\delta\psi_k}, \quad \alpha_k = -\frac{\delta\Gamma}{\delta\bar{\psi}_k},$$

therefore Eq. (B.5) can be rewritten as:

$$\frac{1}{a}\partial_{(y)}^2\partial_{\mu}^{(y)}\mathcal{A}^{\mu}(y) - \partial_{(y)}^{\mu}\frac{\delta\Gamma}{\delta\mathcal{A}_{\mu}(y)} + i\sum_{k=1,2}\bar{e}_k\left[\frac{\delta\Gamma}{\delta\psi_k(y)}\psi_k(y) + \bar{\psi}_k(y)\frac{\delta\Gamma}{\delta\bar{\psi}_k(y)}\right] = 0. \quad (\text{B.8})$$

Taking the derivative  $\frac{\delta}{\delta\bar{\psi}_m(x)}\frac{\delta}{\delta\psi_n(z)}$  ( $\psi$ 's are Grassmann!) of this identity and setting  $\mathcal{A}_{\mu} = \bar{\psi} = \psi = 0$ , we get:

$$\partial_{(y)}^{\mu}\frac{\delta^3\Gamma}{\delta\mathcal{A}_{\mu}(y)\delta\bar{\psi}_m(x)\delta\psi_n(z)} + i\bar{e}_n\delta(y-z)\frac{\delta\Gamma}{\delta\bar{\psi}_m(x)\delta\psi_n(y)} - i\bar{e}_m\delta(y-x)\frac{\delta\Gamma}{\delta\bar{\psi}_m(y)\delta\psi_m(z)} = 0. \quad (\text{B.9})$$

In momentum space the first term represents the three-point 1PI Green's function with a photon and two charginos with masses  $m_m$  and  $m_n$  on the external legs times the momentum of the photon. The second and third terms contain two-point functions of those two charginos. Again, if  $m = n$  we obtain the typical QED-like Ward-Takahashi identity, while for  $m \neq n$  the second and third terms are identically zero due to the absence of mixing between the physical mass states, and, thus Eq. (B.9) forces the three-point function to vanish. This completes our proof.

## Appendix C

# The Lagrangian vertices and Feynman rules

### C.1 Handling C-conjugate and Majorana fermions

The presence of Majorana fields (neutralinos) causes certain complications in constructing Feynman rules based on the Lagrangian vertices (see e.g. [14]). Due to two additional ways to pair Majorana fields:  $\underline{\Psi}\Psi$  and  $\overline{\Psi}\overline{\Psi}$ , two additional types of propagators generally arise when the Wick theorem is applied directly. At the same time, the possibility to rewrite the Lagrangian in a few equivalent forms using the C-conjugation matrix and the anticommutativity of Majorana fermions can result in various confusions for relative signs of Feynman amplitudes [48]. Besides, there are vertices with fermion number violation in the MSSM Lagrangian, and they cause the explicit appearance of the charge-conjugation matrix, which complicates the automation of the calculations.

Several ways to evade these difficulties were proposed in the literature, see e.g. [49]; here we follow the approach by Denner et. al. [38], which naturally incorporates the charge-conjugated fields. The relevant Feynman rules are formulated in compact form using only *one* conventional propagator

$$S(p) = \frac{i(\not{p} + m)}{p^2 - m^2 + i\epsilon} \quad (\text{C.1})$$

for internal fermion (Dirac or Majorana) line. Majorana lines do not possess graphical arrows but use the same propagator (see below). Following [38], we handle graphs with fermion lines in the following way:

1. Rewrite the Lagrangian via the original and/or charge-conjugated fermion fields, absorbing all occurrences of the  $C$ -matrix into the field operators, *until no explicit  $C$ -matrices appear in the vertices*.
2. Draw all possible diagrams for the process *without the fermion arrow on Majorana lines*. As usual, the arrow on the Dirac fermion lines should point in the direction of particle (rather than antiparticle) flow. Dirac particles here are the conventional ones, in our case they are the electron and the positive chargino.
3. Fix an *orientation*: an arbitrary (but continuous) fermion flow direction for each fermion chain.

4. Start at an external leg (or at some arbitrary propagator for a closed loop) and write down the Dirac matrices proceeding against the chosen fermion flow through the chain. The external fermion wave functions (spinors) should be chosen according to the fixed fermion flow direction, and *not* according to the Dirac fermion arrow (even if present).
5. If a Dirac fermion line has the opposite direction to the chosen orientation, the *reversed* (or *dashed*) vertices  $\Gamma' = C\Gamma^T C^{-1}$  (here  $\Gamma$  comes from a Lagrangian vertex  $\bar{\Psi}_a \Gamma \Psi_b \Phi$ , where  $\Psi_a$  and  $\Psi_b$  can be either Majorana or Dirac fermions and  $\Phi$  denotes scalar or vector particle) and the propagator with *reversed momentum*  $S(-p)$  should be used (cf. Eq. (C.1) where, as usual,  $p$  is the four-momentum in the direction of Dirac fermion arrow).
6. As usual, add factor  $(-1)$  for every closed fermion loop.
7. For determination of symmetry coefficients the Majorana fermions can be treated like real scalar or vector fields.

Simply speaking, the trick behind the above rules is to consider a charge-conjugated field as an ordinary field when needed. Indeed, the charge-conjugated field, together with the Dirac conjugated of the latter, are expressed via the same creation and annihilation operators, the only difference with the original field is that the particle and anti-particle creation (annihilation) operators are interchanged. Then, being given a fermion chain with (arbitrarily) fixed orientation, we can always rewrite needed parts of the Lagrangian in a way that the original fields correspond to the lines where the particle flow coincides with our chosen “flow”, and charge-conjugated fields correspond to the lines where these flows are opposite. The explicit  $C$ -matrices do not appear anymore, being, instead, absorbed into the charge-conjugated fields. If one then applies the Wick theorem, “dashed” momentum space vertices arise when Lagrangian terms with ordinary fields are rewritten via charge-conjugated fields, and the reversed propagators (reverse sign of propagator argument) come from the fact (convention) that the momentum in a propagator for a given field is the momentum along the particle flow — this, in turn, comes from the explicit calculation of the pairings. When the charge-conjugated field is considered, the former anti-particle becomes a particle, so the propagator argument changes sign. The Majorana fields are self-conjugated, particles coincide with antiparticles, so nothing changes when we choose the opposite orientation. That is why Majorana lines should not carry any additional arrow, except that of the fermion flow we choose.

To demonstrate how all this works, let us consider an example. The diagram in Fig. C.1 contributes to the  $Z\chi_i\chi_j$  vertex correction. We fix the fermion flow to coincide with the positive chargino flow, so, due to the arrow “clashing”, the electron arrows are opposite to the chosen orientation.

According to the above recipe, we shall start writing down the factors from the right upper corner, namely the wave function for the external  $\chi_i^+$  leg comes first. In our case it is an outgoing particle (both according to the chosen orientation and the Dirac line direction), so the spinor is  $\bar{u}(k_1)$ . Next, there comes a vertex. The relevant Lagrangian term (see Eq. (C.19), Appendix C.2), is ( $m_e = 0$ ):

$$L_4^{LC} = -\frac{g}{2} \{ X_{1j}^\dagger \Psi_{\chi_j}^T C(1 - \gamma^5) \Psi_e \bar{\nu}^\dagger + X_{j1} \bar{\Psi}_e (1 + \gamma^5) C \bar{\Psi}_{\chi_j}^T \bar{\nu} \}, \quad (\text{C.2})$$

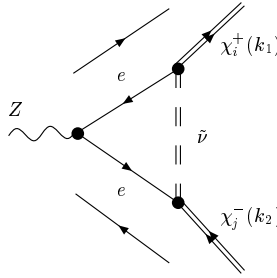


Figure C.1: Example of diagram with “clashed” fermion arrows. The outside arrows show the chosen direction of fermion flow.

where the elements of the mixing matrices  $X$  are irrelevant for the current discussion and will be dropped in this Section. In any representation in  $3 + 1$  dimensions the  $C$ -matrix is conventionally defined in a way that

$$C^{-1} = C^\dagger, \quad C^T = -C, \quad C\gamma^{\mu T}C^{-1} = -\gamma^\mu, \quad (\text{C.3})$$

besides, for real  $C$  in the Weyl basis the relation  $C = -C^{-1} = -C^\dagger$  also holds. The charge conjugated field is defined as:

$$\Psi^c = C\bar{\Psi}^T, \quad (\Psi^c)^c = \Psi, \quad \overline{(\Psi^c)} = -\Psi^T C^{-1}, \quad (\text{C.4})$$

where  $\Psi^c$  is a charge conjugated field and the bar denotes Dirac adjoint. For the solutions of the Dirac equation Eqs. (C.3), the definition (C.4) lead to

$$v(p, \sigma) = C\bar{u}^T(p, \sigma), \quad u(p, \sigma) = C\bar{v}^T(p, \sigma),$$

which is justified by the plane wave expansions:

$$\begin{aligned} \Psi(x) &= \int \frac{d^3p}{(2\pi)^3 2p_0} \{ e^{-ipx} c(p, \sigma) u(p, \sigma) + e^{ipx} d^\dagger(p, \sigma) v(p, \sigma) \} \\ \bar{\Psi}(x) &= \int \frac{d^3p}{(2\pi)^3 2p_0} \{ e^{-ipx} d(p, \sigma) \bar{v}(p, \sigma) + e^{ipx} c^\dagger(p, \sigma) \bar{u}(p, \sigma) \} \\ \Psi^c(x) &= \int \frac{d^3p}{(2\pi)^3 2p_0} \{ e^{-ipx} d(p, \sigma) u(p, \sigma) + e^{ipx} c^\dagger(p, \sigma) v(p, \sigma) \} \end{aligned}$$

( $c^\dagger$  and  $d^\dagger$  create particle and antiparticle, respectively).

Using Eq. (C.4) and dropping the numerical factors we can rewrite the Lagrangian vertex (C.2) as

$$\dots \bar{\Psi}_{\chi_j}^c (1 - \gamma^5) \Psi_e \tilde{\nu}^\dagger + \dots \bar{\Psi}_e (1 + \gamma^5) \Psi_{\chi_j}^c \tilde{\nu}. \quad (\text{C.5})$$

However, as one can see from the picture, this vertex is not exactly the one we need to follow the strategy discussed in the beginning of this Section. Rather, we need it written in terms of  $\Psi_e^c$  and  $\Psi_{\chi_j}$ : if these two are treated as the “ordinary” fields, then the chosen fermion flow will coincide with “ordinary” particle flow.

To get the desired expression, let us complete a simple exercise. Take two *anticommuting* spinor fields  $\chi_a$  and  $\chi_b$  and consider a bilinear product:  $\bar{\chi}_a \Gamma_i \chi_b$ , where  $\Gamma_i$  is some Dirac matrix structure. We rewrite it as:

$$\bar{\chi}_a \Gamma_i \chi_b = (\bar{\chi}_a \Gamma_i \chi_b)^T = (-1) \chi_b^T \Gamma_i^T \bar{\chi}_a^T = \bar{\chi}_b^c C \Gamma_i^T C^{-1} \chi_a^c = \bar{\chi}_b^c \eta_i \Gamma_i \chi_a^c \equiv \eta_i \bar{\chi}_b^c \Gamma_i \chi_a^c \quad (\text{C.6})$$

(no summation over  $i$ ); the  $(-1)$  factor comes from anticommutation of spinor fields,  $\eta_i = 1$  for  $\Gamma_i = 1, \gamma^5, \gamma^\mu \gamma^5$  and  $\eta_i = -1$  for  $\Gamma_i = \gamma^\mu, \sigma^{\mu\nu}$ . In particular, the vertex (C.5) (or (C.2)) can therefore be rewritten as

$$\dots \bar{\Psi}_e^c (1 - \gamma^5) \Psi_{\chi_j} \tilde{\nu}^\dagger + \dots \bar{\Psi}_{\chi_j} (1 + \gamma^5) \Psi_e^c \tilde{\nu}, \quad (\text{C.7})$$

(the momentum space vertex did not change, but obviously it is not always the case).

Next, we come to the propagator. The latter corresponds now to pairing of  $C$ -conjugated fields; one easily checks that the result is:

$$S(p) = \frac{i(\not{p} + m)}{p^2 - m^2 + i\epsilon}, \quad CS^T(p)C^{-1} = S(-p),$$

so the momentum sign in the propagator is opposite to the sign one would choose if the conventional Feynman rules for the graph at Fig. C.1 were used.

Further comes the  $Zee$  vertex, which, according to the chosen fermion flow, we need to rewrite in the  $Ze^c e^c$  form. Eq. (C.6) says that it will lead to the sign change of the vector part (cf. Eq. (C.9), Appendix C.2):

$$\dots \bar{\Psi}_e \gamma^\rho (-4 \sin^2 \theta_W + 1 - \gamma^5) \Psi_e Z_\rho = \dots \bar{\Psi}_e^c \gamma^\rho (4 \sin^2 \theta_W - 1 - \gamma^5) \Psi_e^c Z_\rho.$$

Next comes the second electron propagator which is again directed against the chosen fermion flow and, therefore, its momenta shall change sign. The lower vertex can again be read off from Eq. (C.7). Finally, the scalar propagator is, of course, unchanged.

Assigning loop momenta according to the “s”-parametrization of Section 5.2 (e.g., the first graph in Fig. 5.1 with propagator  $d_2$  contracted to a point), and collecting all the contributions discussed above one gets the loop graph in Fig. (C.1):

$$\begin{aligned} & \dots \times \bar{u}(k_1) (1 + \gamma^5) \times \frac{-(\not{q} - \frac{1}{2}\not{Q}) + m_e}{(q - \frac{1}{2}Q)^2 - m_e^2 + i\epsilon} \\ & \times \gamma^\rho (4 \sin^2 \theta_W - 1 - \gamma^5) \\ & \times \frac{-(\not{q} + \frac{1}{2}\not{Q}) + m_e}{(q + \frac{1}{2}Q)^2 - m_e^2 + i\epsilon} \times (1 - \gamma^5) v(k_2) \\ & \times \frac{1}{(q + \frac{1}{2}P_t)^2 - m_\nu^2 + i\epsilon}, \end{aligned}$$

where “...” of course includes the loop integral over the momentum  $q$ , as well as all the algebraic factors and coupling constants left aside during this discussion (like, e.g., the mixing matrices). The (matrix) multiplication “ $\times$ ” is used as delimiter to highlight the contribution coming from each of the graph elements. The  $m_e$  terms are kept only for clarity, the limit  $m_e = 0$  is always assumed.

One can show that the cross-section obtained in this way is independent of the chosen fermion flow direction. The proof of the latter statement, as well as all the necessary details of derivation of these rules can be found in [38].



## C.2 MSSM Lagrangian vertices used in analytical calculations

In this Section, mainly for the sake of completeness, we assemble the MSSM Lagrangian vertices that are needed to obtain the analytical results quoted in Chapters 3 and 6. For Feynman vertices used in the full 1 loop contribution with vertex corrections the reader is addressed to [36, 34] and references therein as the complete MSSM Feynman rules set is very large (see, e.g., [39]).

The Feynman rules for MSSM in terms of component fields were first collected in [39]. Instead of using the diagrammatic vertices in momentum space quoted in the latter article, here we prefer to list the relevant Lagrangian vertices. Following [39], we work in the 't Hooft–Feynman gauge, where the gauge boson propagators have their simplest form:

$$\frac{-ig_{\mu\nu}}{(k^2 - M^2)},$$

while the neutral and charged (unphysical) Goldstones acquire masses  $M_Z$  and  $M_W$ , respectively (see e.g. [50]). The notations below closely follow [65].

Since the 1-loop analytical calculations were done in the limit of heavy sleptons dropping all the (box) diagrams with internal slepton lines, we do not list the vertices that include sleptons (apart from  $e\tilde{\chi}\tilde{\nu}$  vertex used at tree level where we did not make any assumptions about the masses). Besides, as one can easily see from Chapter 3 (tree) and Chapter 4 (1-loop), the vertices with Higgs/Goldstone bosons do not enter the graphs that give the main CP-odd contribution we focused on. Indeed, it turned out that the Higgs (and Goldstone) lines either bring the  $m_e$  factors into the diagrams (and this factor we always drop), or enter together with slepton fields, and thus, again, the graph has to be dropped. That is why the vertices with Higgs/Goldstone fields were not needed and, hence, not listed below.

As usual, “\*” and “†” denote the complex and hermitian conjugation, respectively. The charge  $e$  is defined to be positive, equal to the charge of the positron. It is connected to the weak coupling by the Weinberg angle:  $g \sin \theta_W = e$ .

For convenience, we divide the vertices into subsections: the Standard Model Lagrangian vertices we need, and the MSSM vertices with SUSY fields we need.

### C.2.1 Standard Model vertices used at tree level and in box calculations

To obtain the analytical expressions analyzed in Chapters 3 and 6 one needs the following Lagrangian vertices involving Standard Model fields:

( $\gamma ee$ ) QED-coupling:

$$L_1^{GQ} = -e A_\rho \bar{\Psi}_e \gamma^\rho \Psi_e \quad (\text{C.8})$$

( $Zee$ )  $Z$  boson – electron – electron:

$$L_3^{GL} = -\frac{g}{4 \cos \theta_W} \bar{\Psi}_e \gamma^\rho (-4 \sin^2 \theta_W + 1 - \gamma^5) \Psi_e Z_\rho \quad (\text{C.9})$$

( $W e \nu$ )  $W$  boson – electron – neutrino:

$$L_5^{GQ} = \frac{g}{2\sqrt{2}} \left\{ W_\rho \bar{\Psi}_\nu \gamma^\rho (1 - \gamma^5) \Psi_e + W_\rho^\dagger \bar{\Psi}_e \gamma^\rho (1 - \gamma^5) \Psi_\nu \right\} \quad (\text{C.10})$$

### C.2.2 MSSM (SUSY) vertices used at tree level and in box calculations

The MSSM vertices we need involve chargino and neutralino mixing matrices, which diagonalize respective mass matrices that arise due to soft-SUSY-breaking terms [46].

The chargino mixing (unitary) matrices  $X$  and  $Y$  are chosen to diagonalize the tree level chargino mass matrix  $M_\chi$ , which is assembled out of quadratic Lagrangian (soft-SUSY-breaking) terms involving charged higgsinos and charged gauginos:

$$\begin{aligned} M_\chi &= \begin{pmatrix} M_2 & \sqrt{2}m_W \sin \beta \\ \sqrt{2}m_W \cos \beta & \mu \end{pmatrix} \\ Y^* M_\chi X^\dagger &= \begin{pmatrix} m_{\chi_1} & 0 \\ 0 & m_{\chi_2} \end{pmatrix}, \quad 0 < m_{\chi_1} < m_{\chi_2}. \end{aligned} \quad (\text{C.11})$$

Here  $M_2$  is the soft-SUSY-breaking gaugino mass parameter,  $\mu$  is the Higgs mixing parameter (higgsino mass parameter),  $\tan \beta$  is the ratio of the two Higgs vacuum expectation values,  $m_W$  is the mass of  $W$  boson,  $m_{\chi_i}$  ( $i = 1, 2$ ) are the masses of the physical chargino states.

In the same manner, the neutralino mixing (unitary) matrix  $U$  is chosen to diagonalize the tree level neutralino mass matrix  $M_N$ , which is assembled out of quadratic Lagrangian (soft-SUSY-breaking) terms involving neutral higgsinos and neutral gauginos:

$$\begin{aligned} M_N &= \begin{pmatrix} M_1 & 0 & -m_Z \cos \beta \sin \theta_W & m_Z \sin \beta \sin \theta_W \\ 0 & M_2 & m_Z \cos \beta \cos \theta_W & -m_Z \sin \beta \cos \theta_W \\ -m_Z \cos \beta \sin \theta_W & m_Z \cos \beta \cos \theta_W & 0 & -\mu \\ m_Z \sin \beta \sin \theta_W & -m_Z \sin \beta \cos \theta_W & -\mu & 0 \end{pmatrix} \\ U^* M_N U^\dagger &= \begin{pmatrix} m_{\chi_1^0} & 0 & 0 & 0 \\ 0 & m_{\chi_2^0} & 0 & 0 \\ 0 & 0 & m_{\chi_3^0} & 0 \\ 0 & 0 & 0 & m_{\chi_4^0} \end{pmatrix}, \quad 0 < m_{\chi_1^0} < m_{\chi_2^0} < m_{\chi_3^0} < m_{\chi_4^0}. \end{aligned} \quad (\text{C.12})$$

Here  $M_1$  is the soft-SUSY-breaking gaugino mass parameter,  $m_Z$  is the mass of  $Z$  boson,  $m_{\chi_i^0}$  ( $i = 1, 2, 3, 4$ ) are the masses of the physical neutralino states.

The  $SU(2)$  gaugino mass parameter  $M_2$  can always be chosen real, while the higgsino mass parameter  $\mu$  (as well as the  $U(1)$  gaugino mass parameter  $M_1$  appearing in the neutralino mass matrix) is in general a complex quantity:

$$\mu \equiv |\mu| e^{i\phi_\mu}. \quad (\text{C.13})$$

The phase  $\phi_\mu$  is one of the main sources of CP violations analyzed in this Thesis; to simplify the calculations in Chapter 6  $M_1$  was always chosen real.

To obtain the analytical expressions analyzed in Chapters 3 and 6 one needs the following Lagrangian vertices involving SUSY fields:

$(\gamma\tilde{\chi}\tilde{\chi})$  photon-chargino-chargino:

$$L_1^{GCN} = e\bar{\Psi}_{\chi_k}\gamma^\rho\Psi_{\chi_l}A_\rho\delta_{kl} \quad (\text{C.14})$$

Note that the sign is opposite to that of  $\gamma ee$  vertex (C.8). This is because following the established convention we treat the positive charginos  $\tilde{\chi}_i^+$  ( $i = 1, 2$ ) as particles, rather than

antiparticles.

$(Z\tilde{\chi}\tilde{\chi})$  *Z boson – chargino – chargino*:

$$\begin{aligned}
 L_2^{GCN} &= \frac{g}{4 \cos \theta_W} \bar{\Psi}_{\chi_j} \gamma^\rho \left\{ \left[ 2\delta_{kj} \cos 2\theta_W + Y_{k1} Y_{1j}^\dagger + X_{j1} X_{1k}^\dagger \right] \right. \\
 &\quad \left. + \gamma^5 \left[ Y_{k1} Y_{1j}^\dagger - X_{j1} X_{1k}^\dagger \right] \right\} \Psi_{\chi_k} Z_\rho \\
 &\equiv \frac{g}{4 \cos \theta_W} \bar{\Psi}_{\chi_j} \gamma^\rho \left\{ G_{V k,j} + \gamma^5 G_{A k,j} \right\} \Psi_{\chi_k} Z_\rho, \tag{C.15}
 \end{aligned}$$

where  $X, Y$  are the chargino mixing matrices, defined by Eqs. (C.11). Note, that the first mass index of  $G_{V k,j}$  and  $G_{A k,j}$  refers to mass of the *annihilated particle*, which is the *positive* chargino. Besides, since  $X$  and  $Y$  are unitary matrices, the following equalities holds:

$$\text{Hermiticity: } G_{V(A)j,k} = (G_{V(A)k,j})^*, \tag{C.16}$$

$$\text{Trace: } \sum_{i=1,2} G_{V i,i} = 2 + 4 \cos 2\theta_W, \quad \sum_{i=1,2} G_{A i,i} = 0. \tag{C.17}$$

$(W\tilde{\chi}\tilde{\chi}_0)$  *W boson – chargino – neutralino*:

$$L_4^{GCN} = \frac{g}{2} \left\{ \bar{\Psi}_{\chi_j} \gamma^\rho (\mathcal{V} + \gamma^5 \mathcal{A}) \Psi_{\chi_a^0} W_\rho + \bar{\Psi}_{\chi_a^0} \gamma^\rho (\mathcal{V}^* + \gamma^5 \mathcal{A}^*) \Psi_{\chi_j} W_\rho^\dagger \right\} \tag{C.18}$$

with

$$\begin{aligned}
 \mathcal{V} &= -U_{a2} Y_{1j}^\dagger - U_{2a}^\dagger X_{j1} - \frac{U_{a3} Y_{2j}^\dagger}{\sqrt{2}} + \frac{U_{4a}^\dagger X_{j2}}{\sqrt{2}}, \\
 \mathcal{A} &= -U_{a2} Y_{1j}^\dagger + U_{2a}^\dagger X_{j1} - \frac{U_{a3} Y_{2j}^\dagger}{\sqrt{2}} - \frac{U_{4a}^\dagger X_{j2}}{\sqrt{2}},
 \end{aligned}$$

where  $X, Y$  are the chargino mixing matrices, and  $U$  is the neutralino mixing matrix, defined by Eqs. (C.11) and (C.12), respectively.

$(e\tilde{\chi}\tilde{\nu})$  *electron – chargino – sneutrino*:<sup>1</sup>

$$L_4^{LC} \stackrel{(m_e=0)}{=} -\frac{g}{2} \left\{ X_{1j}^\dagger \bar{\Psi}_{\chi_j}^T C (1 - \gamma^5) \Psi_e \tilde{\nu}^\dagger - X_{j1} \bar{\Psi}_e (1 + \gamma^5) C^{-1} \bar{\Psi}_{\chi_j}^T \tilde{\nu} \right\} \tag{C.19}$$

$$= -\frac{g}{2} \left\{ X_{1j}^\dagger \bar{\Psi}_{\chi_j}^c (1 - \gamma^5) \Psi_e \tilde{\nu}^\dagger + X_{j1} \bar{\Psi}_e (1 + \gamma^5) \Psi_{\chi_j}^c \tilde{\nu} \right\} \tag{C.20}$$

$$= -\frac{g}{2} \left\{ X_{1j}^\dagger \bar{\Psi}_e^c (1 - \gamma^5) \Psi_{\chi_j} \tilde{\nu}^\dagger + X_{j1} \bar{\Psi}_{\chi_j} (1 + \gamma^5) \Psi_e^c \tilde{\nu} \right\} \tag{C.21}$$

where  $X$  is the chargino mixing matrix defined by Eqs. (C.11) and  $C$  is the charge-conjugation matrix. For convenience we also provided two versions of this vertex expressed via the charge conjugated fields.

---

<sup>1</sup>The additional terms proportional to  $m_e$  can be found in [65] (we drop these terms in the computations). Note, however, that the second term of this vertex gets a wrong sign in [65] (c.f. [39]).



# Bibliography

- [1] Yu. A. Gol'fand and E. P. Likhtman, JETP Letters **13** (1971) 323; D. V. Volkov and V. P. Akulov, Phys. Lett. **46B** (1973) 109; J. Wess and B. Zumino, Nucl. Phys. B **70** (1974) 39; *idid*, Phys. Lett. **49B** (1974) 52. These articles are reprinted in *Supersymmetry*, S. Ferrara, ed. (North Holland/World Scientific, Amsterdam/Singapore, 1987);
- [2] S. Dimopoulos and H. Georgi, Nucl. Phys. B **193** (1981) 150; H. P. Nilles, Phys. Rept. **110** (1984) 1; H. E. Haber and G. L. Kane, Phys. Rept. **117** (1985) 75.
- [3] M. Drees, R. M. Godbole, P. Roy, *Theory and Phenomenology of Sparticles* (World Scientific, Singapore, 2004).
- [4] S. Weinberg, *The Quantum Theory of Fields* (Cambridge University Press, Cambridge, England, 2000), Vols. 1–3.
- [5] O. Buchmueller, et al., JHEP 0809 (2008) 117. [arXiv:0808.4128 [hep-ph]].
- [6] Michael E. Peskin, *Summary of Lepton Photon 2011*, Invited talk at 25th International Symposium on Lepton Photon Interactions at High Energy (LP11), Mumbai, India, 22-27 Aug 2011; [arXiv:1110.3805 [hep-ph]].
- [7] J. Incandela [on behalf of CMS], *Status of the CMS SM Higgs Search*, and F. Gianotti [on behalf of ATLAS], *Status of the SM Higgs Search in ATLAS, joint CMS/ATLAS seminars at CERN, July 4, 2012*; CMS Collaboration, CMS-PAS-HIG-12-020; ATLAS Collaboration, ATLAS-CONF-2012-093.
- [8] S. Akula, P. Nath and G. Peim, arXiv:1207.1839 [hep-ph].
- [9] S. Weinberg, Phys. Rev. D **13** (1976) 974; *ibid.* D **19** (1979) 1277; L. Susskind, Phys. Rev. D **20** (1979) 2619; G. 't Hooft, in *Recent developments in gauge theories*, Proceedings of the NATO Advanced Summer Institute, Cargese 1979, ed. G. 't Hooft *et al.* (Plenum, New York 1980).
- [10] S. Weinberg, Phys. Rev. Lett. **80** (1998) 3702 [hep-th/9803099].
- [11] S. Coleman and J. Mandula, Phys. Rev. **159** (1967) 1251.
- [12] R. Haag, J. T. Lopuszanski, and M. Sohnius, Nucl. Phys. B **88** (1975) 257; reprinted in *Supersymmetry*, [1].
- [13] N. Weiner, *Dark Matter and New Physics*, talk given at *ICHEP2012 - 36th International Conference for High Energy Physics, 4-11 July 2012, Melbourne, Australia*, the slides

are available at:

<http://indico.cern.ch/contributionDisplay.py?contribId=33&confId=181298>

- [14] H. E. Haber and G. L. Kane, Phys. Rept. **117** (1985) 75.
- [15] A. D. Sakharov, Pisma Zh. Eksp. Teor. Fiz. **5** (1967) 32 [JETP Lett. **5** (1967) 24] [Sov. Phys. Usp. **34** (1991) 392] [Usp. Fiz. Nauk **161** (1991) 61].
- [16] J. H. Christenson, J. W. Cronin, V. L. Fitch and R. Turlay, Phys. Rev. Lett. **13**, (1964) 138.
- [17] G. C. Branco, L. Lavoura, J. P. Silva, *CP Violation* (Oxford University Press, Oxford, England, 1999).
- [18] H. P. Nilles, Phys. Rept. **110** (1984) 1; H. E. Haber and G. L. Kane, Phys. Rept. **117** (1985) 75; H. Baer and X. Tata, *Weak Scale Supersymmetry* (Cambridge University Press, Cambridge, England, 2006); see also Vol. 3 of [4].
- [19] J. R. Ellis, S. Ferrara and D. V. Nanopoulos, Phys. Lett. B **114** (1982) 231. W. Buchmuller and D. Wyler, Phys. Lett. B **121** (1983) 321; J. Polchinski and M. B. Wise, Phys. Lett. B **125** (1983) 393; F. del Aguila, M. B. Gavela, J. A. Grifols and A. Mendez, Phys. Lett. B **126** (1983) 71 [Erratum-*ibid.* B **129** (1983) 473].
- [20] Y. Kizukuri and N. Oshimo, Phys. Rev. D **46** (1992) 3025.
- [21] T. Ibrahim and P. Nath, Phys. Rev. D **57** (1998) 478 [Erratum-*ibid.* D **58**, 019901 (1998 ERRAT, D60, 079903. 1999 ERRAT, D60, 119901. 1999)] [arXiv:hep-ph/9708456]; M. Brhlik, G. J. Good and G. L. Kane, Phys. Rev. D **59** (1999) 115004 [arXiv:hep-ph/9810457]; N. Ghodbane, S. Katsanevas, I. Laktineh and J. Rosiek, Nucl. Phys. B **647** (2002) 190 [arXiv:hep-ph/0012031]; A. Bartl, W. Majerotto, W. Porod and D. Wyler, Phys. Rev. D **68** (2003) 053005 [arXiv:hep-ph/0306050]; S. Yaser Ayazi and Y. Farzan, Phys. Rev. D **74** (2006) 055008 [arXiv:hep-ph/0605272].
- [22] E. Accomando *et al.* [ECFA/DESY LC Physics Working Group], Phys. Rept. **299** (1998) 1 [arXiv:hep-ph/9705442]; J. A. Aguilar-Saavedra *et al.* [ECFA/DESY LC Physics Working Group], arXiv:hep-ph/0106315; T. Abe *et al.* [American Linear Collider Working Group], in *Proc. of the APS/DPF/DPB Summer Study on the Future of Particle Physics (Snowmass 2001)* ed. N. Graf, SLAC-R-570 *Resource book for Snowmass 2001, 30 Jun - 21 Jul 2001, Snowmass, Colorado*; G. Weiglein *et al.* [LHC/LC Study Group], Phys. Rept. **426** (2006) 47 [arXiv:hep-ph/0410364].
- [23] Y. Kizukuri and N. Oshimo, in *Proc. of the Workshop on  $e^+e^-$  Collisions at 500 GeV: The Physics Potential*, Munich–Annecy–Hamburg 1993, DESY 93-123C, P. Zerwas (ed.); arXiv:hep-ph/9310224.
- [24] S. Y. Choi, A. Djouadi, H. S. Song and P. M. Zerwas, Eur. Phys. J. C **8** (1999) 669 [arXiv:hep-ph/9812236]; S. Y. Choi, M. Guchait, J. Kalinowski and P. M. Zerwas, Phys. Lett. B **479** (2000) 235 [arXiv:hep-ph/0001175]; S. Y. Choi, A. Djouadi, M. Guchait, J. Kalinowski, H. S. Song and P. M. Zerwas, Eur. Phys. J. C **14** (2000) 535 [arXiv:hep-ph/0002033].

- [25] A. Bartl, H. Fraas, O. Kittel and W. Majerotto, Phys. Lett. B **598** (2004) 76 [arXiv:hep-ph/0406309].
- [26] W. M. Yang and D. S. Du, Phys. Rev. D **67** (2003) 055004 [arXiv:hep-ph/0211453].
- [27] A. Bartl, K. Hohenwarter-Sodek, T. Kernreiter and H. Rud, Eur. Phys. J. C **36** (2004) 515 [arXiv:hep-ph/0403265].
- [28] G. V. Dass and G. G. Ross, Phys. Lett. B **57** (1975) 173; Nucl. Phys. B **118** (1977) 284.
- [29] B. Ananthanarayan and S. D. Rindani, Eur. Phys. J. C **46** (2006) 705 [arXiv:hep-ph/0601199].
- [30] W. Hollik, E. Kraus, M. Roth, C. Rupp, K. Sibold and D. Stockinger, Nucl. Phys. B **639** (2002) 3 [arXiv:hep-ph/0204350].
- [31] B. Ananthanarayan and S. D. Rindani, Phys. Rev. D **70** (2004) 036005 [arXiv:hep-ph/0309260].
- [32] S. Heinemeyer, W. Hollik and G. Weiglein, Phys. Rept. **425** (2006) 265 [arXiv:hep-ph/0412214].
- [33] B. C. Allanach *et al.*, in *Proc. of APS/DPF/DPB Summer Study on the Future of Particle Physics (Snowmass 2001)*, ed. N. Graf, Snowmass, Colorado, p. 125 [arXiv:hep-ph/0202233].
- [34] K. Rolbiecki and J. Kalinowski, Phys. Rev. D **76** (2007) 115006.
- [35] P. Osland and A. Vereshagin, Phys. Rev. D **76** (2007) 036001 [Erratum-*ibid.* 119902].
- [36] Per Osland, Jan Kalinowski, Krzysztof Rolbiecki, Alexander Vereshagin, *Proc. of 2007 International Linear Collider Workshop (LCWS07 And ILC07)* [arXiv:hep-ph/0709.3358].
- [37] G. 't Hooft, Nucl. Phys. B **33** (1971) 173.
- [38] A. Denner *et. al.*, Nucl. Phys. B **387** (1992) 467; *ibid.* , Phys. Lett. B **291** (1992) 278.
- [39] J. Rosiek, Phys. Rev. D **41** (1990) 3464; the version with the most recent corrections is available at: <http://www.fuw.edu.pl/~rosiek/physics/prd41.html>
- [40] H. E. Haber, in *Proc. of the XXI SLAC Summer Institute of Particle Physics: Spin Structure in High Energy Processes, July 26 - August 6, 1993*, ed. L. DePorcel and Ch. Dunwoodie, pp. 231–272 (SLAC – Report – 444, Stanford, California, 1994).
- [41] G. Feinberg and S. Weinberg, Nuovo Cimento **14** (1959) 571.
- [42] T. Blank and W. Hollik, arXiv:hep-ph/0011092.
- [43] G. V. Dass and G. G. Ross, Phys. Lett. B **57** (1975) 173; Nucl. Phys. B **118** (1977) 284.
- [44] Homepage: <http://jaxodraw.sourceforge.net/>

- [45] Homepage: <http://www.reduce-algebra.com/>; REDUCE v3.5 was used in computations.
- [46] L. Girardello and M. T. Grisaru, Nucl. Phys. B **194** (1982) 65.
- [47] B. C. Allanach, A. Dedes and H. K. Dreiner, arXiv:hep-ph/0309196, and references therein.
- [48] J. Schechter and J. W. F. Valle, Phys. Rev. D **24** (1981) 1883; S. K. Jones and C. H. Llewellyn Smith, Nucl. Phys. B **217** (1983) 145.
- [49] E. I. Gates and K. L. Kowalski, Phys. Rev. D **37** (1988) 938; J. Gluza and M. Zralek, Phys. Rev. D **45** (1992) 1693.
- [50] G. 't Hooft, Nucl. Phys. B **33** (1971) 173; K. Fujikawa, B. W. Lee and A. I. Sanda, Phys. Rev. D **6** (1972) 2923.
- [51] G. Passarino and M. J. G. Veltman, Nucl. Phys. B **160** (1979) 151; G. 't Hooft and M. J. G. Veltman, Nucl. Phys. B **153** (1979) 365.
- [52] W. Khater, dr. scient. thesis, University of Bergen, 2003.
- [53] T. Hahn and M. Perez-Victoria, Comput. Phys. Commun. **118** (1999) 153 [arXiv:hep-ph/9807565].  
See also <http://www.feynarts.de/looptools/>
- [54] G. J. van Oldenborgh and J. A. Vermaseren, Z. Phys. C **46** (1990) 425.
- [55] M. A. Diaz and D. A. Ross, JHEP **0106** (2001) 001 [arXiv:hep-ph/0103309]; arXiv:hep-ph/0205257.
- [56] H. Eberl, T. Gajdosik, W. Majerotto and B. Schrausser, Phys. Lett. B **618** (2005) 171 [arXiv:hep-ph/0502112].
- [57] A. Bartl, H. Fraas, T. Kernreiter, O. Kittel and W. Majerotto, arXiv:hep-ph/0310011.
- [58] A. Bartl, H. Fraas, O. Kittel and W. Majerotto, arXiv:hep-ph/0308141.
- [59] A. Bartl, T. Kernreiter and O. Kittel, Phys. Lett. B **578** (2004) 341 [arXiv:hep-ph/0309340].
- [60] G. A. Moortgat-Pick *et al.*, arXiv:hep-ph/0507011.
- [61] M. E. Peskin and D. V. Schroeder, *Quantum Field Theory* (Addison-Wesley, NY, 1997).
- [62] J. D. Bjorken and S. D. Drell, *Relativistic Quantum Mechanics and Relativistic Quantum Fields*, McGraw-Hill, 1964–1965.
- [63] T. Ohl and J. Reuter, Eur. Phys. J. C **30** (2003) 525; arXiv:hep-th/0212224.
- [64] S. Pokorski, *Gauge Field Theories*, Cambridge, 1987.
- [65] B. Kileng, dr. scient. thesis, University of Bergen, 1994.